POLITECNICO DI MILANO
Dipartimento di Elettronica e Informazione

MODELLING, SIMULATION, AND CONTROL OF A GEOTHERMAL POWER PLANT

Modellistica, Simulazione e Controllo
di un Impianto Geotermico

Francesco Casella

Advisor: Prof. Claudio Maffezzoni

– Tesi di Dottorato –
– Dottorato di Ricerca in Ingegneria Informatica e Automatica – 1996/1998

POLITECNICO DI MILANO

DOTTORATO DI RICERCA IN INGEGNERIA INFORMATICA E AUTOMATICA

MODELLISTICA, SIMULAZIONE E CONTROLLO DI UN IMPIANTO GEOTERMICO

Tesi di Dottorato di:

Francesco Casella

Relatore:

Prof. Claudio Maffezzoni

Tutore:

Prof. Nicola Schiavoni

Coordinatore del Dottorato:

Prof. Carlo Ghezzi

XI ciclo

SOMMARIO

Motivazioni e obbiettivi della ricerca

Nell'ambito degli impianti per la produzione di energia elettrica, un'enfasi sempre crescente viene posta sullo sfruttamento efficiente delle fonti di energia, sia per motivi economici che per motivi ambientali. Questo può voler dire, da un lato, un uso più efficiente delle fonti energetiche tradizionali, come il petrolio e il gas naturale, dall'altro, il crescente utilizzo di fonti di energia rinnovabili e non convenzionali. Quali esempi del primo tipo si possono citare gli impianti a ciclo combinato, o gli impianti di co-generazione che producono energia elettrica insieme a calore per tele-riscaldamento domestico o vapore per usi industriali; come esempi del secondo tipo, si possono considerare gli impianti a energia solare, gli impianti geotermici e i termocombustori per rifiuti solidi urbani con co-generazione di energia. In entrambi i casi, l'obbiettivo è di sfruttare a fondo fonti di energia "povere", cioè sostanzialmente a bassa temperatura.

Il costo di questa operazione sta essenzialmente nell'aumento della complessità dei processi di produzione, spesso combinato con la necessità di ricorrere a soluzioni progettuali anche fortemente innovative. Nella maggior parte dei casi, i progettisti dell'impianto si occupano della ideazione del ciclo termodinamico, del progetto delle parti meccaniche, del dimensionamento dei componenti e dei bilanci di massa ed energia a regime; raramente viene affrontata l'analisi dinamica fin dai primi stadi del progetto. Il personale responsabile del progetto del sistema di controllo e delle fasi di commissioning, avviamento e conduzione dell'impianto si trova quindi di fronte a due seri problemi. Prima di tutto, l'elevato numero di componenti, la complessità dell'impianto, spesso dotato di numerosi ricircoli o spillamenti di fluido, e la presenza di svariati sotto-sistemi interconnessi tra loro, fa sì che il comportamento complessivo dell'impianto, sia statico che dinamico, non possa essere dedotto con facilità da quello dei singoli componenti, ma sia fondamentalmente il risultato della loro interazione. Inoltre, nel caso di progetti fortemente innovativi, manca del tutto quell'esperienza su impianti analoghi che di norma funge da guida per affrontare i problemi posti dal nuovo impianto. In particolare, il comportamento dinamico dell'impianto può essere del tutto imprevedibile, sia durante il normale esercizio, sia in caso di guasti.

In queste situazioni, la disponibilità di un adeguato strumento sistemistico di simulazione, che permetta di integrare nell'analisi il modello dinamico del processo, le strategie di controllo automatico e la simulazione delle manovre d'esercizio e delle risposte ai guasti, può essere un validissimo aiuto, permettendo di facilitare e rendere più sicure e veloci le fasi di progettazione, commissioning, avviamento ed esercizio dell'impianto.

Lo studio sistemistico dell'impianto geotermico di Latera, condotto in collaborazione con l'ENEL S.p.A, rientra in questo quadro d'insieme. L'impianto di Latera [ELC89] sfrutta una riserva di acqua calda sotterranea per produrre energia servendosi di turbine a vapore. L'entalpia piuttosto bassa e il contenuto di gas disciolti (soprattutto CO_2) del fluido geotermico primario fanno sì che che solo circa il 12% del fluido estratto dai pozzi passi in fase gassosa, la quale raccoglie la quasi totalità della CO_2. Questa situazione è completamente differente da quella degli impianti geotermici convenzionali, nei quali il fluido estratto dai pozzi è costituito interamente da una fase gassosa, contenente oltre il 98% di vapor d'acqua, che puo' essere direttamente convogliato alle turbine. Nasce quindi la necessità di un processo più complesso che sfrutti in modo efficiente il contenuto energetico della miscela gas-vapore. Inoltre, l'elevata portata di acqua residua prodotta dal processo (circa 350 kg/s per una produzione netta di energia elettrica attorno ai 28 MW) deve essere eliminata tramite la reiniezione in altri pozzi, sia per motivi di tipo ambientale (il fluido contiene sostanze inquinanti), sia per evitare il rapido esaurimento della riserva d'acqua sotterranea. I pozzi di reiniezione sono collocati a 10 km dall'impianto di produzione vapore, allo scopo di evitare il prematuro raffreddamento del campo di produzione; ciò richiede un complesso impianto di reiniezione, sottoposto a vincoli piuttosto critici sul suo funzionamento per evitare l'instaurarsi temporaneo di flussi bifase, con possibili conseguenze traumatiche sull'impianto stesso.

E' stata quindi presa la decisione di coadiuvare la fase finale di progetto del sistema con un simulatore ingegneristico, in grado di rappresentare con buona precisione il funzionamento di tutte le parti fondamentali dell'impianto, cioè: i pozzi di produzione, il processo di separazione di fase, il trasporto dei fluidi alla centrale di produzione vapore, la produzione di vapore pulito dall'acqua geotermica e dalla miscela vapore-CO_2, nonché lo scarico delle acque residue attraverso il sistema di reiniezione. Una delle questioni più impegnative è stata la modellizzazione accurata del "rievaporatore" ("reboiler"), una colonna a piatti avente lo scopo di separare la CO_2 dal vapore; il "reboiler" infatti è un componente innovativo, il cui comportamento dinamico non è mai stato studiato prima d'ora in letteratura. Il simulatore permette lo studio della sua dinamica, anche in caso di grandi transitori e fuori dalle condizioni nominali di progetto.

Il simulatore ha permesso di rispondere ad alcune domande fondamentali, prima che l'impianto venisse effettivamente costruito e in assenza di esperienza su impianti simili da parte del personale addetto, nonchè di dati sperimentali sul funzionamento. La prima domanda riguarda l'adeguatezza della struttura del sistema di controllo, descritta sommariamente nella documentazione di progetto [ELC89], a garantire il funzionamento dell'impianto entro i limiti di sicurezza in tutte le possibili configurazioni di funzionamento, nonché in caso di guasti a componenti critici. Questa parte è cruciale per un rapido svolgimento della fase di commissioning e primo avviamento, seguita poi da una soddisfacente fase di esercizio dell'impianto. La seconda domanda è: si può migliorare la struttura del sistema di controllo, utilizzando le misure disponibili? E' opportuno prendere ulteriori misure sul processo? La terza riguarda l'ottenimento di una taratura (preliminare) dei parametri di tutti i controllori, allo scopo di accelerare al massimo la fase di commissioning. L'ultima questione, non meno importante, è di trovare criteri di esercizio ottimali per l'impianto.

Lo studio del problema di controllo del reboiler ha rivelato una situazione tipica di molti problemi di controllo dei processi, nei quali la struttura del sistema di controllo (ossia quali debbano essere le variablili controllate, quale sia il migliore accoppiamento tra variabili di ingresso e uscita dei regolatori, quali misure addizionali possano essere usate per migliorare le prestazioni, ed infine quali valori vadano assegnati ai setpoint) non e' affatto chiara a priori. Di fatto, l'iniziale problema di controllo è stato inquadrato nel più ampio contesto dell'ottimizzazione della produzione d'energia dell'impianto. Una parte di questa ricerca, non prevista nelle fasi iniziali del progetto, è stata condotta mentre l'autore si trovava in visita presso il Centre for Process Systems Engineering dell'Imperial College di Londra. Un possibile sbocco conclusivo di questa parte del lavoro potrebbe essere un sistema di supporto alle decisioni, che affianchi il personale addetto alla conduzione della centrale nel suo compito di gestione, con lo scopo finale di massimizzare il rendimento complessivo dell'impianto. Lo studio completo di questo sistema va comunque ben oltre l'ambito di questa tesi.

Il simulatore d'impianto, che è stato costruito come parte determinante del lavoro di ricerca, è un simulatore ingegneristico: è sufficientemente accurato da poter essere usato per scopi di progetto, mentre la sua interfaccia utente è piuttosto limitata, e adatta, per il momento, all'utilizzo da parte di personale qualificato, coinvolto nella progettazione e nell'avviamento iniziale. D'altra parte, grazie alle potenzialità di programmazione visuale del sofware impiegato per lo sviluppo (LabView, [Lab97]), essa potrebbe essere abbastanza facilmente estesa, fino ad ottenere un simulatore d'addestramento per il personale che sarà responsabile dell'esercizio ordinario dell'impianto.

Principali risultati ottenuti

I principali risultati di questa ricerca possono essere così sintetizzati.

Innanzitutto viene passato in rassegna l'argomento della simulazione di processo basata su criteri di disaccoppiamento, e vengono presentati alcuni nuovi risultati sulla soluzione delle reti idrauliche tramite disaccoppiamento. Successivamente, viene discussa l'applicazione di questi concetti all'ambiente di simulazione ProcSim, che è stato usato durante tutta la ricerca ed è basato essenzialmente su di essi.

Il secondo risultato innovativo è rappresentato dall'estensione dell'ambiente di simulazione di processo ProcSim all'impiego di fluidi di lavoro bi-componente (acqua+CO_2), con il relativo sviluppo dei modelli di tutti i nuovi componenti che trattano questo tipo di fluido.

ProcSim, precedentemente sviluppato presso il Dipartimento di Elettronica del Politecnico di Milano ([Bar94,95,96,98]), è già stato utilizzato con successo per la simulazione di impianti di produzione di energia tradizionali, costituiti da una rete contenente caldaie, camere di combustione, scambiatori di calore, valvole, pompe e turbine, facenti uso di acqua e vapore come fluidi di lavoro ([Bar95], [Cst95], [Col96]); è stato inoltre validato estensivamente in un caso particolare, nel quale un piccolo impianto pilota era disponibile per una esaustiva serie di esperimenti dinamici ([Bel96], [Lev99]). D'altra parte, il tipo di processo su cui si basa l'impianto di Latera era decisamente differente da questi ultimi, il che ha comportato la scrittura da zero di quasi tutti i modelli dei componenti di processo, mai utilizzati prima d'ora, o comunque un loro adattamento all'utilizzo del fluido bi-componente. E' stato inoltre sviluppato un approccio sistematico alla modellistica di reti idrauliche il cui flusso può essere completamente intercettato durante la simulazione dei transitori.

Un simulatore dinamico completo e accurato dell'intero impianto è stato costruito, per gli scopi sopra descritti. I modelli dei componenti di processo che lo costituiscono sono modelli non-lineari basati sui principi primi; essi tengono conto anche di dettagli quali la CO_2 disciolta in tutti i componenti contenenti acqua liquida, il non perfetto equilibrio termodinamico nelle cavità bifase (in particolare nei piatti del reboiler), e la dinamica ondulatoria nelle condotte di reiniezione. Il codice di simulazione è in grado di descrivere l'avviamento e la fermata di alcune parti di impianto (i pozzi di produzione e le diverse unità dell'impianto di produzione vapore); non è stato però pensato per la simulazione dell'avviamento da freddo, che avrebbe richiesto uno sforzo modellistico molto più elevato. Vale la pena di ricordare che, dopo un breve corso di addestramento, il simulatore è stato usato autonomamente dal personale dell'ENEL per definire completamente la configurazione del sistema

di controllo distribuito, e per ottenere una pre-taratura dei parametri dei regolatori, in modo da permettere un commissioning più rapido dell'impianto.

Per avere un'idea della complessità e della completezza del simulatore, si consideri che esso comprende circa 300 componenti di processo e di controllo, con più di 1000 parametri (alcuni dei quali vettoriali), oltre 700 variabili di processo e 23 anelli di regolazione.

Il simulatore ha permesso di verificare la fattibilità delle manovre operative previste, e la capacità del sistema di controllo di mantenere l'impianto nei limiti di sicurezza in caso di guasti a componenti critici. Data l'assoluta mancanza di esperienza pregressa, questo era un aspetto assolutamente non scontato a priori, in particolare per il funzionamento del reboiler e del sistema di reiniezione. Per questi due sottosistemi, diversi tipi di sistema di controllo sono stati considerati, sia convenzionali (PI con compensazione statica), sia di tipo più avanzato.

Lo studio del sistema di controllo per il ciclo reboiler ha evidenziato il fatto che il problema di controllo in questo caso è prima di tutto un problema di ottimizzazione. L'impianto lavora normalmente in uno stato stazionario, con le turbine al massimo carico consentito dalla produzione dei pozzi e senza alcun bisogno di regolazioni adatte a seguire profili rapidi di variazione di carico. Inoltre, la risposta del ciclo reboiler a transitori causati da guasti o da cambiamenti nella configurazione dei pozzi di produzione si è dimostrata non critica. Il vero obbiettivo del sistema di controllo, che non era stato chiaramente identificato prima di questo lavoro di ricerca, è di massimizzare l'efficienza energetica complessiva dell'impianto, che dipende essenzialmente dalle complesse interazioni che avvengono tra i vari componenti, durante il funzionamento dell'impianto. La struttura del sistema di controllo del reboiler non è affatto scontata, visto che sono disponibili molte più misure rispetto alle variabili di controllo, e che la strategia di controllo non è affatto chiara a priori. Viene quindi proposta una possibile struttura per il sistema di controllo e una politica di gestione dei setpoint, che garantisce il funzionamento dell'impianto molto vicino al punto di lavoro ottimale, in tutte le possibili condizioni operative e in condizioni di sicurezza. L'analisi non è affatto conclusiva, e rimane spazio per un ulteriore lavoro di ricerca sul tema.

Infine, alcuni dei risultati e dei concetti sviluppati in questo lavoro di ricerca sono stati pubblicati: in particolare, lavori sul concetto generale di disaccoppiamento applicato alla simulazione [Cas98c], sulla simulazione del reboiler [Cas98d] e sulla simulazione e controllo dell'impianto di reiniezione [Cas98b].

Schema della tesi

Successivamente all'Introduzione, il Capitolo 2 contiene la descrizione dell'impianto e dei principali problemi che nascono dalla sua peculiare struttura. Vengono descritte le scelte di progetto, i principi su cui si basa il funzionamento e le politiche di gestione dell'impianto, insieme ai diagrammi di flusso semplificati dell'impianto, che verranno poi impiegati per la sua simulazone. Viene poi discusso il grado di dettaglio dell'analisi e della modellistica, motivando le principali ipotesi semplificative, che sono state adottate allo scopo di ottenere un modello e un simulatore al tempo stesso accurati e di complessità ragionevole. Infine, vengono introdotte le principali questioni poste dalla simulazione e dal controllo di un impianto di tipo così innovativo.

Il Capitolo 3 tratta della simulazione dei processi di generazione di energia. Viene presentata una panoramica dello stato dell'arte nella simulazione di tali processi, basata su principi di disaccoppiamento, insieme ad una descrizione dell'ambiente ProcSim, che si basa essenzialmente su tali principi. Vengono inoltre descritti alcuni nuovi risultati sulla stabilità numerica della soluzione delle reti idrauliche mediante disaccoppiamento. Il successivo capitolo descrive le estensioni che è stato necessario apportare all'ambiente di simulazione per trattare il processo di Latera: il trattamento di un fluido di lavoro bifase e bi-componente; la modellistica dei separatori di fase e del reboiler; la modellistica delle condotte di reiniezione includente la dinamica ondulatoria, integrata col resto del processo; il corretto trattamento delle reti idrauliche il cui flusso può essere completamente intercettato, e di particolari strutture di rete idraulica, che non erano mai state incontrate prima d'ora nella simulazione di impianti di generazione convenzionali.

Il Capitolo 5 è dedicato ad una descrizione più dettagliata della modellistica dei componenti di processo innovativi: reboiler (piatti e fondo), separatori di fase, vari tipi di valvole, condotte di trasporto per liquidi e miscele gas-vapore, condotte di reiniezione con dinamica ondulatoria, modelli semplificati dei pozzi di produzione e reiniezione, pompe, vasi d'espansione pressurizzati, turbine. Viene anche brevemente descritta la libreria di componenti di controllo.

Nel Capitolo 6 ci si concentra sul simulatore di processo. Prima di tutto, l'architettura del simulatore nell'ambiente ProcSim viene discussa, dalle specifiche generali, fino ad alcuni problemi specifici di implementazione. Successivamente, vengono descritte le applicazioni del simulatore, cioè: la taratura degli anelli di regolazione e la validazione del sistema di controllo; il test delle manovre operative e delle risposte al guasto di singoli componenti; l'uso del simulatore come sussidio alla fase di commissioning e, in un secondo tempo, come strumento per l'addestramento del personale. Il capitolo termina

con la descrizione del modello statico semplificato dell'impianto, realizzato nell'ambiente di simulazione gPROMS, utilizzato per gli studi di ottimizzazione.

Il Capitolo 7 tratta i problemi di controllo e gestione dell'impianto. Dopo una breve introduzione, i problemi di controllo più interessanti vengono discussi, in particolare il controllo del ciclo reboiler e del sistema di reiniezione. Alcune linee guida per il possibile futuro sviluppo di un sistema di supporto alle decisioni per la gestione dell'impianto concludono il capitolo.

Infine, le conclusioni e i possibili sviluppi futuri della ricerca vengono dati nel Capitolo 8.

RINGRAZIAMENTI

Il Dottorato di Ricerca, come ebbe a dirmi qualche anno fa Nicola Schiavoni, è un'avventura, e come ogni avventura si snoda attraverso un percorso più o meno accidentato, ma confortato dalla compagnia e dal contributo di innumerevoli persone, senza le quali sarebbe impossibile portare il cammino a compimento.

Il primo ringraziamento va al professor Claudio Maffezzoni, per la possibilità che mi ha dato di occuparmi di un problema per me di grande interesse, per avermi costantemente seguito lungo tutto lo svolgersi del lavoro, e per avermi insegnato molto, soprattutto durante le interminabili discussioni, invariabilmente concluse dall'augurio "buon lavoro!", che hanno scandito la nostra quasi triennale collaborazione. Ugualmente devo ringraziare il professor Nicola Schiavoni, che con grande discrezione e rispetto è stato, quasi novello Virgilio, la mia guida nell'intraprendere e portare a termine il percorso, certo non facile, del dottorato.

Uno specialissimo ringraziamento va ad Alberto Leva e ad Andrea Bartolini, innanzitutto per avermi sopportato (a volte non e' facile), ma soprattutto per l'aiuto e il supporto che mi hanno continuamente offerto nel mio lavoro. Chi ha provato a lavorare da solo su un progetto impegnativo, trovandosi spesso incagliato in difficoltà apparentemente insuperabili, sa quale conforto può dare la disponibilità di un consiglio amichevole e competente per rimettersi in carreggiata. La vulcanicità di Alberto, e la professionalità impagabile di Andrea sono state per me un aiuto ed un esempio insostituibili. Ringrazio per il contributo dato ad alcune parti del lavoro i tesisti Cristiano Bonetti (per la modellistica dell'impianto di reiniezione) e Angela Cera (per lo studio delle valvole con orifizio tarato).

Un ringraziamento particolare va a Pasquale Calabrese, dell'ENEL/CRA, agli ingegneri Enrico Arzilli e Martino Pasti dell'ENEL di Pisa, e a tutto il personale dell'ENEL di Larderello che ho avuto modo di conoscere, per la loro stretta e fruttuosa collaborazione al progetto, nonchè per la loro simpatia e amicizia.

Vorrei poi ricordare, rigorosamente in ordine alfabetico, i miei compagni di avventura dell'XI ciclo: Emanuele Carpanzano (il pessimista dal volto umano), Massimo Maroni (mister pi-qu-pitrasposto), Fabio Previdi (una vita spesa per l'università, in tutti i sensi) e Guido Poncia (che ha commesso l'errore di nascere a Ponte Ranica invece che in California). Non posso esimermi dal ricordare anche il mio carissimo amico Emanuele Poli, dottorando in Fisica dell'XI ciclo, che, prima da Pavia e poi dal Max-Planck-

Institut di Garching, mi ha tenuto di buon umore con la sua pungente ironia telematica. Sembrava impossibile, ma ce l'abbiamo fatta! Insieme a loro, ricordo poi tutti gli amici del dipartimento, in ordine sparso: Marco Lovera, Sergio Savaresi, Marco Fabio (Mongio) Mongiovì, Roberto (Giro) Girelli, Alessandra (Lale) Gragnani, Luigi (Piro) Piroddi, Roberto Cordone, Maddalena Aime, Renato Casagrandi, Gianni (Jack) Ferretti, Luca Ferrarini, Luca Villa, Andrea Rizzoli, Roberto Wolfler, Oscar DeFeo, Gianmarco Paris, Paolo Rocco, Emma Tracanella, Marco Broglia, augurandomi di non aver dimenticato nessuno.

Vorrei pure ringraziare il professor Costas Pantelides, che mi ha ospitato all'Imperial College per tre mesi, e tutti i ragazzi e le ragazze del Centre for Process Systems Engineering, che hanno reso piacevole e arricchito umanamente il mio soggiorno di studio in Inghilterra.

Un ringraziamento speciale va a Serena Nassivera, a Graziella Moglia ed a Vincenza Caputo, sempre disponibili, col sorriso sulle labbra, ad aiutarmi nella quotidiana lotta contro la burocrazia del Politecnico.

Infine, il ringraziamento più sentito alla mia famiglia, per il suo continuo supporto (seppure a volte non privo di perplessità); in particolare ringrazio mia madre, che ha pazientemente rivisto tutte le bozze di questa tesi, e a cui va buona parte del merito se la stesura del testo in lingua inglese è risultata perlomeno dignitosa .

x

a Daniela

POLITECNICO DI MILANO

DOTTORATO DI RICERCA IN INGEGNERIA INFORMATICA E AUTOMATICA

MODELLING, SIMULATION, AND CONTROL OF A GEOTHERMAL POWER PLANT

Ph.D. Thesis by:

Francesco Casella

Advisor:
Prof. Claudio Maffezzoni

Tutor:
Prof. Nicola Schiavoni

Supervisor of the Ph.D. Program:
Prof. Carlo Ghezzi

CONTENTS

1. INTRODUCTION

1.1 Motivation and Scope of the Research

In recent times, more and more emphasis has been put on the efficient exploitation of energy sources, both for economical and environmental reasons. This includes a more efficient use of traditional energy sources, such as oil and natural gas, as well as an increasing exploitation of renewable and non-conventional energy sources. As examples of the former, one can consider combined-cycle power plants, or co-generation plants producing electrical power together with heating or steam for industrial use; as examples of the latter, solar power plants, geothermal plants and urban waste incineration plants with electrical power co-generation can be mentioned. In both cases, the aim is to efficiently exploit “low-quality” energy, which in most cases means low-temperature energy sources.

The cost for this is an increasing complexity of the process concept, rather often combined with the need of innovative design. In most cases, plant designers deal with thermodynamic cycle conception, mechanical design, component sizing, and steady-state mass and energy balances, but seldom tackle any dynamic analysis. People involved with control system design, plant commissioning, start-up, and management therefore face two serious problems. First of all, the high part count and the complex arrangement of the plant, featuring numerous flow recirculations and splittings, and connection of several sub-systems, are such that the overall plant behaviour, both static and dynamic, cannot be simply inferred from that of its components, but it is essentially determined by their interaction. Moreover, if the design is really innovative, no previous experience on similar plants is available as a guideline, and the dynamic behaviour of the plant can be difficult or even impossible to predict, both during normal operation and in the occurrence of faults.

In these situations, the availability of an adequate system simulation tool, integrating the process dynamic model, the automatic control strategies, and the simulation of the operating manoeuvres and fault responses in the analysis, can be an invaluable aid to support a safer, faster and more successful plant design, commissioning, start-up and operation.

The system study of the Latera Geothermal Plant, carried out jointly with ENEL, the Italian Electricity Board, falls into that scheme. The Latera Plant

[ELC89] exploits an underground hot water reservoir to produce energy by steam turbines. The low enthalpy and the dissolved gas content of the geothermal fluid (mainly CO_2) is such that only about 12% of the extracted fluid goes into the vapour phase, which collects almost all of the CO_2, with the rest of the fluid remaining in the liquid phase. This situation is completely different from the conventional geothermal plants, where the extracted fluid is made up entirely of a gas phase, containing over 98% water vapour, which is directly conveyed to the turbines; a more complex process is thus required to efficiently exploit the energy content of the gas-vapour mixture. Moreover, a huge flow of exhaust water is produced (around 350 kg/s for 28 MW of net electrical power), which must be disposed of by reinjection into other wells, both for environmental reasons and to avoid the early depletion of the underground reservoir. The reinjection wells are displaced 10 km away from the plant, in order to avoid the premature cooling of the reservoir; this requires a complex reinjection plant, with critical constraint on its operation to avoid dangerous two-phase plug flow.

The decision was taken to support the late phase of the system design with an engineering simulator, accurately representing the operation of all the relevant parts of the plant, namely: the production wells, the phase separation process, the fluid transport to the main plant, the production of pure water steam from both the hot water and the steam-CO_2 mixture, and, finally, the exhaust water disposal through the reinjection system. One of the most challenging issues has been the accurate modelling of the “reboiler” (the plate-column device separating the CO_2 from the steam), which is an innovative device whose dynamic behaviour has never been studied before in the literature. The simulator permits the study of the dynamic behaviour of the plant, even under large transients and off-design conditions.

The simulator has allowed to answer some fundamental questions, before the plant was actually built and in absence of any previous operational experience and experimental data on similar plants. The first question is whether the control system structure, sketched in the original design document [ELC89], is adequate to operate the plant within the safety limits, in all the predictable situations and configurations, and in case of critical component failures. This of course is crucial for a fast commissioning phase, followed by a successful operation of the plant. The second question is: can this structure be improved, using the available measurements? Should other measurements be taken on the process? The third is to obtain a (preliminary) tuning of the parameters of all the controllers, in order to speed up the commissioning phase. The last, but not least, issue is to find optimal operating criteria for the plant.

The study of the reboiler control problem has revealed a situation which is typical of many process control problems, in which the control system structure, i.e. which should be the controlled variables, which is the best input-

output variable pairing, which extra measurements can possibly be used to improve the performance, and what values should be assigned to the setpoints, is not at all clear a-priori. As a matter of fact, the initial control problem has been placed in the wider context of the optimisation of the plant power output. Part of this research, which had not been planned at the beginning, was carried out while the author was visiting the Centre for Process Systems Engineering of the Imperial College, London. The possible final outcome of this part of the research could be a Decision Support System to help the plant personnel in the plant management task. The full study and implementation of this system is however beyond the scope of this thesis.

The plant simulator, which was built as a part of the research work, is an engineering simulator: it is quite accurate, so that its output can be used for design purposes, but its user interface is rather limited and its use at the moment is restricted to skilled engineers. However, thanks to the visual programming capabilities of the software that has been used for its development [Lab97], it could be rather easily extended to obtain a training simulator for the personnel who will be involved with ordinary plant operation.

1.2 Main Results

The main results of this research work can be summarised as follows.

First of all, the topic of thermo-hydraulic process simulation based on decoupling concepts is reviewed, and some new results are presented, pertaining to the decoupled solution of hydraulic networks by splitting. The application of these concepts in the ProcSim simulation environment, the simulation tool used throughout the whole research, heavily based on those concepts, is briefly discussed.

The next result is the extension of the ProcSim process simulation environment to deal with a two-component (water+CO_2) working fluid, and the associated modelling of all the new, specialised process components. ProcSim, formerly developed at the Dipartimento di Elettronica of the Politecnico di Milano ([Bar94,95,96,98]), had been previously used for simulation of traditional power generation plants, consisting of networks of boilers, combustion chambers, heat exchangers, valves and turbines, using pure water and steam as working fluids ([Bar95], [Cst95], [Col96]); moreover, it was thoroughly validated in a particular case, where a small pilot plant was available for extensive dynamic test trials ([Bel96], [Lev99]). However, the process concept under the Latera Plant design was quite different, so that almost all of the process component models have either had to be created from scratch, since they had never been used before (reboiler, phase separators), or at least re-written (valves, pipes), to adapt them to the particular two-

component working fluid. A systematic approach has also been developed to deal correctly with network components (valves, pipes) whose flow can be completely cut off during the simulation transients.

A complete and accurate dynamic simulator of the whole plant has been built, for the purposes stated in the previous section. The simulator is based on first-principle, non-linear models, taking into account details such as dissolved CO_2 in all the process components containing liquid water, thermal non-equilibrium in the two-phase vessels, and exact wave dynamics in the long reinjection pipelines. The simulation code can deal with start-up and shut-down of some plant sections (namely the production wells and steam processing sub-sections); however, it has not been designed to simulate the cold plant start-up, since this feature would imply a much harder modelling effort. It is worth mentioning that, after a short training course, the simulator was used autonomously by the personnel of the ENEL Control and Automation Department to define the distributed control system configuration in full and to obtain a preliminary tuning for faster plant commissioning [Cal98].

To appreciate the complexity and completeness of the simulator, consider that the number of process and control components included in the model is over 300, with more than 1000 parameters (some of them vector parameters, such as the control valve flow characteristics), over 700 process variables and 23 control loops.

The simulator allowed to assess the feasibility of the predicted operating manoeuvres, and the capability of the control system to keep the plant within safety limits in case of critical component faults. Given the total lack of a-priori information and experience, this was a non-trivial issue, in particular for the reboiler and reinjection system operation. For these two sub-systems, different control systems were considered, both conventional (PI plus static feedforward) and more sophisticated.

The study of the control system for the reboiler section showed that the control problem is essentially an optimisation problem: the plant normally operates in a steady state, with the turbines processing all the available steam, without any need of fast tracking regulations; moreover, the response of the reboiler system to transients due to failures or to changes in the production well configuration is not critical. The true aim of this control system, which had not been clearly identified before this research work, is to maximise the overall energetic efficiency of the plant, which depends essentially on all the complex interactions between the different components, taking place during its operation. The structure of the reboiler control system is not at all trivial, since many more measurements than control variables are available, and the control policy is not at all clear a-priori. A possible solution is proposed for the system control structure and the setpoint management policy, in order to always operate safely and close to the optimal operating point, in all the possible

operating conditions. The analysis is however by no means conclusive, leaving room for further research on the subject.

Finally, some of the results and concepts developed in this research work are published: in particular, on general decoupling concepts applied to simulation [Cas98c], on the subject of the reboiler simulation [Cas98d], and on the subject of modelling and control of the plant reinjection system [Cas98b].

1.3 Outline of the Dissertation

Chapter 2 contains a description of the plant and of the main issues arising from its particular structure. The design choices, working principles and management policy are briefly described, along with the simplified flowsheets of the plant, which will be used for its simulation. The degree of detail in the analysis is also discussed, motivating the main simplifying assumption which have been introduced to obtain an accurate, yet manageable, process model and simulator. Finally, an introduction to the main issues in the simulation and control of such an innovative plant is given.

Chapter 3 deals with the simulation of power generating processes. An overview of the state-of-the-art in simulation of such processes based on decoupling principles is given, along with the description of the ProcSim environment, which is extensively based on such principles. Some new results are given on the stability analysis of the decoupled solution for hydraulic networks. The following chapter describes the extensions which were needed to deal with the Latera Plant process: handling of two-phase, two-component (water plus CO_2) working fluid; modelling of the phase separators and of the reboiler; modelling of long pipelines with wave propagation, seamlessly integrated with the rest of the process; correct handling of hydraulic networks whose flow can be completely cut off, and special hydraulic network structures, which were not previously encountered in the simulation of conventional power plants.

Chapter 5 is devoted to a more detailed description of the modelling of the innovative process components: reboiler plates and bottom, phase separators, various kinds of valves, transport pipes for both liquid and gas-vapour mixture, long pipelines for liquid transport taking into account wave propagation phenomena, simplified production and reinjection wells, pumps, turbines, and pressurised tanks. The control library is also briefly described.

The focus of Chapter 6 is on the process simulator. First, the simulator architecture in the ProcSim environment is discussed, from the general specifications, down to the specific implementation issues. Then, the simulator applications are discussed, namely: single-loop tuning and control system validation; test of operating manoeuvres and response to component failures;

use of the simulator as an aid for the commissioning phase and, eventually, as a tool for personnel training. The chapter ends with the description of the simplified static model of the plant, implemented in the gPROMS process modelling environment, which has been used for the optimisation studies.

Chapter 7 deals with plant control and management problems. After a brief introduction, the most interesting control problems on the plant are discussed, in particular the control of the reboiler section and the reinjection system. The guidelines for the possible development of a decision support system (DSS) for plant management conclude the chapter.

Finally, summarising conclusions and future research directions are given in Chapter 8.

2. THE LATERA GEOTHERMAL PLANT

2.1 Plant Description

The Latera Power Plant, located near Lake Bolsena in Central Italy, is designed [ELC89] to exploit a low-enthalpy underground geothermal source, to produce electrical power by means of steam turbines. A simplified schematic flowsheet of the plant is shown in figure 2.1.

The geothermal fluid is a mixture of water and dissolved gases (mainly CO_2), with a specific enthalpy of about 900 kJ/kg and a mass fraction of the dissolved gas varying between 3% and 6%. Therefore, at the typical pressures found at the well heads (between 11 and 16 bars), the fluid is a two-phase mixture; due to the rather low fluid enthalpy, the gas phase only amounts to about 12% of the total mass flowrate, collecting almost all the dissolved CO_2. After the primary phase separation, two fluids are available: hot geothermal water at a temperature of about 175 °C, and a steam-CO_2 mixture with a 30% CO_2 mass fraction.

The production wells are located in two distinct production areas, about 500 m away from the main plant. Since the transport of the two-phase fluid over such a distance would be very critical, the two phases must be separated near the production wells and then conveyed to the main plant through separate pipes.

The main plant is divided into three main functional units to obtain clean steam from the primary fluids. The first one (the *reboiler cycle)* processes the steam-CO_2 mixture through a circuit containing a specialised plate-column device, called *reboiler,* which is a 14-plate column with two countercurrent flows (liquid water with dissolved CO_2 flowing downward and steam+CO_2 mixture rising up) mixing in each plate. The gas-vapour mixture coming from below gradually condenses its steam fraction by coming into contact with colder water flowing from above; the multi-stage countercurrent configuration maximises the mass and energy transfer efficiency. The final outcome is that the water gets heated, and the vapour fraction is almost completely removed from the gas-vapour mixture, which is then discharged into the atmosphere. The hot water is then flashed twice and processed by cyclone phase separators, to obtain clean steam and colder water, which is again recirculated in the reboiler. To avoid build-up of salts in the continuously recirculated water, with

subsequent scaling of components, a very small fresh water flowrate, taken from a nearby river, is added to the circuit, and a correspondingly small flowrate is bled from the low pressure phase separator.

The second unit of the main plant produces steam from the hot water by simply flashing it twice, and again processing the flashed fluid in two cyclone phase separators.

Both units produce steam at two different pressures to increase the energetic efficiency. In general, splitting up the hot water flashing in a greater number of stages would reduce the overall irreversibility of the thermodynamic process, thus increasing the net mechanical energy available by the steam processing in the turbines. However, the cost of more than two different pressure levels in terms of added process components would far exceed the slight increase in the overall process efficiency.

In the third unit, the steam coming from the two previous units is mixed and fed to two standard 20 MW steam turbines, connected to electrical generators.

The huge flow of exhaust water coming from the hot water processing unit (350 kg/s at a temperature of about 130 °C), can be used as a low-temperature source, e.g. for greenhouse heating; after that, it cannot be disposed of in surface streams, both for environmental reasons, since it contains toxic elements, and to avoid early depletion of the underground geothermal reservoir. During normal operation, it is conveyed by a pumping system to faraway reinjection wells, which are located 10 km away from the main plant, beyond a 100-metre-high hill. The reinjected water flows then through the underground hot rocks of the geothermal reservoir, where it gets reheated before being extracted again from the production wells. Two pressurised tanks are added to the system, one immediately after the pump regulating valve and the other at point of maximum elevation in the circuit; these should damp out the pressure and flow oscillations in the whole system, in order to avoid as much as possible the formation of a vapour phase, which could cause severe mechanical stress in the pipeline once the pressure rises again.

In case of failures in the reinjection system, an auxiliary reinjection well (V2) can be used. This well is located at a lower altitude than the plant, so that no pumping is necessary for its operation, which is made possible by gravity alone. However, its draining capacity is limited to 140 kg/s, for which reason the production rate of the extraction wells must be limited to 40% of the full capacity (the so-called *"reduced flowrate operating mode"*). It is important for the plant to keep operating in these conditions, while the reinjection system is being serviced; it follows that the switching between the *reduced flowrate mode* and the *normal flowrate mode* is a crucial manoeuvre on the plant. Note,

however, that the V2 well should not be used permanently, since it is has no underground connection to the geothermal reservoir of the production field.

This plant is completely different from the ordinary geothermal plants, such as, e. g., the plants operated by ENEL in the Larderello district. These plants exploit higher specific-enthalpy sources, resulting in a primary fluid made up entirely with a gas phase, which contains over 95% water steam, mixed with other gases and substances in a much smaller proportion. This fluid does not need any phase separation and is easily transported through a pipeline network from the production wells to the main plants collectors, which directly feed the turbines. The most critical problem with these plants is the turbine wear: the working fluid is much more corrosive than ordinary, pure steam, so that special materials have to be used for the turbine blades and for all the mechanical equipment in general.

The plant is divided into six functional units, as follows:

1. northern production fields, with geothermal production wells, phase separators, and transport pipes to the main plant;
2. southern production fields, with geothermal production wells, phase separators, and transport pipes to the main plant;
3. gas-vapour mixture processing unit (reboiler cycle);
4. geothermal water processing unit;
5. turbine unit;
6. reinjection system.

The general plant management policy is to provide base-load power to the electrical grid, i.e. to work 24 hours a day at full load, using all the available steam; the normal operating mode of the plant is therefore a steady-state. The reason behind this is that the start-up and shut-down of geothermal wells is a lengthy and complex operation, and, in general, frequent changes of production flowrate should be avoided to obtain the best production performance from the geothermal field. For economic reasons, after the initial operational phase, the plant should ordinarily run unattended, under full automatic control, without any permanent on-site personnel. Plant supervision and surveillance should be provided remotely by personnel working in the Larderello geothermal production site, 200 km away; routine maintenance teams should visit the plant only every once in a while.

In case of failures in one of the units, the plant should be automatically brought to a safe condition; this should be accomplished while avoiding as much as possible a complete plant shut-down, as well as the shut-down of production wells, which would imply costly, undesirable, and unnecessary plant downtime and start-up manoeuvres. To achieve this goal, the functional unit design is such that, in case of a failure, every single unit can be isolated, leaving the other running, possibly with reduced performance. The entire

manoeuvre should be performed by the automatic control system. Some examples are given:

- in case of failures in the reboiler cycle, unit 3 must be isolated from the feed pipe and from the turbines, and separately shut down; the gas-vapour mixture is discharged into the atmosphere, without any need of shutting down the production wells and the hot water processing unit;
- in case of failures in the geothermal water processing unit, unit 4 and 6 must be shut down, temporarily sending the water coming from the production areas to a large pool connected with the V2 well; the shut-down of the production wells is again avoided;
- in case of failure of the reinjection system, unit 6 is shut down, the exhaust water is sent to the V2 well, and the production rate is reduced to 40% of the full load;
- in case of a turbine trip, the corresponding steam is discharged into the atmosphere, without any need for further unit shut-down.

In case of one of these fault events, the maintenance team can be sent to the site to take appropriate remedy actions and eventually either re-start the units which were shut down or, in case of serious problems, shut down the whole plant, depending on their judgement of the situation.

The modularity in the plant design allows a gradual plant start-up; for instance:

1. start-up of one or two production wells, with the production flows being discharged into the atmosphere, first in the production areas and then, after the connection of the fluid transport pipes, in the main plant areas;
2. start-up of units 3 and 4 of the main plant, using the flows made available by step 1, discharging the exhaust water into the V2 well and the clean steam into the atmosphere;
3. start-up of unit 5 (turbine system), and connection to the electrical grid;
4. start-up of the reinjection system (unit 6);
5. start-up of more production wells, until the full production rate is achieved.

Moreover, some of the production wells can be started up or shut down for maintenance reasons, while always keeping the main plant working, even though with reduced power output.

It is clear from the preceding discussion that the main motivation for a full dynamic simulator of the plant is to assess its behaviour during all of these configuration changes, either planned or due to accidental failures in the plant. In particular, the main objective is to verify whether the control system is able to keep the plant within the safety limits (pressures, levels, etc.) during the most severe transients.

As a final remark, it should be emphasised that the Latera plant is radically different from fuel-based power plants, since there is no combustion and no heat exchanger, while there are very complex circuits with mixing and recirculation of two-component fluids. In some respects, it could even be said that the analysis of the Latera plant falls more into the realm of chemical engineering rather than of power plant engineering. A considerable modelling effort is thus required.

2.2 Degree of Detail in the Analysis

The full P&I diagrams describing the plant are by far too complicated to be directly used to build a simulation model: the part count amounts to several hundred components, many of which are used only for the cold start-up or the maintenance of the plant, and are thus beyond the scope of the simulator. On the other hand, the most interesting transients take place during the plant configuration changes, when some functional units are isolated or re-connected to the plant, so that an excessively simplified model would lack the ability to describe them. Moreover, the only reasonable boundary conditions for the model are the production wells, reinjection wells, direct vents to the atmosphere and steam turbines, since there are no other points in the plant where pressures, flowrates, mass fractions and temperature can be considered as fixed. The simulator should therefore include, at least in a simplified way, all the six functional units.

The production wells L2 and L2bis (see Fig. 2.1), with their relative cyclone phase separators and control valves, are very similar and run in parallel before their output flowrates are merged at the head of the transport pipe to the main plant, so that an equivalent parallel representation is quite natural. To avoid an excessive proliferation of similar plant sections in the model, the decision was then taken to merge the similar components of the northern production site into single equivalent components. The equivalent components have multiple volumes and cross-sections, and, under equal pressure drops and control valve openings, multiple flowrates. The same was done with the southern site (wells L4, L4bis, L3D). The results obtained in terms of control loop tuning are equivalent to those of a single production well, while the net effect on the rest of the plant remains unchanged. A simple change in the component parameters allows to represent only one of the production wells instead of the parallel of the two (or three).

As already said, all the hand valves and piping, which are only related to manual start-up and maintenance operations, have not been considered in this study, as well as the electrical part of the plant and all the auxiliary plant services, such as drainage collection, pressurised air production for equipment operation, etc. On the contrary, the on-off valves which can isolate the different

functional units have been kept in the model, in order to be able to simulate the configuration change transients. The resulting, simplified P&I diagrams corresponding to the simulator model are shown in Figure 2.2 (units 1 and 2), Figure 2.3 (units 3, 4, and 5), and Figure 2.4 (unit 6). A detailed diagram of the reboiler is shown in Figure 2.5.

All the pipes inside the main plant have not been explicitly modelled, for the following reasons: first, their volume is small, if compared to the tanks to whom they are connected; second, since the design pressure is only 20 bars, the pipe walls are rather thin when compared to typical power plants, so that their heat capacity is negligible; third, detailed data of the actual pipe lengths was not available at the time of the model building. The only exceptions are given by the two recirculation pipes AC318 and AC329, whose length and difference in elevation between head and tail have a considerable effect on the plant, in terms of head differences in the pumping systems and hot fluid transport delays.

2.3 Main Issues

2.3.1 Simulation

The first, fundamental issue arising from the simulation of this plant is the two-component nature of the circulating fluids; this will be the subject of Chapter 4 and then, in more detail, of Chapter 5, where the modelling of individual components will be discussed.

The second issue is the strong motivation supporting the development of a full system simulator, caused by the very strong interaction between the plant components in a rather complex structure. This can be clearly seen by two examples.

First, consider the pressure control valves PC3005A/B (Fig. 2.1 and 2.3): their primary aim is to keep the reboiler pressure at the setpoint value; however, when units 1 and 2 are connected to the main plant, these valves actually determine the pressures in the primary separators V101-2 and V201-2, which are equal to the reboiler pressure minus the head losses across the connection pipes VP301 and VP302; these pressures in turn determine the mass fraction of the vapour phase which separates from the production well fluids. As a consequence of that, the dynamic response to a variation in the opening of those valves is the result of the very complex interaction between the reboiler (with its flow recirculations and mass and energy transfers between the two phases in each plate), the connection pipes (whose volume is not at all negligible), and the primary phase separators of both production areas, all at the same time. Without a complete system simulator it is therefore impossible to give even a gross estimate on the dominant time constant of the dynamic

response. Moreover, the decomposition of the system model in a block diagram, resulting from the connection of causal input-output dynamic systems, is not feasible, since the pressure-flowrate relations are a-causal [Cel91], like currents and voltages in a electrical circuits.

As a second example, one can consider that, during normal full-load operation, the two turbines are not controlled, to avoid costly pressure drops across the four valves PV500XA, which are kept completely open. This implies that the pressures of the secondary separators of unit 3 (V311-2 and V313-4) are strongly coupled with the corresponding pressure of the secondary separators of unit 4 (V401-2 an V403-4); the same can be said of their temperature, since they contain saturated water and steam coming from the flashing of hot water. On the other hand, due to the turbine characteristics, these pressure are approximately proportional to the inlet flowrates of the turbines. Suppose now, for instance, that the flowrate of geothermal water coming from the production areas decreases for some reason: this will induce a reduced steam flowrate going into the high pressure turbine, a lower pressure in the two connected primary separators, and a consequently lower temperature of the reboiler recirculation flows, which in turn will modify the reboiler operating conditions, and so on.

From these two examples, it should be clear how difficult it is to give estimates on the dynamic behaviour of the plant without the aid of a full system simulator, and the impact this situation has on control system design.

Another issue is the simulation of the reboiler: from a mechanical point of view, this component closely resembles a distillation column, but the similarities almost stop at this point. In ordinary distillation columns, the circulating fluids are mixtures of two (or more) substances which can be either in the liquid or vapour phase at the operating pressure; here instead, in the typical operating conditions (pressures up to 16 bars and temperatures between 80 and 175 °C) only one of the substances (H_2O) can condense or evaporate, with significant mass and energy transfer between the two phases, while the other is an almost ideal gas, which can only have a rather small dissolved fraction in the liquid phase (typically less than 0.1%). Another crucial difference is the absence of a condenser, which is always found on top of the distillation columns: this means that the pressure dynamics is governed by the top exhaust valve opening instead of the cooling fluid flowrate in the condenser. Summing up, the equations governing the reboiler, even if based on the same mass and energy balance principles, are completely different from those of typical distillation columns (see, e.g., [Luy90]). The vast literature on distillation column modelling and control is therefore of little or no use, and in particular the simplifying assumptions which often permit to obtain reasonably-sized column models, which can be directly used for advanced control system design. The processes which more closely resemble the one implemented by

the reboiler (see, e.g., [Per85]) are the *drying processes*, which, however, are usually carried out using different devices and under different operating conditions, typically with much lower H_2O contents than in this case. Finally, the estimated efficiency of the column plates (i.e. their ability to bring the incoming flows close to the thermodynamic equilibrium) is quite low. One common modelling approach is to build a model having a correspondingly lower number of plates; this however is not very satisfactory from the point of view of dynamic analysis, since the mass storage of both liquid and gas-vapour mixture has to be redistributed over larger, fictitious plates, whose state during transients does not correspond to the physical state of the real plates. In this study, the decision was taken to employ a model which does not assume a situation of thermodynamic equilibrium in each plate, by introducing a Murphree-like efficiency parameter [Luy90], and taking into account a different temperature of the liquid and vapour phases in each plate. This gives a more accurate representation of the actual device operation, and will permit an easier tuning of the plate efficiency parameter, once experimental data become available.

The last, crucial issue is arisen by the reinjection unit. The exhaust fluid (at a temperature between 80 and 130 °C, depending on operating conditions and on the possible secondary use of the fluid for heating) is pumped to the reinjection wells through two long pipelines, the former (3.4 km long) climbing a 100-metre-high hill, and the latter (6.8 km long) going 100 metre downhill on the other side. The management and control of this plant unit is very critical, especially during fast transients: if the pressure in the highest part of the pipelines falls below saturation level (2-3 bars), transient two-phase flow could result, with possibly devastating effects once the pressure rises again; on the other hand, the tail pressure of the second pipeline should not exceed the design pressure, to avoid damage to the pipe itself. Accurate dynamic modelling is therefore mandatory; since the length of the pipes corresponds to wave travelling times of several seconds, distributed parameters models should be employed, taking the wave dynamics into account. This accuracy is needed both for control system design and validation, and to assess if the plant can withstand the most critical event, i.e. the reinjection pump trip.

The simulator will not be able to reproduce the cold start-up of the plant, which would imply a much greater modelling effort. However, it will be able to simulate the connection and disconnection of the different plant units, as well as the start-up sequence sketched in section 2.1 and the corresponding shut-down sequence, provided all the vessels already contain hot water and steam.

2.3.2 Control

One of the key features required by the project is the possibility to simulate all of the 37 control loops which will be deployed in the plant. Most of them are rather trivial level controls, or pressure controls acting on relief valves. For example, consider the valves PV3001 and PV3002, with their relative control loops: in case of reboiler cycle shut-down, unit 3 is isolated from unit 1 and 2 by closure of the on/off valves PV3009A and PV3009C; the pressure then rises up until the controllers open the relief valves which discharge the gas-vapour mixture to the atmosphere. For all these single-loop controllers, the control structure is well-defined, i.e. it is absolutely clear which are the control variables (actuators) and controlled variables (sensors) for each loop. Therefore, the simulator can be used for a preliminary tuning of the controller parameters, which will be useful, among other things, to speed up the plant commissioning phase dramatically. The controllers employed for these loops are standard PI controllers with auto/manual and anti-windup features. Where necessary, a static input/output non-linear function is applied to the controller output to compensate for valve non-linearity, in order to obtain a linear loop transfer function over a wide range of operating condition. The simulator itself can be used to calculate those functions, by computing the relationship between the valve opening and the corresponding sensor output under different operating conditions. This implies that the valve models should contain the actual flow characteristics for each different valve, as given by the manufacturer. The model library has been conceived in order to make this possible, i.e. very accurate valve models have been included.

Note that many of these control loops are replicated in similar part of the plants (e.g. unit 1 and 2), so that the tuning effort is slightly less than apparent at first sight. These loops are tuned in order to have a sufficient disturbance rejection during the most severe transients, without exceeding the bandwidth allowed by the valve actuators.

Three non-standard control system emerge after a careful analysis of the plant structure: the reboiler cycle control, the level controls in unit 3, and the pressure control of the top pressurised tank in the reinjection unit. For these control systems, as it often happens in process control problems, the control strategy is not at all clear a-priori: before tackling the synthesis of the control law (which is only the last step), many structural decisions have to be taken. First of all, the aim of the control system should be clearly identified; on that ground, the control system designer should select the appropriate sensors, actuators, controller structure (centralised or decentralised), input/output pairings (in case of decentralised structure), possible use of extra measurements, and setpoint value management strategy. This fact has been recognised for a long time, in particular in the chemical process engineering

(see, e.g., [Fos73]): it is a very complex subject, where many very different aspects such as equipment cost, control performance robustness against process perturbations, process uncertainties, measurement noise and bias, response to sensor and actuator faults, automatic fault detection and control reconfiguration, and, last but not least, control system manageability by plant personnel, have to be taken into account simultaneously. Unfortunately, even if many partial design tools and methods have been developed to help in this stage of the design, (see, e.g., [Mor89], [Sko96], [Fra90-96]), a systematic approach has not emerged so far, and in most cases ad-hoc solutions based on the particular plant structure must be carefully conceived.

In the case of the Latera plant, the controller outputs are the commands to the valve actuators; their location and number were fixed in the early design stage, and thus not subject to change. Moreover, the general design rule is to employ local single-loop controllers wherever possible, for simplicity, reliability and cost reasons. On the other hand, more measurements than control variables are available, which gives many degrees of freedom in the choice of the actual control system structure; moreover, in some cases, a simple single-loop feedback structure might not be adequate to satisfy the control system requirements.

The reboiler cycle, apart from the three level controls which can be designed independently, has three degrees of freedom, corresponding to the three valve actuators PV3005A/B (top reboiler exhaust valves), FV3012 (medium temperature recirculation), and TV3013 (low temperature recirculation). On the other hand, many more sensors are available, namely: PT3005 (top plate pressure), TT3013 (gas exhaust temperature), TT3014 (low-temperature recirculation temperature); FT3012 and FT3013 (high- and low-temperature recirculation flowrates); FT3014 and FT3015 (gas-vapour mixture flowrate entering the reboiler from units 1 and 2); FT3102 (steam flowrate coming from the high pressure phase separator); FT5001 (total steam flowrate entering the high pressure turbine). The control system aim, stated in high-level terms, should be to operate the cycle safely and efficiently, but how to translate this requirement into an actual control system structure is a subtle issue, as will be discussed in thorough detail in section 7.2. As it will become clear, the original structure proposed in [ELC89] is probably not the best one, and some better alternatives are proposed.

The three controlled levels in the reboiler cycle (in the reboiler bottom, in the water tank of the high pressure separator and in the water tank of the low pressure separator) are coupled, since the total amount of water contained in the reboiler cycle is approximately constant. This could be exploited to obtain a smarter control solution than the simple, completely decentralised structure proposed in [ELC89]. Details will be given in section 7.3.

The reinjection unit of the plant is perhaps the most critical one, from the point of view of the control system, due to the hill-climbing structure of the pipeline. The control system should simultaneously ensure that:

1. the minimum pressure in the system (i.e. the pressure in the top pressurised tank) never falls below the saturation value, to avoid two phase flow;
2. the maximum pressure in the system (i.e. just before the regulating valve of the reinjection wells) does not exceed the design limit of the pipe.

Note that the two constraints are conflicting, and the range of steady-state operating points satisfying both is rather narrow. The control of this part of the plant is therefore very critical, because even moderate-size oscillations, caused by changes in the pump flowrate, could lead to the constraints violation. The most critical situation is the pump trip, with the flowrate going to zero almost instantaneously.

The control system structure here is actually rather obvious: the top tank pressure, which is the lowest of all the circuit, is the controlled variable, and the opening of the valve on the reinjection wells is the control variable. The setpoint for the top pressure should be chosen in order to allow the widest possible oscillations around it in case of disturbances, without violating any of the two constraints. However, the transfer function of the plant shows a large phase lag, due to the wave propagation delay through the 6.8 km pipe, and a resonance caused by the interaction between the capacity of the two pressurised tanks and the inertia of the fluid contained in the connecting pipe (the hydraulic equivalent of an electrical LC circuit); consequently, the feedback loop is constrained to have a very low bandwidth. Since the measurement of the pump flowrate is available, it can be usefully employed to introduce an additional feedforward compensation. In case of a pump trip, a suitable open-loop transient is triggered for the closure of the valve on the reinjection wells. The availability of an accurate, non-linear simulator has allowed to evaluate this closing transient accurately, and to verify that the operational limits of the plant are satisfied, even though with a rather narrow safety margin. More details on the subject can be found in section 7.4.

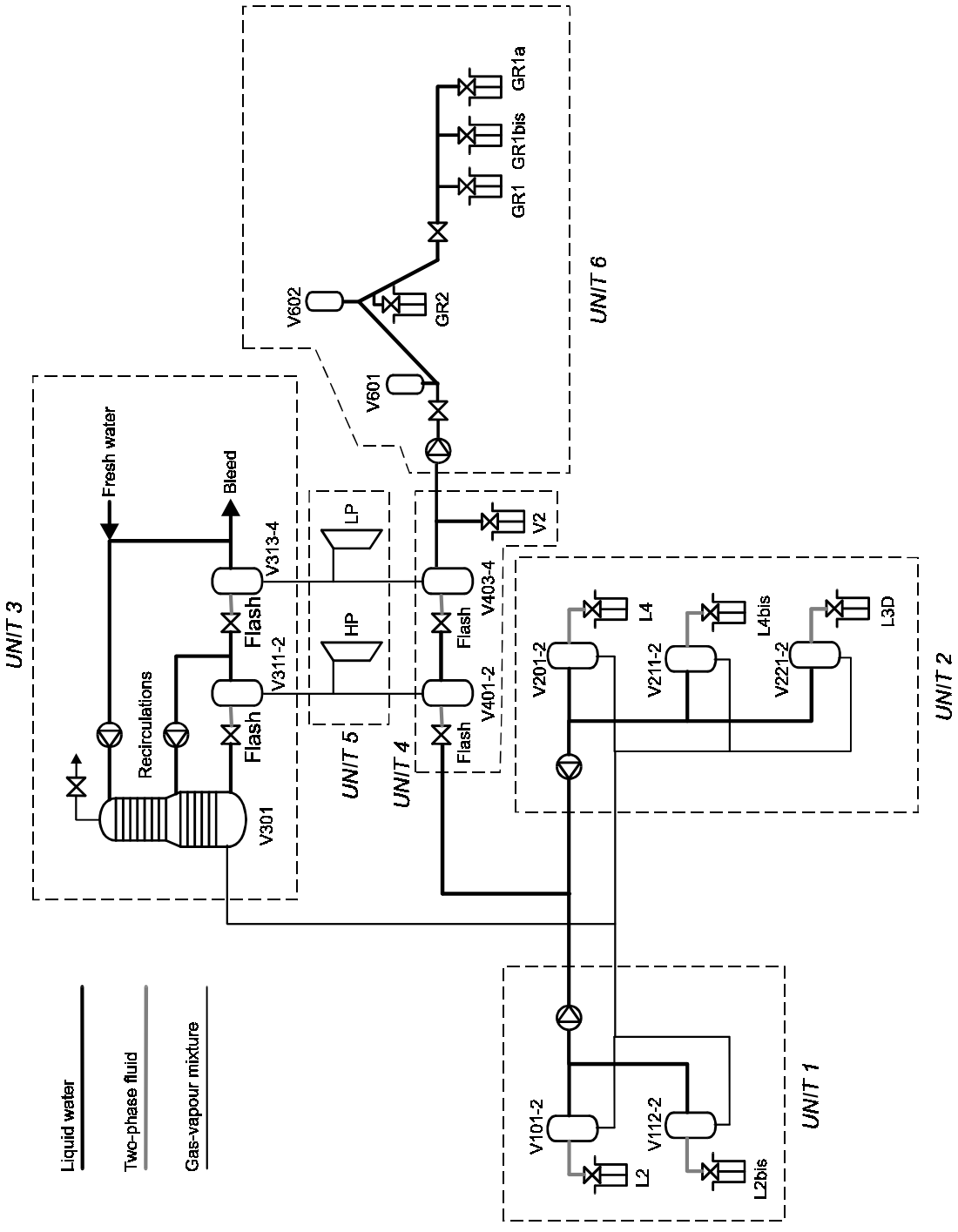

Figure 2.1: Simplified flowsheet of the Latera Geothermal Plant

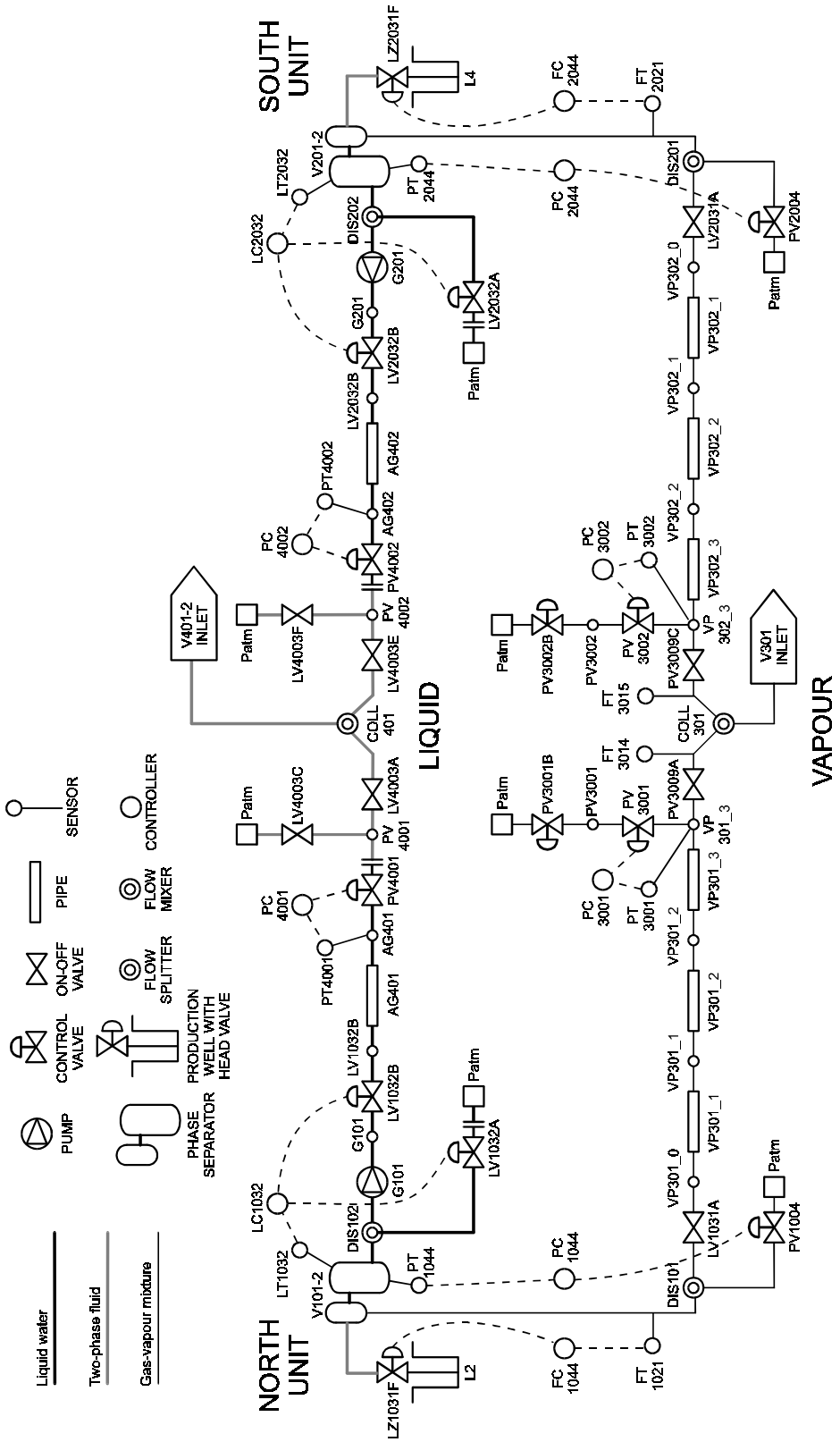

Figure 2.2: Production Units 1 and 2

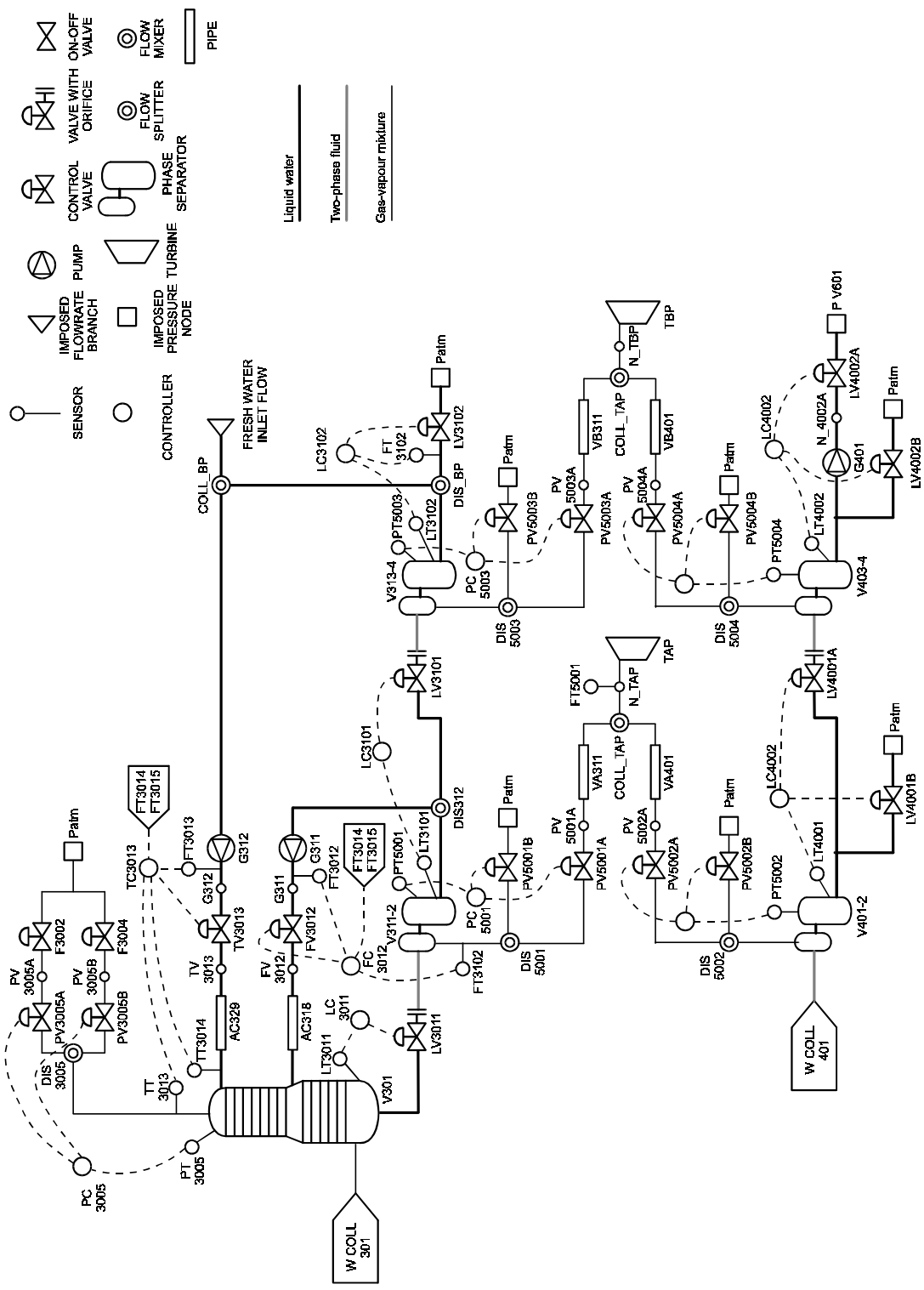

Figure 2.3: Main plant (Units 3, 4, 5)

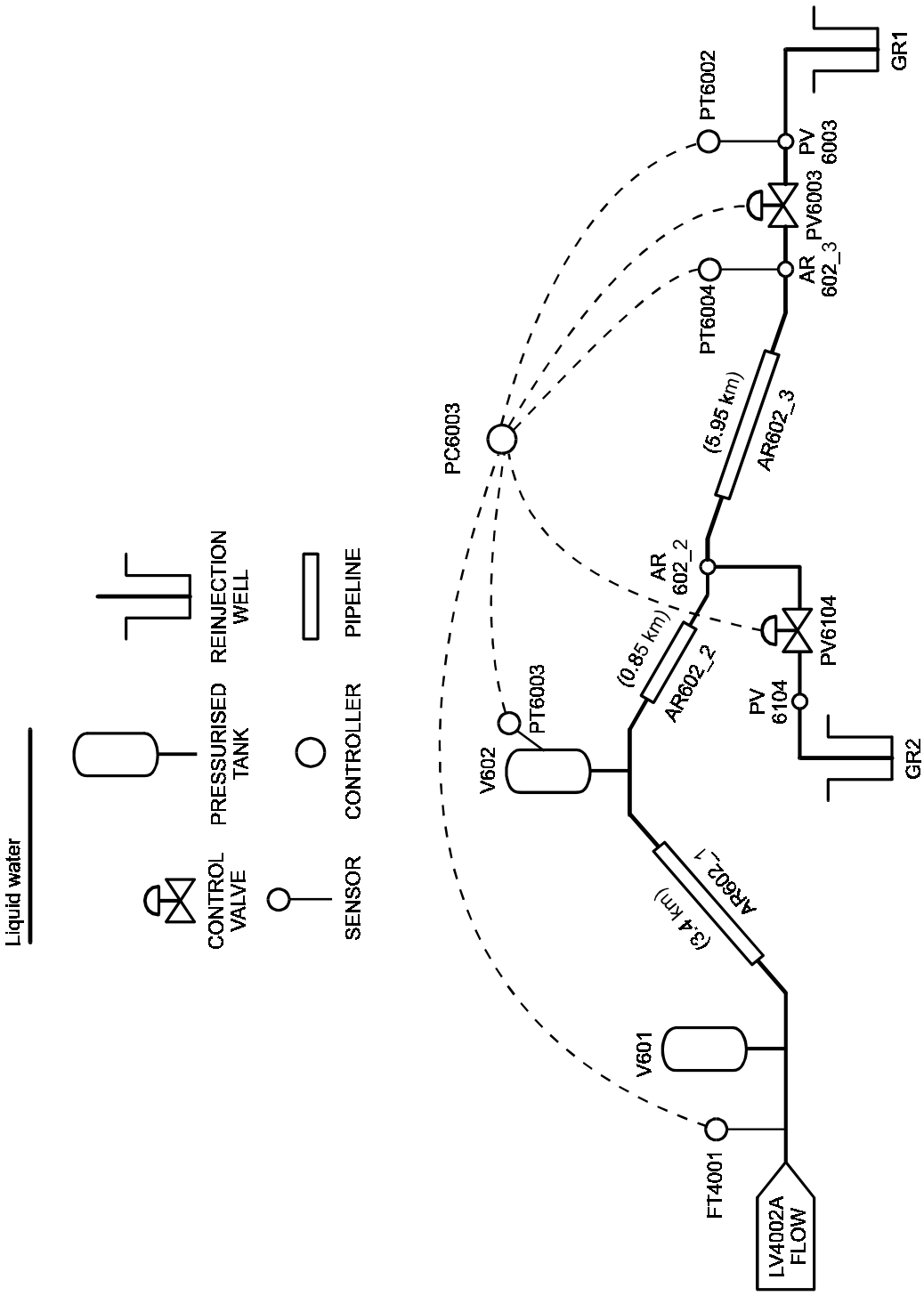

Figure 2.4: Reinjection system (Unit 6)

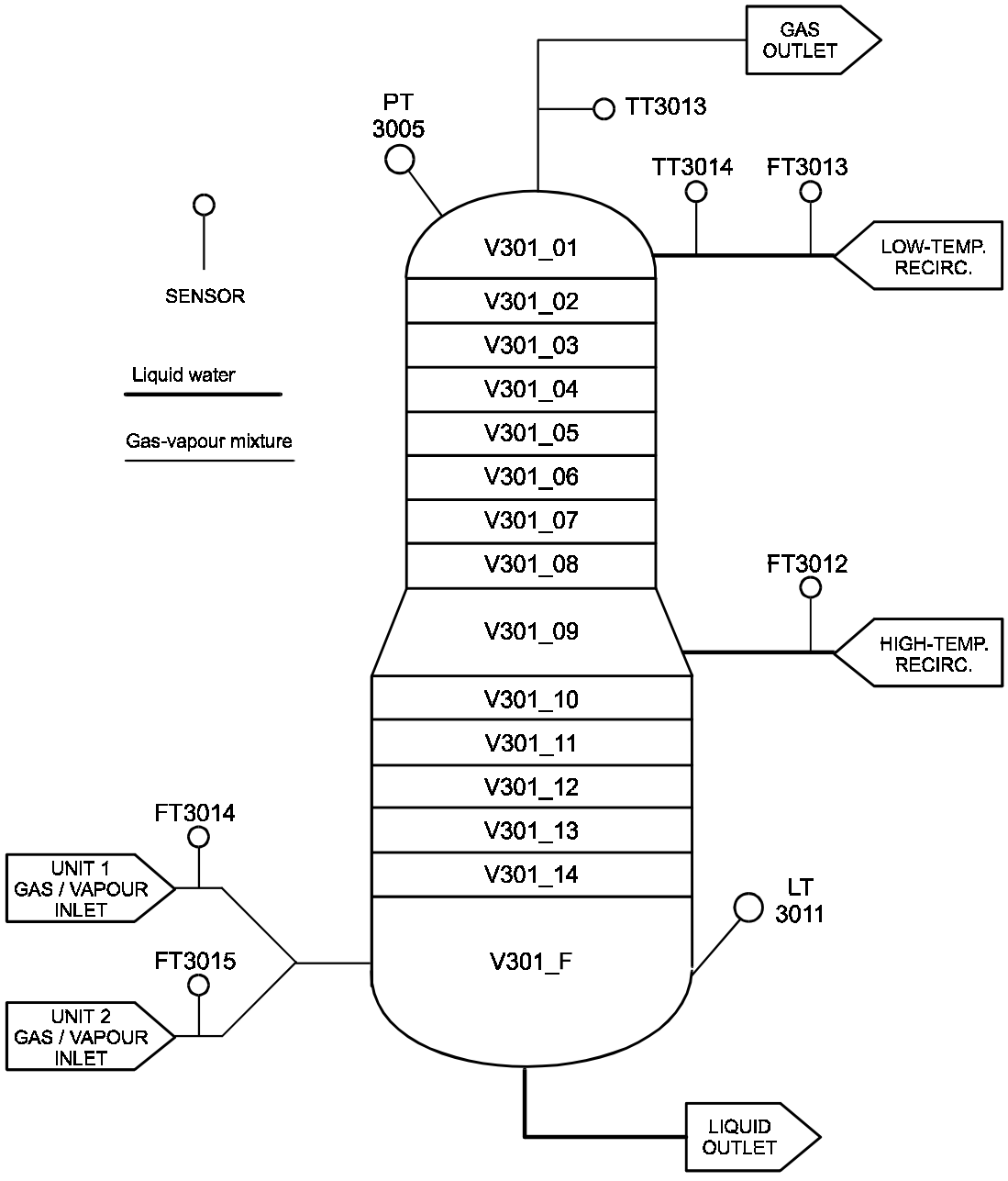

Figure 2.5: Reboiler (detail)

3. SIMULATION OF POWER GENERATION PROCESSES BASED ON DECOUPLING

3.1 Introduction

The study of the dynamics of power generation plants has been an active research field for more than thirty years, the first pioneering works dating back to the last fifties [Chi58]; a review of basic issues in modelling and simulation of such plants, as well as references to relevant papers in the field can be found, for instance in [Maf92].

The research has been focused primarily on fossil-fired power plants and nuclear power plants, driven by many different motivations.

The main interest in the case of the conventional (fossil-fired) plants lies in the availability of a dynamic model of the plant, which is essential for better control system analysis and design, for control equipment checkout, for personnel training, and to reduce the time required by the plant commissioning and initial start-up phases. This is true for plants of innovative design (e.g., combined cycle plants), where little or no previous experience is available, as well as for older, already existing plants, when, for instance, they are re-allocated to perform daily load cycling duties instead of the base-load power production for which they were originally designed.

In the case of nuclear plants, the emphasis is put primarily on safety issues, i.e. on the study of the plant dynamic behaviour in case of failures; this requires the greatest modelling effort to achieve the highest possible accuracy of the results, since the outcome of the simulations has to be used to assess the plant safety in case of accidents, which is obviously a very critical issue.

Operator training is another field which can greatly benefit from the availability of plant simulators; the accuracy required in this case can be lower than for design and engineering purposes. Operator training on simulators can help avoid unit trips and costly plant downtime, as well as generally increase the efficiency in the operation of the plant.

Two main research trends can be identified, leading to two main categories of models: simple global plant models, and detailed plant models, often based on modular approaches.

The aim of the former is typically to understand the gross behaviour of existing plants, for effective synthesis of advanced “model based” control systems, as well as for educational and training use. These models can be either simplified models based on first-principle equations and drastic modelling simplifications, or low-order approximations of the real dynamic response of the plant, coming from some system identification procedure. In most cases, they are formulated analytically, either as low-order dynamic systems, or as block diagrams consisting of low-order transfer function and, possibly, simple non-linear elements. These models are rather easily understandable by a skilled control engineer, and can be directly employed for control system design. On the other hand, they rest on foundations given by prior experimental data and experience on the plant behaviour, or at least on detailed and accurate models, together with extensive numerical simulation. The reason behind that is evident in the case of identification models, but also in the case of first-principle, simplified models, the often very drastic approximations which are introduced can only be justified a-posteriori on the grounds of the agreement between the simplified model behaviour and the real plant behaviour. As a final remark, many of these models are linear models, describing the plant behaviour near a certain operating point; these are obviously unsuitable to simulate large plant transients.

The latter category of models, instead, concerns the problem of predicting the dynamic behaviour of the plant accurately when little or no experimental data and experience is available, as in the case of new plant designs, possibly under operating conditions far from the nominal one. This is the realm of the engineering simulators, for which detailed models are needed, their equations being based on first principle laws (such as conservation of mass, energy, and momentum), semi-empirical correlations, such as the formulae to calculate heat transfer coefficients, and accurate calculation of fluid thermodynamic properties. These models are definitely too complex to be treated analytically, and consequently need numerical simulation environments to be used effectively. To cope with the complexity of such models, modularity concepts are widely adopted, ranging from the basic modularisation approaches employed by almost all the simulation environments, to hierarchical modelling (such as the sub-unit concept of the gPROMS environment, [Pan93], [Brt94], [gPR97]) through to object-oriented modelling [Mat93a]. The application of O-O modelling concepts in the field of power plant process simulation is still in its infancy, being much more mature in the field of mechanical system simulation.

As already mentioned in Chapter 2, the modelling approach used in this research is the second one: the plant design is radically innovative, so that the purpose of modelling and simulation is to understand the dynamic behaviour of the plant in all the possible operating conditions, both during normal operation

and in case of failures, mainly for the purpose of control system design. This must be accomplished before the actual plant is built and operated, so that the whole modelling process, based exclusively on the available design data, has to be rather accurate to be reliable. It should be noted, however, that the issue of global and simplified models vs. detailed numerical ones is not so clear-cut as it could seem at first sight, since some parts of the process might need a coarser degree of detail than other ones, depending on the focus of the application. In the case of the Latera Plant, for instance, the steam turbines are modelled as very simple flow-pressure boundary conditions, while much greater detail is put in the modelling of the reboiler and phase separators; in other cases, when turbine speed control is a fundamental issue, very accurate turbine models must be employed, including the electrical generator model and a simplified model of the connection to the electrical grid.

Typical process components found in fossil-fired or nuclear power plants are: steam generators, steam turbines, condensers, electrical generators, valves, pumps. Steam generators are usually made of a combustion chamber surrounded by a complex structure of heat exchangers, plus an optional vessel in case of drum boilers, which is instead absent in once-through boilers. Combined cycle plants also include gas turbines. The typical working fluids are water and steam, for the water circuit, and a gas mixture for the combustion chamber and flue gas circuits, as well as for the gas turbine. Some basic references on the modelling problem for such devices can be found in [Maf92].

The review of all the codes that have been developed for the simulation of such processes is not at all a trivial task. Simulation codes range from modular simulation environments developed in-house by some electricity companies (such as the SICLE code of Eléctricité de France [SIC72-79] or the LEGO code of ENEL [LEG83]) or by power equipment production companies (such as the KWU-Siemens code [KWU83]), to prototype software developed by universities or research centre (such as the ProcSim environment employed in this research, [Bar94,95,96,98]), to commercial general-purpose code, such as APROS from VTT Finntech, or Pro-Trax from Trax Corporation. Much research work has also been done using general-purpose commercial dynamic system simulators, such as Matlab/Simulink from The MathWorks, MatrixX from Integrated Systems, etc. (see, e.g., [Ord94]); these models, however, are often obtained with rather crude approximations, and usually lack the flexibility given by the full modularity (i.e. the one-to-one correspondence between each process component and a software module). Dynamic simulators used in the field of chemical engineering, such as HYSYS from Hyprotech, AspenPlus and SpeedUp from Aspen Technology, or gPROMS from Process Systems Enterprise could also be evaluated. All these codes differ by many aspects, such as:

- degree of modularity;
- need of ad-hoc treatment of model equations to fit in the software structure;
- availability of specialised software structures to deal with typical power plant equipment, and special plant arrangements, such as the complex structure of the heat exchangers in the steam generator;
- integration algorithms;
- graphical vs. textual model representation;
- model libraries for power plant processes;
- degree of detail of the models;
- possibility and ease of extension and customisation of the existing libraries;

In addition, the availability of such codes can be a problem for many different reasons:

- proprietary nature of the code;
- high cost, in the case of fully engineered products;
- prototype development stage and lack of support and extensive documentation, for packages developed in the universities and research centres;
- obsolescence of the underlying software technology (e.g. FORTRAN-based simulation codes, for instance, tend to be overcome by graphically-oriented simulation environments).

It is therefore beyond the scope of this dissertation to provide a detailed comparison of these software packages. In this chapter, the state of the art in power plant process simulation, based on decoupling principles, will be discussed. The aim is to review the concepts on which the ProcSim simulation environment is based, in order to be able to understand the following discussion. At the same time, some original material is added, that is a comprehensive re-formulation of the hydraulic network modelling, and the stability analysis of the decoupled solution of hydraulic network by splitting, which were not previously available. In the following chapter, instead, the extensions needed to model the Latera Plant will be discussed, this material being entirely original.

3.2 Thermo-Hydraulic Decoupling

The approach to process simulation employed in the ProcSim simulation environment is based on the (possibly partial) decoupling among some of the equations describing the dynamic behaviour of the components. The decoupling among equations permits to solve them independently, thus reducing the computational burden on the numerical integration algorithm. This decoupling might exist among the equations of a single component, as will be

discussed in this section, or among the equations of different components, which will be the subject of Section 3.3.

The idea to exploit the decoupling between hydrodynamic and thermal phenomena to reduce the computational burden in power process simulation can be traced back to the SICLE code [SIC72-79], where it was extensively used to solve efficiently equations describing heat exchangers. It has also been used for efficient implementation of training simulators [Bus85]. This approach is rather difficult to formulate in abstract terms, but it is better described in terms of examples. It is always assumed that the partial derivative equations (PDE) are reduced to ordinary differential equations (ODE) by means of some discretisation method (e.g., the method of lines), and that the ODE are solved by a fixed-step algorithm, such as Euler's forward (implicit) method [Lam91].

Example 1: Horizontal cylindrical pipe with incompressible fluid.

The describing equations are:

$$P_{in} - P_{out} = \frac{k_f}{\rho} w^2 \tag{3.1}$$

$$\frac{\partial \rho A e}{\partial t} + \frac{\partial w h}{\partial x} = \omega \varphi_\omega \tag{3.2}$$

Equation (3.1) is the momentum conservation equation, where P_{in} and P_{out} are the inlet and outlet pressure, k_f is a friction coefficient, ρ is the (constant) fluid density, and w is the mass flowrate; (3.2) is the energy conservation equation, where A is the (uniform) pipe cross-section, e the specific energy of the fluid, h its specific enthalpy, ω the pipe perimeter and φ_ω the linear thermal flux along the pipe. For an incompressible fluid, enthalpy and energy are a function of temperature only; thus, assuming constant specific heats c_v and c_p

$$e = c_v T, \quad h = c_p T \tag{3.3}$$

eq. (3.2) can be formulated as

$$\rho A c_v \frac{\partial T}{\partial t} + w c_p \frac{\partial T}{\partial x} = \omega \cdot \varphi_\omega \tag{3.4}$$

The incidence matrix for this system is shown in Tab. 3.1. In this extreme case, it has a block triangular structure, meaning that the hydrodynamic equation (3.1) and the thermal equation (3.4) can be solved independently at each time step, provided (3.1) is solved first. In this case the decoupling is perfect, so that the independent solution of eq's. (3.1) and (3.4) does not imply any approximation.

	P_{in}	P_{out}	w	T
(3.1)	X	X	X	
(3.4)			X	X

Table 3.1: Incidence matrix

Example 2: Horizontal cylindrical pipe with compressible fluid.

The exact equations for mass and momentum conservation lead to a model describing the propagation of pressure and flow waves along the pipe, along with thermal phenomena. If the wave travelling time is small compared to the fundamental time constants of the process (i.e. for pipes shorter than about 100 m), the model can be simplified with the following assumptions:

1. the wave propagation delays are neglected (i.e. it is assumed that the speed of sound is infinite);
2. the distributed pressure drop, which is usually small compared with the absolute pressure, is lumped at the end of the pipe and assumed as function of the outlet flow w_{out}, (or of the inlet flow w_{out}) thus assuming a uniform pressure $P(x)=P_{in}$ (or P_{out}) along the whole pipe.

The equations describing the process become the following:

$$A\frac{\partial \rho}{\partial t}+\frac{\partial w}{\partial x}=0 \qquad \textit{(mass conservation)} \qquad (3.5)$$

$$P_{in}-P_{out}=\frac{k_f}{\rho}w^2 \qquad \textit{(momentum conservation)} \qquad (3.6)$$

$$A\frac{\partial \rho e}{\partial t}+\frac{\partial wh}{\partial x}=\omega\cdot\varphi_{\omega} \qquad \textit{(energy conservation)} \qquad (3.7)$$

Since $\rho=\rho(P_{in},h)$ and $e=h-P_{in}/\rho$, the hydrodynamic equations (3.5), (3.6) are coupled with the thermal equation (3.7) through the density (which was assumed constant in Example 1), as is easily seen in Tab. 3.2, so that they must be solved simultaneously. If, however, the fluid is such that

$$\frac{\partial \rho}{\partial h}\cdot\frac{dh}{dt}\cong 0 \qquad (3.8)$$

as in the case of liquids, the influence of the variation of h in (3.5)-(3.6) is very small, so that (3.6) and (3.5) can be solved independently of (3.7), using the value of h at the previous integration step, without making significant errors. This is known as the *weakening approach* ([Cas98c], [Car99]); the variable whose previously computed value can be used in solving a certain equation is called a *weak variable*. It will be denoted by a W in the following tables. To be more precise, h can be considered weak in (3.5)-(3.6) if the *mutual* influence of h in determining the solution of (3.5)-(3.6) *and* of P_{in}, P_{out}, and w in determining the solution h of (3.7) is small.

	P_{in}	P_{out}	w	h
(3.5)	X		X	W
(3.6)	X	X	X	W
(3.7)	X	X	X	X

Table 3.2: Incidence matrix

When (3.8) does not hold, e.g. in case the fluid is an ideal gas, better decoupling can be achieved by using

the entropy form of the energy conservation equation, instead of (3.7):

$$\rho A T \frac{\partial S}{\partial t} + wT \frac{\partial S}{\partial x} = \omega \cdot \varphi_\omega \tag{3.9}$$

where $\rho=\rho(P_{in},S)$, $T=T(P_{in},S)$, S is specific entropy of the fluid, and the term describing heat generated from friction has been neglected. If (3.9) is linearised around the steady state solution satisfying

$$\overline{w}\,\overline{T} \frac{\partial \overline{S}}{\partial x} = \omega \cdot \overline{\varphi}_\omega \tag{3.10}$$

the following equation is obtained

$$\overline{\rho} A \overline{T} \frac{\partial \delta S}{\partial t} + \overline{w}\,\overline{T} \frac{\partial \delta S}{\partial x} + \delta(wT) \frac{\partial \overline{S}}{\partial x} = \omega \cdot \delta\varphi_\omega \tag{3.11}$$

describing the small variations $\delta\xi(x,t) = \xi(x,t) - \overline{\xi}(x)$ of the process variables around the steady state condition. It is clear from the analysis of (3.11) that the influence of the hydrodynamic variables P_{in} and w in the solution of (3.9) is weak, provided the process dynamics does not move away too much from the steady-state condition, i.e. at low frequency. For large transients, the influence of those variables remains weak, provided the integration step is not too large, so that the effect of their variation along an integration step is small, when compared to the other terms. This again gives origin to a triangular structure of the incidence matrix (Tab. 3.3), which in turn permits to solve the thermal equation (3.9) independently of the hydrodynamic equations (3.6) and (3.5). Even if the influence of P_{in} and w in the solution of (3.9) is not so weak, the only important thing is that also the influence of S in the solution of (3.5)-(3.6) (terms marked with Y) is sufficiently weak, so that the *mutual* coupling between the two sub-systems of equations remains small.

This simple example shows two important concepts: the first is that the solution of the different equations describing a process can be split into the sequential solution of smaller size problems, even if the equations are not rigorously decoupled, provided the mutual coupling is sufficiently weak; the second is that the choice of the actual hydrodynamic and thermal equations and state variables can be crucial to achieve a more effective decoupling among equations.

Finally, note that the independent solution of the two systems is not possible when there is a strong *mutual* influence of the hydrodynamic variables in the thermal equations *and* of the thermal variables in the hydrodynamic equations. In this case, the delay of one

	S	P_{in}	P_{out}	w
(3.9)	X	W		W
(3.6)	Y	X	X	X
(3.5)	Y	X		X

Table 3.3: Incidence matrix

integration step, which is introduced by solving the two systems in sequence, can lead to instability of the numerical solution, and must therefore be avoided. Conversely, the independent solution of the two systems is possible if the influence of the hydrodynamic variables in the thermal equation, or vice-versa, exists in one direction only (triangular structure), or is at least predominant in one direction, as it happens when weak coupling variables are present; the effect of decoupling the solution will only be a small approximation error, proportional to the integration stepsize.

Example 3: Pipe with compressible gas, thick metal wall and high gas-metal heat transfer coefficient

This case is the same as Example 2, except that the fluid exchanges heat with the pipe wall by forced convection. Assuming uniform temperature across the wall thickness and neglecting the thermal conduction along the pipe length in the metal wall, the describing equations are:

$$A\frac{\partial \rho}{\partial t} + \frac{\partial w}{\partial x} = 0 \qquad \textit{(gas mass conservation)} \qquad (3.12)$$

$$P_{in} - P_{out} = \frac{k_f}{\rho} w^2 \qquad \textit{(gas momentum conservation)} \qquad (3.13)$$

$$A\frac{\partial \rho e}{\partial t} + \frac{\partial wh}{\partial x} = k_c(T_m - T_f) \qquad \textit{(gas energy conservation)} \qquad (3.14)$$

$$\rho_m c_m A_m \frac{\partial T_m}{\partial t} = k_c(T_f - T_m) \qquad \textit{(metal energy conservation)} \qquad (3.15)$$

where T_f is the fluid temperature, $\rho=\rho(P_{in},T_f)$, $e=e(T_f)$, $h=h(T_f)$, and ρ_m, c_m, A_m, T_m are the metal wall density, specific heat, cross-section and temperature, respectively. If the heat transfer coefficient k_c is sufficiently high, the temperature dynamics of the fluid will closely follow that of the metal, which will be slow due to the high heat capacity of the metal compared to that of the gas. It ensues that the hydrodynamic equations (3.12) and (3.13) can be solved using the gas temperature computed in the previous integration step without introducing a significant modelling error. In other words, the fluid temperature can be considered a weak variable in 3.12, since its variation along an integration step is small, due to the nature of the thermal equations. The basic assumption here is that the integration stepsize is sufficiently short to model the

	P_{in}	P_{out}	w	T_f	T_m
(3.12)	X		X	*X*	
(3.13)	X	X	X		
(3.14)	X		X	X	X
(3.15)				X	X

Table 3.4: Incidence matrix

fundamental thermal dynamics accurately, i.e. that of the wall temperature. The system decoupling structure is shown in Tab. 3.4.

In this case, a very important consideration can be done: depending on the boundary conditions of the pipe (which will close the system of equations), it will generally happen that the dynamics of the hydrodynamic variables (P_{in}, P_{out}, w) will be much faster than that of the thermal variables (T_f , T_m). A *multirate* integration algorithm could be then employed, with a shorter step size for the hydrodynamic equations than for the thermal equations, thus improving the overall efficiency of the integration algorithm without introducing significant errors [Bus85].

Example 4: Liquid-liquid countercurrent heat exchanger with thick wall

Consider the idealised model of a heat exchanger depicted in Fig. 3.1, where two liquids flow in a countercurrent fashion, separated by a thick thermal wall. Suppose, for simplicity, that the two flowrates are fixed by volumetric pumps, so that there's no need to formulate any hydrodynamic equation; as in the previous example, assume a uniform temperature across the wall thickness and zero thermal conduction along the pipe length in the metal wall.

The equations modelling the (thermal) process are:

$$\rho_1 A_1 c_{v1} \frac{\partial T_1}{\partial t} + w_1 c_{p1} \frac{\partial T_1}{\partial x} = k_{c1}\left(T_m - T_1\right) \qquad \textit{(liquid 1 energy conserv.)} \quad (3.16)$$

$$\rho_2 A_2 c_{v2} \frac{\partial T_2}{\partial t} - w_2 c_{p2} \frac{\partial T_2}{\partial x} = k_{c2}\left(T_m - T_2\right) \qquad \textit{(liquid 2 energy conserv.)} \quad (3.17)$$

$$\rho_m c_m A_m \frac{\partial T_m}{\partial t} = k_{c1}(T_1 - T_m) + k_{c2}(T_2 - T_m) \qquad \textit{(metal energy conserv.)} \quad (3.18)$$

where variables with subscripts 1, 2 and *m* correspond to liquid 1, liquid 2 and metal wall, respectively.

Due to the counter-current configuration, after the PDE's are discretised without any decoupling assumption, a fully coupled ODE system of high order results, whose computational burden can be high if implicit methods are employed. However, if the heat capacity of the metal wall is sufficiently high, and the heat transfer coefficients k_{c1} and k_{c2} are sufficiently small, the thermal inertia of the wall is such that the metal temperature cannot change too much

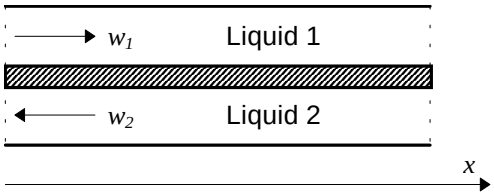

Figure 3.1: Idealised heat exchanger

along an integration step. In case the heat transfer coefficients are not so small, this is still true, provided a sufficiently short time step is used. This allows to solve (3.16) and then (3.17) using the values of T_m computed at the previous time-step, and only then to update the solution of (3.18) using the newly computed values of T_1 and T_2. In this case, T_m is considered weak in both (3.16) and (3.17) (see Tab 3.5). Note that, with such an arrangement, the large ODE system resulting from the discretisation of the PDE's (3.16) and (3.17) will typically have a triangular structure, in spite of the counter-current structure of the process, which implies that very efficient solution algorithms can be applied.

In case k_{c1} is small, but k_{c2} is not, it is still possible to consider T_m weak in (3.16), solve that equation, and then solve (3.17) and (3-18) simultaneously, integrating their discretised PDE's backwards in the direction of liquid 2 (see Tab 3.6). The resulting large ODE system will again have a (block) triangular structure, in spite of the counter-current flow in the heat exchanger, still allowing an efficient numerical solution.

This example shows clearly how elements possessing inertia (in this case thermal inertia) can be used to decouple the equations of a model. Once again, the whole procedure is sound if the integration stepsize is shorter than the fundamental temperature dynamics of the metal wall.

The procedure illustrated above in an idealised case can be successfully employed in much more complex cases, such as the one shown in Fig. 3.2. In this case the external fluid can be a hot flue gas, and the configuration of the heat exchanger banks can be a hybrid of transversal and counter-current flow. The wall thermal inertia again permits to solve separately the equations describing the inner and outer fluid flow and temperature dynamics, leading to drastic simplifications in the numerical computations. This kind of configuration is typical in gas duct of fossil-fired power plants, where the geometry of the heat exchangers can be quite complex, both for efficiency and mechanical reasons.

	T_1	T_2	T_m
(3.16)	X		W
(3.17)		X	W
(3.18)	X	X	X

Table 3.6: Incidence matrix - 1

	T_1	T_2	T_m
(3.16)	X		W
(3.17)		X	X
(3.18)	X	X	X

Table 3.5: Incidence matrix - 2

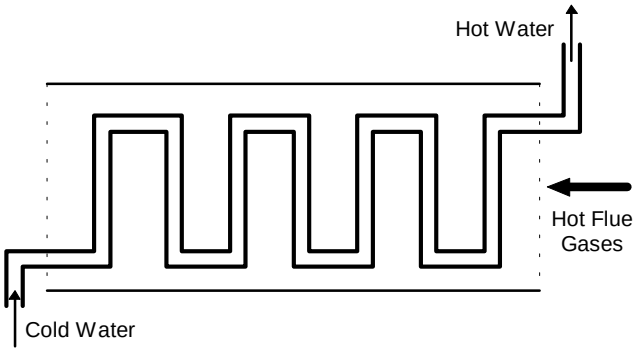

Figure 3.2: Complex heat exchanger structure

Example 5: Boiler-turbine system with multirate simulation

The previously illustrated concepts can be applied not only to single components, but also to complex systems, which is the most interesting case. Consider, for example, the power plant sketched in Fig 3.3. First of all, the system of hydrodynamic equations can be decoupled from the system of thermal equations; once flows and pressures have been computed, the thermal equations can be solved component by component; to this aim, the thermal inertia of the cooling liquid and metal walls of the condenser can be used to break the loop made by the condenser, the pre-heaters, the boiler, the super-heaters and re-heaters, and the turbines (no turbine extractions are considered here, for the sake of simplicity).

Moreover, the hydrodynamic and thermal phenomena occur within two different time scales. Thermal phenomena are conditioned by the high inertia of the heat exchanger walls, and by the massive storage of water in the boiler drum and in the condenser, with typical time constants in the range between 10 s and 500 s, depending on the boiler load. On the contrary, flow and pressure dynamics can be very fast: the turbine regulation valves must be closed in a few tenths of a second in case the generator is disconnected from the electrical grid, to avoid the turbine gaining excessive angular speed. Consequently, the turbine speed control system must have a bandwidth of 20-40 rad/s. For an accurate

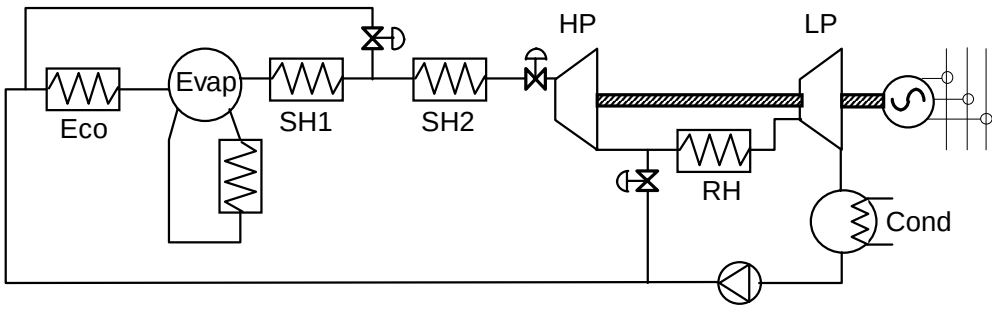

Figure 3.3: Simple power plant

dynamic simulation of the control loop, the hydrodynamic process equations, coupled with the electro-mechanical equations of the turbine-generator unit, must be integrated with a stepsize of 10-20 ms. If the decoupling approach is employed, a multirate integration algorithm can be used: for instance, the hydrodynamic equations, the electro-mechanical turbine equations and the controller equations should be integrated with a step size of 20 ms, while the thermal equations (which far outnumber them) can be integrated with a much longer step size of 1 s. This results in a tremendous saving of computation time, which can be of great benefit, especially in real-time simulation applications.

As a final remark, the decoupling approach allows to split the whole process simulation task into several sub-tasks, communicating through a shared database, containing the values of the process variables; each sub-task, involved with the solution of a subset of the process equation, can be allocated on a different processor, implementing a distributed, parallelised simulator.

The reader interested in the details of the decoupling approach applied to typical components of fossil-fired power plants (boilers and heat exchangers) is referred to [SIC72] and [Cst95], which also contain some analysis on the numerical stability issues which arise when using the decoupling approach in different cases.

3.3 Hydraulic Decoupling and Hydraulic Network Splitting

3.3.1 Ideal Hydraulic Networks and Electrical Equivalents

Let's now concentrate on hydraulic networks. An *ideal* hydraulic network is made of *nodes*, associated to its pressure, and *branches*, associated to its flowrate. Each node corresponds to an equation of the kind:

$$\alpha \frac{dP}{dt} = \sum w_{in} - \sum w_{out} \tag{3.19}$$

where α is the (possibly zero) node capacitance, w_{in} and w_{out} are the flowrates entering and leaving the node, respectively. Each branch correspond to an equation of the kind:

$$P_{in} - P_{out} = \beta \frac{dw}{dt} + \gamma(w) \tag{3.20}$$

in case one desires to include in the model the inertance β of the fluid, or of the kind

$$w = f(P_{in}, P_{out}) \tag{3.21}$$

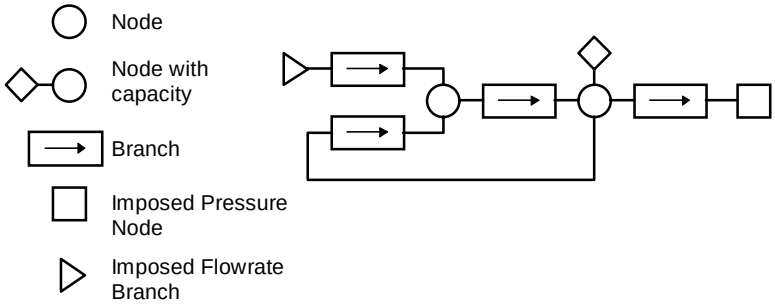

Figure 3.4: Example of hydraulic network

in case there's a direct algebraic relationship between inlet and outlet pressure, which is not necessarily a function of the pressure drop P_{in}–P_{out} (e.g. like in the case of valves operating in choked flow conditions).

An ideal network can also contain *imposed pressure nodes* and *imposed flowrate branches*; the corresponding values of pressure and flowrate are exogenous, and considered as given when solving the network. Their typical use is to describe boundary conditions, or to split the solution of larger networks, as will be explained in the following.

An example of such network is given in Fig. 3.4.

The equations of the single components (which are a-causal by themselves) can be assembled following the network topology, to obtain a closed model of the whole network. The resulting system of Differential-Algebraic Equation (DAE) can then be solved, for instance, by using Euler's forward (implicit) method, solving the resulting non-linear system of equations by Newton's method.

The behaviour of these networks may be better understood by considering the small-signal electrical circuit equivalent to the hydraulic network undergoing small perturbations around the steady state condition, which can be obtained with the following substitutions (see the example in Fig. 3.5):

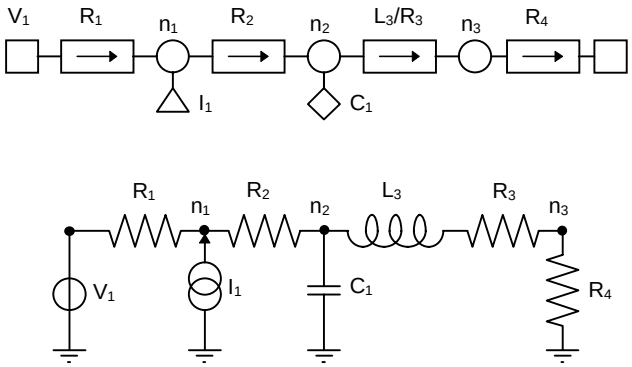

Figure 3.5: Hydraulic network and electrical equivalent

- Pressure variation ⇒ Voltage
- Flowrate variation ⇒ Current
- Hydraulic node ⇒ Electrical node, possibly connected to the ground with a condenser having capacity $C=\alpha$
- Hydraulic branch ⇒ Non-linear resistor, having resistance $R = d\gamma / dw$, possibly connected in series with an inductor having inductance $L = \beta$

3.3.2 Hydraulic Network Splitting: a Simple Case

To explain how the solution of hydraulic networks can benefit from the decoupling approach, by splitting the problem into the solution of smaller sub-networks, a very simple case, taken from [Cas98c], is briefly described; subsequently, the general case is discussed.

Consider the simple electrical network shown in Fig. 3.6. The differential-algebraic system describing its operation is equivalent to the form:

$$\dot{x} = Ax + Bu \tag{3.22}$$

with $x=[V_b\ V_c]$' and $u=E$, while A and B are the appropriate matrices. Suppose that (3.22) is integrated using Euler's *implicit* integration algorithm, to ensure unconditional stability; then, at every time step, the following linear system must be solved:

$$Hx_{k+1} = x_k + f_{k+1} \tag{3.23}$$

where $H = I - A \cdot \delta t$, $f = Bu \cdot \delta t$, and δt is the integration time step. Note that matrix H has to be inverted; in the general non-linear case, H is the system Jacobian matrix, which should be inverted at each time step.

On the other hand, if Euler's *explicit* integration algorithm is employed, the solution is given by

$$x_{k+1} = Fx_k + f_k \tag{3.24}$$

where $f = I + A \cdot \delta t$. No matrix inversion is needed; however the solution is numerically stable only for $\delta t<2T_{min}$, where T_{min} is the smallest time constant of matrix A (i.e. the inverse of the opposite of its largest eigenvalue). If the circuit is characterised by fast dynamics, mixed with slow dynamics, the explicit algorithm is not appropriate, since it forces to use very small time steps.

Assume now that R_2 and C_2 are sufficiently large: the variation of voltage Vc within an integration step is likely to be small, therefore having a weak influence on current I_2: it is then possible

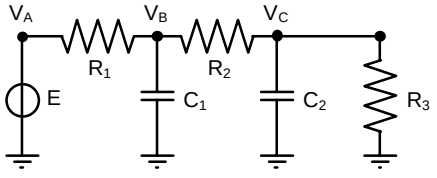

Figure 3.6: Electrical network

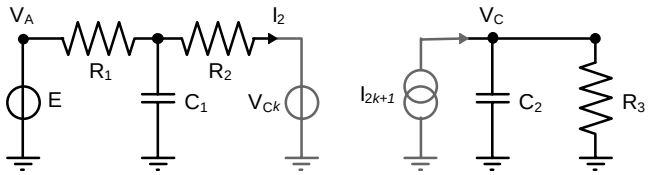

Figure 3.7: Split electrical network

to split the network, decoupling its solution in the solution in sequence of two smaller networks, shown in Fig 3.7.

The left part of the circuit is solved by implicit Euler's integration, but assuming V_c fixed at the value computed at the previous time step. Then, the right part of the circuit is solved assuming I_2 fixed at the value thus calculated in the left part. This means that a mixed implicit-explicit integration algorithm is employed; therefore the solution will always converge to the true one as $\delta t \to 0$. The solution formula corresponding to this procedure is:

$$G_L x_{k+1} = G_R x_k + f_{k+1} \,, \tag{3.25}$$

where

$$G_L = \begin{bmatrix} 1+\dfrac{\delta t}{RC_1} & 0 \\ -\dfrac{\delta t}{R_2 C_2} & 1+\dfrac{\delta t}{R_3 C_2} \end{bmatrix}, \quad G_R = \begin{bmatrix} 1 & \dfrac{\delta t}{R_2 C_1} \\ 0 & 1-\dfrac{\delta t}{R_2 C_2} \end{bmatrix}. \tag{3.26}$$

The solution of the discretised equation is much simpler: due to the *triangular* nature of G_L, matrix inversion is trivial. However, the numerical stability of the solution is greatly enhanced, compared with the explicit integration case. This can be easily seen from the following numerical examples, where the following sets of values for the components are considered:

$$R_1=0.1;\ C_1=1;\ R_3=1;\ C_2=\{1;\ 3;\ 5\};\ R_2=[0.1\text{–}10]\,. \tag{3.27}$$

The stability regions of the fully explicit algorithm and of the mixed algorithm employing the decoupling between the two sub-networks are shown in Fig. 3.8. Stability regions correspond to the points below the curves. Note the very different time scales for *dt* (the integration stepsize). Also note that, in case R_2 is sufficiently large, the decoupling (or *weakening*) approach yields unconditional stability like the fully implicit algorithm, despite the reduced computational burden.

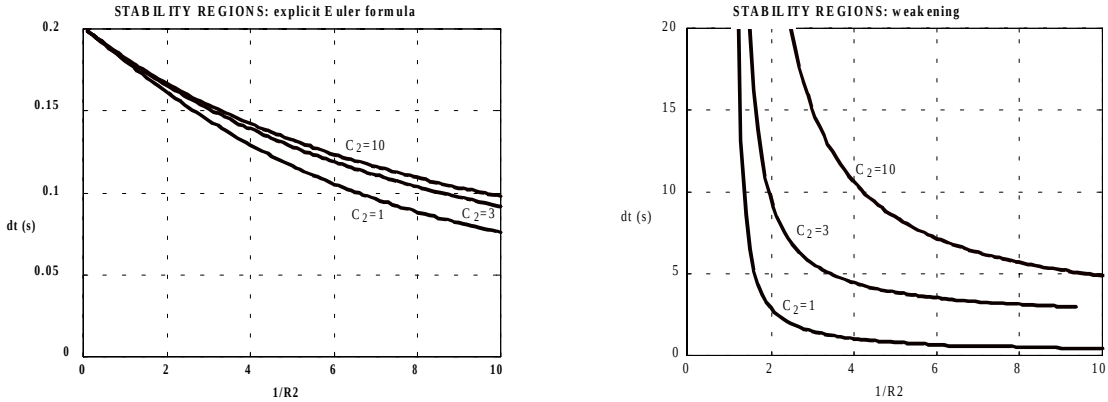

Figure 3.8: Stability regions of the two integration algorithms

In terms of hydraulic network, the analysis carried out above corresponds to the situation sketched in Fig. 3.9. Instead of solving the network as a whole, the two sub-networks are solved in sequence. The boundary conditions for the split networks are taken equal to the last computed value of the corresponding variable (pressure or flowrate).

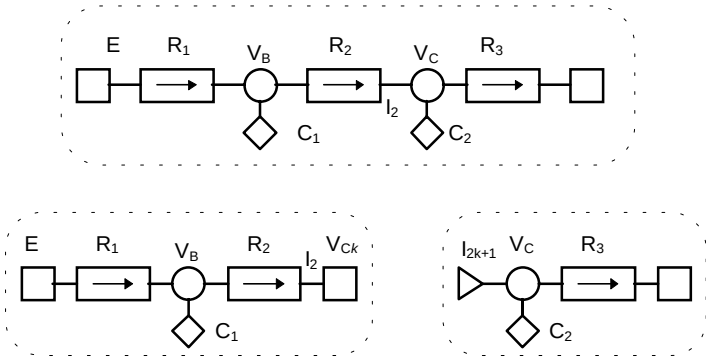

Figure 3.9: Hydraulic networks equivalent to Fig's. 3.6-3.7

3.3.3 Hydraulic Network Splitting: General Case

The general case, in which a linear electrical network is solved by decoupling, will now be discussed, with respect to the numerical stability of the discretised, decoupled solution. Since the model of any non-linear hydraulic network undergoing small perturbations around a steady state is equivalent to that of a linear electrical network, the result can then be easily interpreted in terms of hydraulic network decoupling.

Consider a generic electrical network, consisting of two sub-networks connected by a node. For the purpose of this analysis, the two sub-networks can be substituted with their equivalent Thévenin circuits, having impedance $Z_1(s)$ and $Z_2(s)$ (Fig. 3.10, left); the equivalent series voltage generators can be

neglected, since they do not affect stability. To implement the decoupled solution, the network is then split across the node, a voltage generator is connected to the first one, and a current generator is connected to the second one (Fig. 3.10, right).

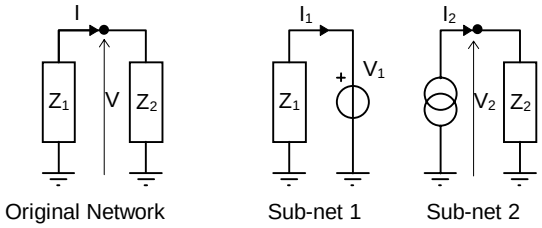

Figure 3.10: General network splitting

At this point it is possible to solve one integration step of Sub-net 1 using the previously calculated value of V_1 and then solve Sub-net 2 with the resulting value of I_2, or vice versa, obtaining the two solution schemes sketched in Fig. 3.11, where z^{-1} is the time delay operator. The minus sign in the loop results from the fact that the current I_1 *goes out of* the dipole Z_1, contrary to the usual passive dipole conventions.

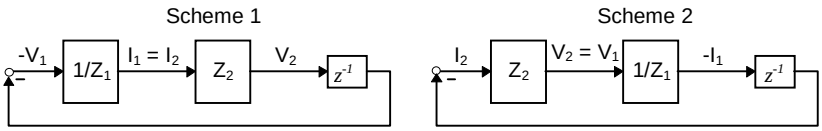

Figure 3.11: Decoupled solution schemes

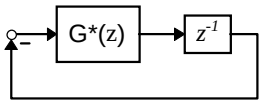

Figure 3.12: Equivalent block diagram

It is obvious that, from the point of view of stability, the two schemes are perfectly equivalent, since the loop transfer function is the same. The stability of the decoupled integration algorithm is therefore equivalent to the stability of the discrete-time system shown in Fig. 3.12, where

$$G^*(z) = \frac{Z_2^*(z)}{Z_1^*(z)} \tag{3.28}$$

comes from the discretisation of the original continuous-time transfer function

$$G(s) = \frac{Z_2(s)}{Z_1(s)} \tag{3.29}$$

via Euler's forward (implicit) formula $s = \frac{z-1}{z \cdot \delta t}$, that is,

$$G^*(z) = G\left(\frac{z-1}{z \cdot \delta t}\right) . \tag{3.30}$$

The stability study would be much easier if the continuous-time transfer function $G(s)$, which often has a clear physical meaning, could be used instead of $G^*(z)$, which is difficult to interpret and, moreover, changes with δt.

Suppose to deal only with stable $G(s)$ transfer functions (corresponding to passive RLC electrical networks, which are the small-signal equivalent of ideal hydraulic networks); since Euler's implicit formula preserves stability [Atk89], $G^*(z)$ will also be a stable (discrete time) transfer function. Let

$$L^*(z) = G^*(z) \cdot z^{-1} . \tag{3.31}$$

be the loop transfer function of the feedback block diagram in Fig. 3.12. The Nyquist Stability Criterion for discrete-time systems then states that the closed-loop system of Fig. 3.12 is stable if and only if the polar plot of

$$L^*(\exp(j\omega_n)) \ , \ -\pi \le \omega_n \le \pi \tag{3.32}$$

with

$$\omega_n = \omega \cdot \delta t \tag{3.33}$$

does not turn around the point −1 (note that the feedback is negative). Three cases will cover the vast majority of possible instances:

- $|L^*(\exp(j\omega_n))| < 1 \ \forall \omega_n \quad \Rightarrow$ unconditional stability
- $|L^*(\exp(j\omega_n))| = 1$ for $\omega_n = \omega_{nc} \quad \Rightarrow$ stability if $\arg[L^*(\exp(j\omega_{nc}))] > -180°$
- $|L^*(\exp(j\omega_n))| > 1 \ \forall \omega_n \quad \Rightarrow$ unconditional instability

The problem is now how to estimate the discrete-time frequency response $L^*(\exp(j\omega_n))$ starting from the continuous time frequency response $G(j\omega)$. From (3.30), (3.31), and (3.33) follows that:

$$G^*(\exp(j\omega_n)) = G\left(\frac{\exp(j\omega_n)-1}{\exp(j\omega_n) \cdot \delta t}\right) = G\left(j\omega + O(j\omega^2)\right) \tag{3.34}$$

$$G^*(\exp(j\omega_n)) \cong G(j\omega), \ \text{for} \ \omega < 0.5\frac{1}{\delta t} . \tag{3.35}$$

$$L^*(\exp(j\omega_n)) \cong G(j\omega) \cdot \exp(-j\omega \cdot \delta t), \ \text{for} \ \omega < 0.5\frac{1}{\delta t} . \tag{3.36}$$

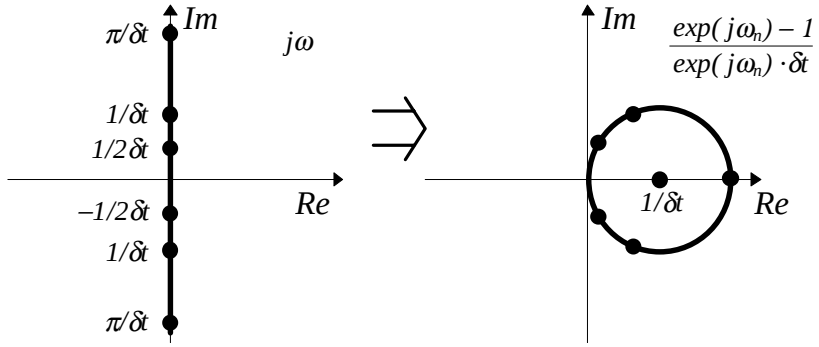

Figure 3.13: Non-linear transformation induced by Euler's discretisation

Up to the limit indicated in (3.35), the discrete-time frequency response of the loop transfer function can be well approximated by the continuous-time one. At higher frequencies, the deformation induced by Euler's non-linear transformation introduces some distortion, as can be seen in Fig. 3.13. When evaluating (3.34), the contribution given to the frequency response by each binomial $(s-\alpha_i)$ of the transfer function can be compared with that of the continuous-time frequency response $G(j\omega)$ by examining Fig. 3.14:

- **Slow poles** (having time constant $\tau >> \delta t$): with increasing ω, the modulus of the discrete-time frequency response decreases less than the corresponding continuous-time one, while the contribution to the phase lag tends to come back towards zero.
- **Slow zeros** (having time constant $\tau >> \delta t$): with increasing ω, the modulus of the discrete-time frequency response increases less than the corresponding continuous-time one, while the contribution to the phase lag tend to come back towards zero.
- **Complex-conjugate poles and zeros:** the pole damping is increased.
- **Fast poles and zeros** (having time constant $\tau << \delta t$): the contribution to the frequency response is approximately equal to the static gain.

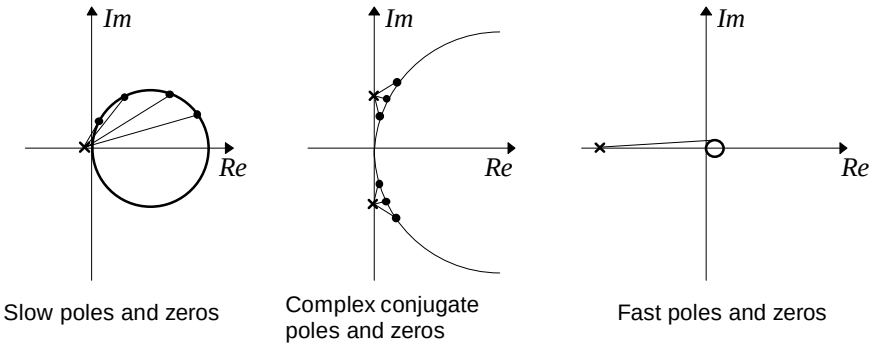

Figure 3.14: Contributions of poles and zeros to $G^*(exp(j\omega))$

This analysis, among other things, explains clearly some facts which are well-known when using fixed-step implicit Euler's integration:

- the fundamental dynamics is computed accurately if the corresponding time constants are at least 2-5 times longer than the integration time step;
- the damping of oscillatory dynamics is increased artificially by the integration method;
- fast dynamics, characterised by much shorter time constants than the integration time step, are approximated by their corresponding steady-state gain.

It is now possible to complete the stability analysis of the decoupling approach, by studying the stability of the block diagram of fig. 3.12, whose loop transfer function is $L^*(z)$.

The analysis will be essentially based on (3.36), that is on the fact that the frequency response of $G^*(z)$ is very similar to that of $G(s)$, except for the above-mentioned approximations. Note that, if the network splitting is reasonable, the parts of the Bode plot where the approximation is cruder will probably lie where the loop gain is well below unity, so that the approximation will have no influence on the stability analysis. It is therefore possible to work directly with the corresponding continuous-time frequency response

$$L(j\omega) = G(j\omega)\cdot\exp(-j\omega\cdot\delta t)\ . \tag{3.37}$$

Real applications will almost always fall under one of these three cases:

1. $|G(j\omega)|>1\ \forall\omega$: the numerical integration by decoupling will be unconditionally unstable, no matter how small a stepsize is used; this means that a completely wrong splitting point has been chosen;
2. $|G(j\omega)|<1\ \forall\omega$: the numerical integration by decoupling will be unconditionally stable for every possible stepsize; this is the most favourable condition (see for instance the case shown in Fig 3.8 (right) for R_2>1).
3. $|G(j\omega)|=1$ at $\omega=\omega_c$: let $\varphi_c=\arg(G(j\omega_c))$ and $\varphi_m=180°-|\varphi_c|$; if φ_m<0 then the integration algorithm is unconditionally unstable; otherwise, stability is preserved if $\arg(L(j\omega_c))>-180°$, which implies

$$\delta t<\frac{\varphi_m}{\omega_c}\cdot\frac{\pi}{180°}\ . \tag{3.38}$$

To preserve the stability of the decoupled integration algorithm with a large step size δt it is therefore necessary to have small |G| (condition 2), and/or small ω_c (condition (3.37)). Since $G(s)=Z_2(s)/Z_1(s)$, this means having:

- small resistance and/or large capacitance on the voltage source side (Z_1)
- large resistance and/or small capacitance on the current source side (Z_2)

The criteria that brought to the splitting of the simple network in section 3.3.2 can now be explained more precisely.

The models of components found in typical power processes are much more complex than the ideal hydraulic network components, whose small-perturbation behaviour is equivalent to the above-discussed electrical network. However, one can assume that, for each component, one or two equation like (3.19), (3.20) or (3.21) can be isolated, thus explaining the (usually fast) pressure-flowrate dynamics; other terms appearing in those equations will be generally related to slower thermal phenomena, and will then be decoupled. The hydrodynamic equations will be then solved first, using the past computed values of all the other variables, as shown throughout section 3.2. When solving the hydrodynamic equations, in addition to thermo-hydraulic decoupling, the solution of the global plant hydraulic network can be split into the solution of several sub-networks, provided the appropriate conditions hold. This pushes the decoupling approach to its maximum extent, allowing to split the solution of the process equation system into the solution of a large number of rather small systems of implicit equations.

3.4 Process Modelling in the ProcSim Environment

3.4.1 Introduction

The ProcSim simulation environment ([Bar94-95-96-98]) was originally developed at the Control Laboratory of Dipartimento di Elettronica of the Politecnico di Milano to simulate conventional, fossil-fired power plants, thus containing networks of drum boilers, heat exchangers, combustion chambers, tanks, pumps, valves and turbines. The simulation approach is heavily based on the concepts explained in sections 3.2 and 3.3, which essentially determine the software structure. The fundamental modelling concepts in ProcSim will be briefly reviewed in this section.

First of all, a fixed stepsize implicit Euler's algorithm is employed throughout the whole environment. The use of an implicit algorithm is mandatory in process modelling; otherwise the fast dynamics, which is invariably associated with the slow fundamental dynamics of interest, would lead to unnecessarily short integration step size during simulation.

This algorithm is very simple, and may appear a bit crude when compared with more sophisticated integration algorithms, such as adaptive stepsize BDF [Gea91], the DASSL code [Bre96], the DASOLV code used by gPROMS [Jar92] or implicit Runge-Kutta codes such as RADAU5 [Hai96]. On the other hand, it allows several features that are much more difficult, or impossible, to implement with more sophisticated equation solvers:

- decoupling approach to the solution of the system of equation describing the whole process, which leads to the solution of many small systems of equations instead of a big one;
- possibility of multirate simulation of different parts or groups of equation;
- possibility of a distributed architecture of the simulator based on decoupling, where many processing units, communicating through a shared database, solve part of the equations independently of each other;
- possibility of real-time simulation (e.g. for training, or for hardware-in-the-loop control system testing): once that suitable simulation step sizes have been selected, ensuring numerical stability and satisfying precision throughout all the possible operating conditions, the ratio of real-time vs. simulation-time ratio on a given hardware architecture is fixed, and there is no possibility that the simulation time lags behind the real time in case of particularly severe perturbations, which could instead happen when using variable stepsize algorithm.

The ProcSim environment is fully modular, i.e. each process component (pump, valve, phase separator, reboiler plate) corresponds to a software structure, composed of a *datasheet* (containing all the component dimensional and functional parameters) and one or more *sub-modules*, each one involved in the solution of a subset of the equation describing it. The model of a particular process is obtained by suitably assembling the modules corresponding to its components. As a general rule, each component will have a *hydraulic* sub-module (describing the pressure-flowrate relationship) and one or more *thermal* or, generally speaking, *causal* sub-modules, which deal with the remaining equations. Many different combinations are possible, as will become clear in Chap. 5.

The basic assumption, upon which the whole environment is based, is that the hydrodynamic equations are decoupled from the other model equations, so that they can be solved independently of them (see section 3.2). However, the hydrodynamic equations of a single component are a-causal, and consequently they cannot be solved one at a time, component-wise; instead, suitable software structures are necessary to assemble a closed model of a hydraulic network from its components, which is then solved as a whole. Once the pressures and flowrates at time $t+\delta t$ have been calculated, under appropriate decoupling assumption the equations contained in the other sub-modules can be solved sequentially, usually following the direction of the fluid flow across the network. Note that, in general, flow reversal is not allowed, since it will greatly increase the modelling complexity, and it is usually not necessary for the vast majority of process components, which are usually designed to have pre-defined (entering or leaving) flow directions at their interfaces. Last, but not least, once all the process variables have been calculated at time $t+\delta t$, the control system modules can compute their output based on the input values

coming from the process. The control modules are causal by definition, so that there is no problem in solving them separately, at least if a decentralised control structure is adopted.

All the sub-modules performing parts of the integration task read and write a database containing all the process variables, whose state can be saved and retrieved at any time.

When facing the problem of modelling a new kind of component, the following steps should be undertaken:

1. Identify the model equations and variables, which ensure the maximum decoupling between the hydrodynamic equation(s) and the other ones; in particular, select the hydrodynamic equations which best capture the pressure-flowrate relationship, having at the same time the minimum coupling with all the other phenomena: usually they are mass conservation equations (for nodes) and momentum conservation equations (for branches).
2. Build the corresponding hydraulic sub-module(s) according to the method described in section 3.4.2
3. Discretise the remaining equations with Euler's implicit method, and build the causal sub-modules(s) as described in section 3.4.3.

The actual procedure may vary, depending on the kind of component. For instance, when modelling a pipe with compressible fluid, the following steps can be taken:

1. Since the pressure drop is usually small, it can be lumped at the end of the pipe, assuming constant pressure along the pipe for the rest of the equations. This equation will be put in a branch-type hydraulic sub-module.
2. The mass conservation equation (which is originally a PDE) can be lumped into a single equivalent ODE, which will result in a hydraulic sub-module of node type, with non-zero capacitance.
3. The energy conservation PDE must be written in the entropy form, in order to have the largest possible decoupling from the hydrodynamic equations. It must then be reduced in a set of ODE's by some suitable method (e.g. by the finite difference method, or the finite element method); the ODE's are then discretised using Euler's implicit method, resulting into a thermal sub-module.

When assembling the pipe in the plant model, the node and branch sub-modules will be a part of the hydraulic network to which the pipe is connected, while the thermal sub-module will be placed in the sequence of causal sub-modules, and used to solve the thermal equations after the hydraulic network (as a whole) has been solved.

As a general rule, standard interfaces are defined for every water- or steam-processing component: every component inlet and outlet is characterised by a pressure P, a mass flowrate w and a specific enthalpy h. The use of the

specific enthalpy instead of the temperature allows to describe the state of the substance completely, even under two-phase conditions.

While the approach used by the ProcSim environment is fully modular, it offers no possibility of hierarchical model aggregation, nor any object-orientation. However, even if these approaches, used by simulation environments such as gPROMS ([Pan93], [Brt94], [gPR97]), OMOLA ([Mat93b]), Dymola ([DYM94]), MOSES ([Maf98]), are very attractive for modelling complex mechanical systems or chemical engineering processes, often containing repetitive equation structures, their usefulness in power process modelling is more questionable, at least if the aim is to obtain accurate engineering simulators. For the latter, especially in case of innovative process concepts, much ad-hoc modelling has to be done, and the strictly structured, inheritance-based concepts of O-O modelling can more often be an obstacle than a benefit. The continuously evolving simulation technology could of course change this situation in the future.

3.4.2 Hydraulic Network Modelling and Simulation

As already said, many process components are characterised by possibly fast pressure and flowrate dynamics. The corresponding a-causal equations are, in most cases, mass conservation equations (for network nodes) and momentum conservation equations (for branches). The approach to modelling and simulation which will now be presented was first introduced by [Bar94], but it is reformulated here in the most general case, taking into account the extensions introduced by the following development of new components in [Cas95], [Col96] and in the present research work.

General hydrodynamic equations can be of three kinds:

$$\alpha \frac{dP}{dt} = \sum w_{in} - \sum w_{out} + \Lambda \qquad \text{(mass balance)} \qquad (3.39)$$

$$P^{in} - P^{out} = \beta \frac{dw}{dt} + \gamma(w,d) + \zeta(d) \qquad \text{(momentum balance)} \qquad (3.40)$$

$$w = w(P^{in}, P^{out}, d) \qquad \text{(algebraic flow relationship)} \qquad (3.41)$$

where P is the node pressure, α is the node capacitance

$$\alpha = \frac{\partial M}{dP} \ , \qquad (3.42)$$

Λ collects all the remaining terms in the mass balance equation, P^{in} and P^{out} are the inlet and outlet pressures of the branch, β is the branch inertance, γ is the friction term and ζ is the piezometric term.

The difference between (3.39)-(3-41) and (3.19)-(3.21) (ideal network equations) lies in the presence of the additional term Λ in (3.39) and of the additional (vector) term d in (3.40) and (3.41). These terms can depend on other variables (specific entropy, liquid level, etc.) which are considered *weak variables*, and therefore considered as constants along the integration step, following the decoupling approach. Equation (3.39) must be carefully selected in order to have the smallest possible mutual influence between the node pressure and the decoupled term Λ.

Equation (3.40) is integrated by Euler's implicit method, giving

$$P_{k+1}^{in} - P_{k+1}^{out} = \frac{\beta}{\delta t} w_{k+1} - \frac{\beta}{\delta t} w_k + \gamma(w_{k+1}, d_k) + \zeta(d_k) \tag{3.43}$$

where the subscripts indicate the integration step. Note that the weak terms are included with their value computed in the previous integration step. Supposing (3.43) can be solved for w_{k+1} in closed form, one obtains

$$w_{k+1} = f(P_{k+1}, w_k, d_k) \tag{3.44}$$

where P is the vector containing the network pressures. In case there is no fluid inertia to be taken into account, (3.41) can be used, leading directly to

$$w_{k+1} = f(P_{k+1}, d_k) \ . \tag{3.45}$$

Now, (3.39) can be discretised, again using Euler's method, resulting in

$$\frac{\alpha}{\delta t} P_{k+1} - \frac{\alpha}{\delta t} P_k - \sum w_{k+1}^{in} + \sum w_{k+1}^{out} - \Lambda_k = 0 \tag{3.46}$$

that is, considering now w as the whole vector of the network flowrates

$$g(w_{k+1}, P_{k+1}, P_k, \Lambda_k) = 0 \ . \tag{3.47}$$

where the second and third arguments are only present for non-zero node capacitance. If Λ is a function of P, it is possible to consider it implicitly (i.e. at step $k+1$) with respect to P in the discretisation, thus improving the stability of the solution; the following equation, instead of (3.46), is obtained:

$$\frac{\alpha}{\delta t} P_{k+1} - \frac{\alpha}{\delta t} P_k - \sum w_{k+1}^{in} + \sum w_{k+1}^{out} - \left(\Lambda_k + (P_{k+1} - P_k) \frac{\partial \Lambda}{\partial P} \right) = 0 \tag{3.48}$$

Now, if (3.44) is substituted into (3.47), the equation solving one integration step for the whole network is obtained:

$$h(P_{k+1}, P_k, w_k, \Lambda_k, d_k) = 0 \ . \tag{3.49}$$

where the second argument is present in case of non-zero capacitance of some node, the third is present in case inertance is taken into account in some branch, and the last two are present if the hydrodynamic equations are not ideal, but weakly interacting additional terms are present.

Equation (3.49) is a non-linear, implicit equation, and must be solved by some iterative method. The choice is to use the well-known Newton's method, using the past values of the pressures P_k as an initial guess P_{k+1}^0 for the solution P_{k+1}; the first Newton iteration corresponds to solving the following equation:

$$h(P_k, P_k, w_k, \Lambda_k, d_k) + \left.\frac{\partial h}{\partial P_{k+1}}\right|_{P_k} \cdot (P_{k+1} - P_k) = 0 \ . \tag{3.50}$$

that is solving the linear equation

$$J \cdot P_{k+1} = J \cdot P_k - r_k \tag{3.51}$$

where J is the Jacobian matrix of h and r is the residual term, given by the leftmost term of (3.50). If the step size is not too large, a single Newton iteration for each integration step is sufficient to attain a good accuracy of the solution.

It can be easily shown that the elements of J are as follows: the diagonal (i,i) elements contain the capacitance of the corresponding nodes, plus the optional partial derivative of Λ, plus the partial derivatives of the flowrates of the branches connected to the node with respect to the node pressure

$$J^{ii} = \frac{\alpha^i}{\delta t} - \frac{\partial \Lambda_k^i}{\partial P} - \frac{\partial}{\partial P_{k+1}^i} \sum w_{in,k}^i + \frac{\partial}{\partial P_{k+1}^i} \sum w_{out,k}^i \tag{3.52}$$

where all the terms with superscript i refer to the *i-th* node, and in particular w_{in}^i are the flowrates of the branches entering the *i-th* node, while w_{out}^i are the flowrates of the branches leaving the *i-th* node. The off-diagonal *(i,j)* terms contain the partial derivatives of the flowrates of the branches connected to the *i-th* node with respect to the pressure of the *j-th* node.

$$J^{ij} = -\frac{\partial}{\partial P_{k+1}^j} \sum w_{in,k}^i + \frac{\partial}{\partial P_{k+1}^i} \sum w_{out,k}^i \tag{3.53}$$

After some easy substitution, the elements of the residual term r_k result as follows:

$$r_k^i = -\sum \tilde{w}_{in,k}^i + \sum \tilde{w}_{out,k}^i - \Lambda_k^i \tag{3.54}$$

with

$$\tilde{w}_k = f(P_k, w_k) \tag{3.55}$$

The Jacobian matrix and residual vector thus illustrated can be computed by adding the contributions given by each single component of the hydraulic network.

Contributions of node *i*

$$J^{ii} \leftarrow \frac{\alpha_k^i}{\delta t} - \frac{\partial \Lambda_k^i}{\partial P} \tag{3.56}$$

($J^{ii}=0$ if the node is only connecting two branches, without corresponding to any process component)

$$r_k^i \leftarrow -\Lambda_k^i \tag{3.57}$$

Contributions of branch *i* →*j*

$$J^{ii} \leftarrow +\frac{\partial w_{k+1}}{\partial P_{k+1}^i} \tag{3.58}$$

$$J^{ij} \leftarrow +\frac{\partial w_{k+1}}{\partial P_{k+1}^j} \tag{3.59}$$

$$J^{ji} \leftarrow -\frac{\partial w_{k+1}}{\partial P_{k+1}^i} \tag{3.60}$$

$$J^{jj} \leftarrow -\frac{\partial w_{k+1}}{\partial P_{k+1}^j} \tag{3.61}$$

$$r_k^i \leftarrow +\tilde{w}_k \tag{3.62}$$

$$r_k^j \leftarrow -\tilde{w}_k \tag{3.63}$$

If the equations of a branch-type component (e.g. a pipe with compressible fluid) also include a mass conservation equation, giving origin to a branch capacitance in addition to the branch resistance and inertance, the capacitance contribution can be directly added to the Jacobian matrix by the branch sub-module, either upstream

$$J^{ii} \leftarrow \frac{\alpha_k}{\delta t} - \frac{\partial \Lambda_k}{\partial P} \tag{3.64}$$

or downstream

$$J^{jj} \leftarrow \frac{\alpha_k}{\delta t} - \frac{\partial \Lambda_k}{\partial P} \tag{3.65}$$

The structure of hydraulic sub-modules should now be clear: each node-type sub-module and each branch-type sub-module should calculate their contribution to the Jacobian matrix and to the residual vector, which are obtained from the hydrodynamic equations (3.39)-(3.41).

The network solver will collect the contributions, according to the topology of the network, thus assembling the discretised equation (3.51) describing the network dynamics. Then the (linear) equation will be solved, obtaining the new pressure values P_{k+1}. Finally, each branch sub-module will calculate the new flowrate value w_{k+1} using (3.44) or (3.45).

3.4.3 Simulation of Causal Equations

Once the hydrodynamic equations have been solved, via the decoupling approach, and the corresponding new pressure and flowrate values P_{k+1} and w_{k+1} have been computed, the remaining equations of most components can be re-arranged in a generalised state-space form, which is causal:

$$A(x)\frac{dx}{dt} = f(x,u,v) \tag{3.66}$$

$$y = y(x,u,v) \tag{3.67}$$

where x is the vector of the other state variables of the component (e.g. specific entropy, specific enthalpy, level, etc.), u is the vector of the variables which have already been computed elsewhere (e.g. pressures, flowrates, inlet specific enthalpies, etc.), v is the vector of the weak variables (whose past computed value will be used to perform the integration step) and y is the vector of the output variables.

Equation (3.66) is again discretised by Euler's implicit method, using the so-called *semi-linearisation* method [SIC72]:

$$A_k(x_{k+1} - x_k) = \delta t \cdot f(x_{k+1}, u_{k+1}, v_k) \tag{3.68}$$

$$A_k(x_{k+1} - x_k) \cong \delta t \cdot f(x_k, u_{k+1}, v_k) + \delta t \cdot \frac{\partial f}{\partial x}(x_{k+1} - x_k) \tag{3.69}$$

$$\left(A_k - \delta t \frac{\partial f}{\partial x}\right)x_{k+1} \cong \left(A_k - \delta t \frac{\partial f}{\partial x}\right)x_k + \delta t \cdot f(x_k, u_{k+1}, v_k) \tag{3.70}$$

Equation 3.70 is then solved for x_{k+1}, and subsequently y_{k+1} is computed using (3.67). Strictly speaking, full implicit integration would imply using A_{k+1}, but the difference lies in a second-order term (as already seen in Example 2, Section 3.2) which is supposed to be negligible when the process is near a steady state, or when the stepsize is sufficiently small. As a final remark, note that many elements of the Jacobian matrix of function f will be structurally very small (e.g. derivatives of the density of a liquid with respect to the temperature); therefore they may be entirely omitted without affecting the numerical stability of the solution, which is mainly affected by the thermo-hydraulic decoupling.

The methods illustrated in this section (3.4) have been employed for the accurate simulation of a drum-boiler industrial steam generator [Cst95], and of a steam generation plant for water desalinisation [Col96]. Moreover, they have been successfully validated in the study of a small pilot power plant, designed for experimental purposes by the CISE research centre [Bel96], [Lev99].

4. EXTENSIONS FOR THE LATERA PLANT

4.1 Two-Component Working Fluid

The first fundamental difference between the ordinary steam/water power processes and the Latera plant process is the extensive use of a two-component working fluid (water plus carbon dioxide) throughout the whole plant. Other gases and substances are present in the geothermal fluid, but they can be neglected.

The only case in which a mixture of steam with an incondensible gas (ordinary air) is considered in ordinary power plants is when simulating the start-up of boilers and condensers; however, this is rather uncommon and, moreover, a great modelling accuracy is usually not needed, the main interest being in the possibility to simulate the initial pressurisation transient, after which normal operation is carried out with water and steam only.

The operation of the Latera plant process instead is essentially based on two-component fluid processing, particularly in the phase separators and in the reboiler. Moreover, despite the rather low solubility of CO_2 in liquid water, the dissolved fraction must be taken into account, due to the huge liquid flowrates involved. As an example, during normal reboiler operation, the dissolved CO_2 flowing downwards is more than 10% of the CO_2 going upwards in the gas phase, and thus not at all negligible. After the flashing of the hot water obtained from the reboiler, the dissolved CO_2 goes almost entirely in the gas phase, so that the resulting steam contains over 2% of CO_2; this in turn implies the need to use a medium-sized compressor to extract the incondensible gas from the condenser, in order to avoid a rapid pressure increase at the turbine outlet. This part of the process is not simulated explicitly, but it is important to know the CO_2 mass fraction going into the high pressure turbine to calculate the turbine efficiency correctly.

4.1.1 Modelling of the Liquid Phase

The modelling of the interaction between CO_2 and liquid water is a very complex (and studied) subject, involving many physico-chemical equilibria [Ger76], [Dom90]. Basically, the following equilibria take place:

- The molar fraction of the dissolved CO_2 is proportional to the partial pressure of the CO_2 in the gas phase, according to *Henry's law:*

$$P_g = H^* \cdot [CO_2]_{acq} \tag{4.1}$$

  where H^* is Henry's constant, which in fact is a function of the temperature, lying in the range 1500-7000 bar/mol. This relationship is valid up to partial pressures of around 30 bars. The equilibrium at very high pressures (100-500 bars) obeys different laws, which are of no interest in this case.
- The dissolved CO_2 reacts with water, producing carbonic acid:

$$CO_2 + H_2O \leftrightarrow H_2CO_3 \tag{4.2}$$

- The carbonic acid reacts again with water, in a two-stage ionisation process:

$$H_2CO_3 + H_2O \leftrightarrow HCO_3^- + H_3O^+ \tag{4.3}$$

$$HCO_3^- + H_2O \leftrightarrow CO_3^{--} + H_3O^+ \tag{4.4}$$

All these equilibria are governed by thermodynamic equilibrium constants. Since the carbonic and hydrocarbonic acids are weak acids, the equilibrium constants are very small; consequently, for values of $pH<6$, the concentration of carbonic and hydrocarbonic ions in the solution is negligible, compared with that of the dissolved CO_2. A detailed modelling of the *pH* in the solution is out of question in this context, since it would involve many more chemical equilibria with other substances (salts) which are present in the geothermal fluid. Moreover, if the pH were high, the water would absorb much more CO_2 than the quantity predicted by Henry's law alone, since most of it would be stored in the form of ions, and then released into the gas phase when flashing the liquid. This is contrary to the main purpose of the process, which is to separate the CO_2 content in order to obtain pure steam for the turbines. Consequently, either the *pH* is low by itself, or some chemical additive should be employed to keep it low. In both cases, it is possible to assume that the chemical reactions will give a negligible contribution, and that the solution process will be governed by Henry's law only. From now on, for the sake of simplicity, Henry's law will be formulated in terms of mass fractions instead of molar fractions:

$$P_g = H(T) \cdot x_g \tag{4.5}$$

where $H(T)$ is Henry's constant expressed in terms of mass fraction and x_g is the mass fraction of the dissolved CO_2. The plot of $H(T)$ is shown in Fig. 4.1,

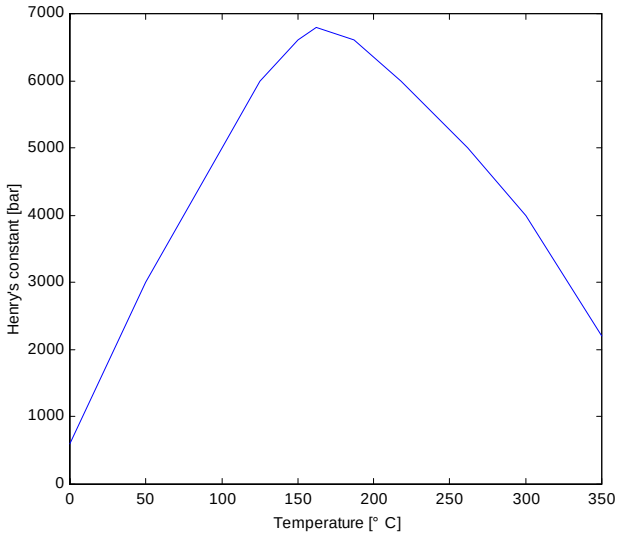

Figure 4.1: Henry's constant for the CO_2 in water

and is the one currently used by the geothermal production department of ENEL. It is interesting to note that plots obtained from other sources are slightly different, probably due to some difference in the experimental conditions.

Since the mass fraction of the dissolved CO_2 never exceeds 0.1%, both its heat of solution and its influence on the liquid density are neglected. Therefore, the liquid density will be assumed equal to the pure water density at the same pressure and temperature conditions; the liquid enthalpy will be the sum of the water enthalpy and of the CO_2 enthalpy, which will be equal to that of the gas phase CO_2 at the same temperature.

4.1.2 Modelling of the Gas Phase

The gas phase found in the Latera process is a mixture of water steam and CO_2. The properties of pure steam are available from the *steam table* software module of the ProcSim environment, based on [ASM93], which calculates all the thermodynamic properties of steam and water, along with their partial derivatives, as a function of (P,S) or (P,h), where P is the pressure, S the specific entropy and h the specific enthalpy. Within the operating regime of the Latera processes (0-10 bars, 80-180 °C), the CO_2 properties can be very well approximated by an ideal gas having a molar weight of 44. The state equation is therefore the standard

$$\frac{P}{\rho} = RT \tag{4.6}$$

where P is the pressure, ρ is the density, R is the ideal gas constant divided by the gas molecular weight, and T is the absolute temperature. According to the ideal gas approximation, the specific enthalpy h is a function of the temperature only

$$h=h(T) \tag{4.7}$$

which can be approximated by a suitable formula, valid in the temperature range of interest.

The problem now is to calculate the properties of the mixture starting from the (known) properties of the components. To this purpose, many methods are available (see, e.g., [How87], [Hol88], [War88]). Most of them are valid for mixtures of *ideal gases*, but some more advanced methods exist, e.g., for mixture of gases which are near their critical conditions. A rather standard method is used to calculate the properties of *humid air*, which is actually a mixture of an incondensible gas with water vapour; however, the partial pressure of the vapour and the mixture temperature are much lower than in the Latera case. After some analysis, the best approximation in the typical conditions found in the Latera process is the so-called *Gibbs-Dalton's rule:*

> "Every component of the mixture behaves as if it was alone, filling the total volume, at the same temperature of the mixture."

According to this rule, if the total pressure P, the temperature T and the mass fraction of the CO_2 x_g are known, after some computations the partial pressures of the vapour P_v and of the CO_2 P_g result as follows:

$$\begin{aligned} P_g &= \frac{x_g M_v}{Z(1-x_g)M_g + x_g M_v} P \\ P_v &= \frac{Z(1-x_g)M_g}{Z(1-x_g)M_g + x_g M_v} P \end{aligned} \tag{4.8}$$

where $Z(Pv,T)$ is the compressibility factor of the steam at its temperature and partial pressure, M_v and M_g are the molecular weights of water and CO_2. However, in the range of operating points of the Latera process, $Z>0.9$, so that (4.8) can be approximated by the formulae valid for a mixture of ideal gases ($Z=1$), in which Dalton's law applies:

$$\begin{aligned} P_g &= \frac{x_g M_v}{(1-x_g)M_g + x_g M_v} P \\ P_v &= \frac{(1-x_g)M_g}{(1-x_g)M_g + x_g M_v} P \end{aligned} \quad ; \tag{4.9}$$

in other words, the partial pressures are proportional to the molar fractions. The worst-case approximation error in the partial pressures is about 2.5%, but is

usually much less. Consequently, (4.9) can be used, which is much simpler since it does not contain $Z(P_v,T)$.

According to Gibb's phase rule, the state of the gas-vapour mixture is completely specified by three state variables, e.g. $X=X(P, h, x_g)$, where X is a generic property of the mixture, P is the *total* pressure and h is the specific enthalpy *of the mixture*. To compute the mixture properties, it is necessary first to calculate the properties of the single components, and then to combine them using Gibbs-Dalton's law. It can be shown that this implies solving a system of implicit non-linear equation, due to the constraint $T_v=T_g$ enforced by Gibbs-Dalton's law.

The calculations are more straightforward if the mixture is in thermodynamic equilibrium with the liquid phase; this actually implies that the vapour fraction is in state of saturation, hence all its specific properties (enthalpy, entropy, density, temperature) can be directly derived from its partial pressure P_v, through a simple access to the saturated steam tables. The mixture properties are then computed very easily.

Let the *a* subscript denote the quantities related to the mixture, the *v* subscript those related to the saturated vapour fraction, the *g* subscript those related with the CO_2 fraction, and the *vsat* subscript denoting the saturated steam properties. Finally, let α be the ratio between the steam molecular weight and the CO_2 molecular weight. It will be now shown that, according to the simplified equations (4.9) and to Gibbs-Dalton's law, all the relevant mixture properties (T_a, ρ_a, h_a) can be easily computed as a function of (P,xg)*:*

$$P_g = \frac{\alpha x_g}{1+(\alpha-1)x_g} P \tag{4.10}$$

$$P_v = \frac{1-x_g}{1+(\alpha-1)x_g} P \tag{4.11}$$

$$T_a = T_{vsat}(P_v) \tag{4.12}$$

$$\rho_v = \rho_{vsat}(P_v) \tag{4.13}$$

$$\rho_g = \frac{P_g}{RT_a} \tag{4.14}$$

$$\rho_a = \rho_v + \rho_g \tag{4.15}$$

$$h_v = h_{vsat}(P_v) \tag{4.16}$$

$$h_g = h_g(T_a) \tag{4.17}$$

$$h_a = (1-x_g)h_v + x_g h_g \tag{4.18}$$

The corresponding partial derivatives with respect to P and x_g are omitted for brevity, but can be found analytically without any particular problem.

The gas-vapour mixture found throughout the Latera process is either in equilibrium condition with water (e.g. just after flashing), or very near the saturation conditions, since only condensation processes take place and no heating is present. Therefore, the assumption that the gas-vapour mixture is always in saturation state is made, which permits to compute all the thermodynamic quantities as a function of two state variables only (P, x_g), as shown. The enthalpy error is small, since the mixture enthalpy is mostly determined by the latent heat of vaporisation of the vapour fraction (1-x_g) and not by its temperature; the temperature error is small, since no heating is ever applied to the mixture, which is always near the saturation state; the density error is small for the same reason.

4.1.3 Modelling of the Flashing Process

A recurrent situation in the Latera process is the flashing of hot water (with dissolved CO_2), occurring just before every phase separator. This process results in a two phase-flow, and the properties of each phase, assuming perfect separation, must be computed. Assume a valve inlet flow characterised by a flowrate w with a state (P_{in}, h, x_g), with $P_{in} > P_{vsat}$ in order to have a single liquid phase. The flashing process preserves the total fluid enthalpy h, bringing the fluid to a pressure $P < P_{vsat}$, so that a two-phase fluid comes out (see Fig. 4.2). Assuming the two phases are perfectly separated, the equations describing the two outlet flows (liquid and gas phase) will be now given and solved, on the grounds of the approximations described in sections 4.1.1 and 4.1.2.

Let P_v be the vapour partial pressure, x_{wl} the ratio between the flow of H_2O in the liquid phase and the total flow, x_{gl} the ratio between the flow of CO_2 in the liquid phase and the total flow, x_{va} the ratio between the flow of steam in the gas phase and the total flow, x_{ga} the ratio between the flow of CO_2 in the gas phase and the total flow, h_v the specific enthalpy of the steam in the gas phase, h_l the specific enthalpy of the water in the liquid phase and h_g the specific enthalpy of the CO_2, which is equal in the two phases, since the heat of solution is neglected. The eight equations governing the process are the following:

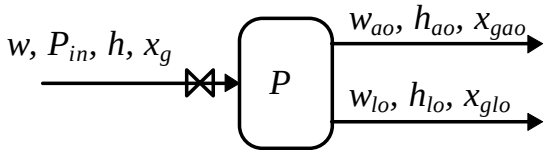

Figure 4.2: Two-component flashing

$$h_l = h_l(P, T_{sat}(P_v)) \cong h_{lsat}(P_v) \tag{4.19}$$

$$h_v = h_{vsat}(P_v) \tag{4.20}$$

$$h_g = h_g(T_{sat}(P_v)) \tag{4.21}$$

$$x_{gl} = x_{wl} \frac{P - P_v}{H(T_{sat}(P_v))} \qquad \text{(Henry's Law)} \tag{4.22}$$

$$x_{ga} = x_g - x_{gl} \qquad (CO_2 \text{ mass conservation}) \tag{4.23}$$

$$h_v x_{va} + h_g x_g + h_l x_{wl} = h \qquad \text{(energy conservation)} \tag{4.24}$$

$$x_{wl} = 1 - x_{va} - x_g \qquad \text{(total mass conservation)} \tag{4.25}$$

$$\frac{P - P_v}{P_v} = \alpha \frac{x_{ga}}{x_{va}} \qquad \text{(Dalton's law)} \tag{4.26}$$

Selecting P_v as a tearing variable, the system (4.19)-(4.26) can be rearranged as seven chained assignments

$$h_l \cong h_{lsat}(P_v) \tag{4.27}$$

$$h_v = h_{vsat}(P_v) \tag{4.28}$$

$$h_g = h_g(T_{sat}(P_v)) \tag{4.29}$$

$$x_{va} = \frac{h - h_l + x_g(h_l - h_g)}{h_v - h_l} \tag{4.30}$$

$$x_{wl} = 1 - x_{va} - x_g \tag{4.31}$$

$$x_{gl} = x_{wl} \frac{P - P_v}{H(T_{sat}(P_v))} \tag{4.32}$$

$$x_{ga} = x_g - x_{gl} \tag{4.33}$$

and one implicit equation in the tearing variable P_v,

$$P_v\left(1 + \alpha \frac{x_{ga}}{x_{va}}\right) - P = 0 \tag{4.34}$$

which can be solved by Newton's method. The required derivatives were computed analytically, but are not shown here for the sake of brevity. Once P_v is known, the assignments (4.27)-(4.33) can be used to compute the other variables. Finally, the liquid and gas flowrates at the outlet w_{lo} and w_{ao}, their CO_2 content x_{glo} and x_{gao}, and their specific enthalpies h_{lo}, h_{ao}, can be computed:

$$w_{lo} = (x_{wl} + x_{gl})w \;; \qquad w_{ao} = (x_{va} + x_{ga})w \tag{4.35}$$

$$x_{glo} = \frac{x_{gl}}{x_{wl} + x_{gl}} \; ; \qquad x_{gao} = \frac{x_{ga}}{x_{va} + x_{ga}} \tag{4.36}$$

$$h_{lo} = (1 - x_{glo})h_l + x_{glo}h_g \; ; \qquad h_{ao} = (1 - x_{gao})h_v + x_{glo}h_g \tag{4.37}$$

4.2 Two-Phase Process Components

Throughout the whole Latera plant, a recurrent process building block can be identified, i.e. a vessel containing the two-component fluid H_2O+CO_2 both in the liquid and gas phase, which can be assumed perfectly separated by a planar liquid-gas interface surface. This is the case of the primary phase separators tanks V101-2, V201-2, of the secondary phase separators tanks V311-2, V313-4, V401-2, V403-4, of the reboiler plates and of the reboiler bottom. A fundamental decision has to be made when modelling such components, i.e. whether to assume thermodynamic equilibrium between the two phases or not. The resulting model equations are quite different, and can be treated differently with respect to the thermo-hydraulic decoupling. After some analysis, the following hypotheses were chosen:

- **Primary phase separators:** the gas mixture resulting from the flashing of the geothermal fluid coming from the production wells contains a mass fraction of CO_2 around 30%; at the typical pressure of 11 bars, the partial pressure of the CO_2 is more than 1.5 bars. This implies that, due to the CO_2 partial pressure, a decrease in the tank pressure does not result in the boiling of the water, unless it is overwhelmingly rapid, but only in a superficial evaporation, which is much slower. Therefore, thermodynamic equilibrium between the two phases cannot be assumed, and a non-equilibrium model, in which the two phases exchange mass and energy proportionally to some suitable driving force, has to be considered; moreover, it is assumed that the liquid phase never undergoes boiling.
- **Secondary phase separators:** the CO_2 mass fraction is around 2% in the high pressure separators and less than 0.1% in the secondary separators: in this case it is possible to assume thermodynamic equilibrium between the two phases, which is a good approximation, at least at low frequencies. The resulting model is much simpler.
- **Reboiler bottom:** the situation here is very similar to the tank of the primary separators, thus the same modelling hypotheses apply.
- **Reboiler plates:** the modelling issues here are subtler: on one hand the CO_2 partial pressure is high (between 1.5 and 8.5 bars), so that the boiling of the liquid phase is impossible; on the other hand, the plates are specifically designed to bring the liquid and the gas into intimate contact: the gas-vapour mixture coming from below bubbles through the liquid layer, thus promoting

the mass and energy exchange between the two. However, it is known that the exchange efficiency is not unitary, i.e., the two phases do not actually reach the thermodynamic equilibrium state. A popular modelling approach is to assume equilibrium conditions anyway, and then to include in the column model a number of so-called *theoretical plates* which is smaller than the real one. Here, instead, no equilibrium condition has been assumed a-priori, and a Murphree-like efficiency parameter has been introduced, to take into account the fact that the plate behaviour is not ideal.

Note that, when using one-component fluid (such as water/steam), each flow can be specified in general by the couple (w, h). In the case of a two-component flow, three variables are needed (w, h, x_g), x_g being the CO_2 mass fraction.

The general modelling approach to the two situations (equilibrium and non-equilibrium) is now described. It will then be specialised for each component in Chap. 5.

4.2.1 Two-Phase Vessel in Equilibrium Conditions

The schematic diagram of the process is shown in fig. 4.3. The model equations are:

$$\frac{dM}{dt} = w_i - w_{lo} - w_{ao} \qquad \text{(Total mass conservation)} \qquad (4.38)$$

$$\frac{dM_g}{dt} = w_i x_{gi} - w_{lo} x_{glo} - w_{ao} x_{gao} \qquad \text{(Total } CO_2 \text{ mass conservation)} \qquad (4.39)$$

$$\frac{dE}{dt} = w_i h_i - w_{lo} h_{lo} - w_{ao} h_{ao} \qquad \text{(Energy conservation)} \qquad (4.40)$$

Now, three state variables must be chosen, to put the equations in the appropriate form; in this case the total pressure P, the CO_2 partial pressure P_g and the liquid level y have been selected. According to the hypotheses assumed to model the two components, and assuming all the flowrates are given, all the terms in (4.38)-(4.40) can be expressed as a function of the three state variables, leading to a model of the kind:

$$\frac{\partial M}{\partial P}\dot{P} + \frac{\partial M}{\partial P_g}\dot{P}_g + \frac{\partial M}{\partial y}\dot{y} = w_i - w_{lo} - w_{ao} \qquad (4.41)$$

$$\frac{\partial M_g}{\partial P}\dot{P} + \frac{\partial M_g}{\partial P_g}\dot{P}_g + \frac{\partial M_g}{\partial y}\dot{y} = w_i x_{gi} - w_{lo} x_{glo}(P, P_g) - w_{ao} x_{gao}(P, P_g) \qquad (4.42)$$

$$\frac{\partial E}{\partial P}\dot{P} + \frac{\partial E}{\partial P_g}\dot{P}_g + \frac{\partial E}{\partial y}\dot{y} = w_i h_i - w_{lo} h_{lo}(P, P_g) - w_{ao} h_{ao}(P, P_g) \qquad (4.43)$$

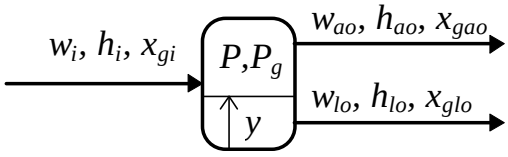

Figure 4.3: Two-phase vessel in equilibrium conditions

Now, since thermodynamic equilibrium is assumed, the pressure P is bound to have a slow dynamics, because a change in P implies a change in the energy stored in the tank, which is large. Therefore, there is no need to decouple the hydrodynamic equation energy from the other ones, so that the system (4.41)-(4.43), which is in the form of (3.66)-(3.67), can be put into a causal model, and thus integrated as explained in section 3.4.3. When the tank is connected to a hydraulic network, it will correspond to an imposed pressure node, and its pressure will be calculated independently of the other pressures of the network.

4.2.2 Two-Phase Vessel Outside the Equilibrium Conditions

The model equations for the primary phase separator, reboiler plate and reboiler bottom are very similar to each other. As an example, a model which is valid for the reboiler plate and bottom is discussed here. The model of the separator is slightly different because there is one only two-phase inlet flow, instead of three different inlet flows, which is then separated (see Sect. 4.1.3), with the resulting flows directly entering the corresponding control volume. These details will be discussed in Chap. 5. Since there is no thermodynamic equilibrium hypothesis, the pressure could change very rapidly, and therefore a hydrodynamic equation must be selected which best captures the interaction between the total pressure and the flowrates, to be included as a hydraulic sub-module in a hydraulic network.

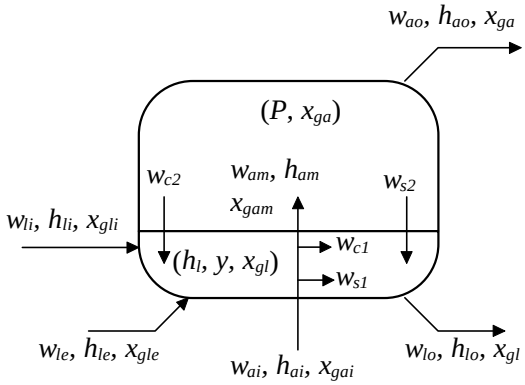

Figure 4.4: Reboiler plate schematic diagram

The schematic diagram of the reboiler plate is given in fig. 4.4; it is subdivided into two control volumes, the lower one containing the liquid phase, and the upper one containing the gas phase. Each flow is described by its mass-flow rate w, its specific enthalpy h and the mass fraction of CO_2 x_g, as usual. The gas mixture input flow (*ai* subscript) enters the liquid control volume, possibly releasing a water vapour condensation flow w_{c1} and a CO_2 solution flow w_{s1}, then enters the gas control volume (*am*); the gas mixture output flow goes out of the gas control volume. The liquid input flow (*li*), output flow (*lo*) and optional extra liquid input flow (*le*, used for recirculation flows) all directly go in and out of the liquid control volume. Moreover, a water vapour condensation flow w_{c2} and a CO_2 solution flow w_{s2} may exist at the interface between the two phases. Finally, note that the fraction of CO_2 dissolved in the liquid phase x_g may be more or less than predicted by Henry's law, giving rise to the corresponding mass transfer flows.

Six state equations would be needed to describe the component behaviour, being two mass equations and one energy equation for each control volume. However, the assumption of saturated vapour in the gas phase is equivalent to an implicit energy equation (i.e. it implies a heat exchange with the liquid phase such that the gas-vapour temperature is always equal to the saturation temperature of the vapour). Therefore, five ODE must be written to describe the behaviour of the component in full. The particular equations, and the corresponding state variables, must be accurately selected in order to maximise the decoupling among them, thus enabling a simpler numerical solution.

The proposed model ([Cas98a]) has five state variables: the pressure P, the mass fraction of CO_2 in the gas mixture x_{ga}, the specific enthalpy of the liquid water h_l, the level y and the mass fraction of CO_2 in the liquid mixture x_{gl}. Five balance equations can be written:

$$\dot{M}_a = w_{ai} - w_{ao} - w_{c1} - w_{s1} - w_{c2} - w_{s2} \tag{4.44}$$

$$\dot{M}_g = w_{ai}x_{gai} - w_{ao}x_g + w_{li}x_{gli} - w_{lo}x_{gl} + w_{le}x_{gle} \tag{4.45}$$

$$\dot{E} = w_{ai}h_{ai} - w_{ao}h_{ao} + w_{li}h_{li} - w_{lo}h_{lo} + w_{le}h_{le} \tag{4.46}$$

$$\dot{M}_{wl} = w_{li}(1-x_{gli}) - w_{lo}(1-x_{gl}) + w_{le}(1-x_{gle}) + w_{c1} + w_{c2} \tag{4.47}$$

$$\dot{M}_{gl} = w_{li}x_{gli} - w_{lo}x_{gl} + w_{le}x_{gle} + w_{s1} + w_{s2} \tag{4.48}$$

where (4.44) is the conservation of the total mass in the gas control volume, (4.45) is the conservation of CO_2 mass in the whole volume, (4.46) is the conservation of energy in the whole volume, (4.47) is the conservation of water mass in the liquid control volume and (4.48) is the conservation of CO_2 mass in the liquid control volume. The left-hand-side terms can be written as a function of the state variables of the component, taking into account the geometric

features of the volume, the water and steam tables, and the properties of the ideal gas CO_2:

$$M_a = M_a(P, x_{ga}, y) = \rho_a(P, x_{ga}) \cdot V_a(y) \tag{4.49}$$

$$M_g = M_g(P, x_{ga}, h_l, y, x_{gl}) = \rho_l(P, h_l) \cdot x_{gl} \cdot V_l(y) + \rho_g(P, x_{ga}) \cdot V_a(y) \tag{4.50}$$

$$\begin{aligned} E = E(P, x_{ga}, h_l, y, x_{gl}) = \rho_l(P, h_l) \cdot \left[h_l + x_{gl} h_{gl}(P, h_l)\right] \cdot V_l(y) + \\ + \rho_a(P, x_{ga}) \cdot h_a(P, x_{ga}) \cdot V_a(y) - PV \end{aligned} \tag{4.51}$$

$$M_{wl} = M_{wl}(P, h_l, y) = \rho_l(P, h_l) \cdot V_l(y) \tag{4.52}$$

$$M_{gl} = M_{gl}(P, h_l, y, x_{gl}) = \rho_l(P, h_l) \cdot x_{gl} \cdot V_l(y) \tag{4.53}$$

where ρ_l is the density of the liquid water, ρ_a is the density of the gas mixture, ρ_g is the density of the CO_2 in the gas mixture, V_l and V_a are the volumes of the liquid and gas phases, V is the total volume, h_a is the specific enthalpy of the gas mixture and h_{gl} is the specific enthalpy of the CO_2 in solution.

The right-hand-side terms can also be functions of the state variables of the plate above or of the plate below. Note that in the plates, due to the presence of weirs, the liquid flowrates w_{lo} are a function of the liquid level y only. In the reboiler bottom, instead, w_{lo} will be determined by the outlet valve.

Among all the possible mass conservation equations, (4.44) has been selected as the hydrodynamic equation, to be included in a hydraulic network for the following reasons:

- it is a mass conservation law of the appropriate kind (i.e. flowrates only appear in the right-hand side)
- the stronger mutual interaction between pressure and flowrates is between the gas phase storage and the gas-vapour mixture flowrates w_{ai} and w_{ao};
- selecting the total mass (gas+liquid phases) conservation equation would not have been a good choice, since the mutual influence between the pressure and the *liquid* flowrates w_{li}, w_{lo} and w_{le} is negligible, and the term depending on dy/dt going into the residual Λ would have been very large, giving rise to significant approximation errors in the pressure value during level transients.

The hydrodynamic node equation will then be:

$$\frac{\partial M_a}{\partial P} \dot{P} = w_{ai} - w_{ao} + \Lambda \tag{4.54}$$

$$\Lambda = -\frac{\partial M_a}{\partial x_g} \dot{x}_g - \frac{\partial M_a}{\partial y} \dot{y} - w_{c1} - w_{s1} - w_{c2} - w_{s2} \tag{4.55}$$

where Λ collects all the remaining terms of (4.44), which will be considered as weak, and thus taken equal to their last computed value, as usual in the decoupling approach. This also includes some derivatives, which implies that

the process variable database should memorise the last two values of the variable, in order to be able to provide the past value of the derivative. This can be critical, since a system of differential equations of order n is solved by a system of difference equations of order $n+k$, where k is the number of "past derivative values" included in the integration algorithm. As a consequence, as δt goes to zero, n poles of the discretised system will tend to the values given by the sampling transformation

$$z \rightarrow exp(s \cdot \delta t) \tag{4.56}$$

while the other k "parasite" poles could tend to any position in the z-plane, possibly leading to unconditional instability of the integration algorithm. It is therefore important that the coefficient of these derivatives and/or the derivatives themselves be small, in order to have a stable integration algorithm for sufficiently small δt. A study of this subject in a (simplified) model of heat exchanger is given in [Cst95].

Let now consider the plates only. The liquid inlet flowrates w_{li}, w_{le} will be exogenous variables, while the gas-vapour mixture flowrates w_{ai} will strongly depend upon the pressure drop across the plate bottom, i.e. on difference between the pressure of the plate under consideration and that of the plate below:

$$\Delta P = k_f w_{ai}^2 + \rho_l \cdot g \cdot y \tag{4.57}$$

which in turn depends partly on the friction caused by the gas flow through the plate holes, and partly on the liquid layer head. Equation (4.57) is then a branch-type hydraulic equation, where the gravitational acceleration g is a constant, while the liquid density ρ_l and the liquid level y are considered as weak variables.

The nodes and branches will be assembled in a network, with the appropriate boundary conditions (e.g. the top exhaust valve, and the feed pipes coming from the production areas). Once solved, all the values of the pressures and of the gas-vapour mixture at step $k+1$ are available.

Now consider equations (4.45)-(4.48). If the plate under consideration is part of a stack of 14 plates, it is clear that the solution of the equations depends both on the state of the plate above (which determines w_{li}, h_{li}, x_{gli}) and of the plate below (which determines h_{ai} and x_{gai}). Without any further decoupling, the 14 corresponding blocks of equations should be solved simultaneously. Consider again eq. (4.45), remembering that the new values of the gas-vapour flowrates and of the pressure (along with its derivative) have already been calculated:

$$\frac{\partial M_g}{\partial x_g}\dot{x}_g = w_{ai}x_{gai} - w_{ao}x_g + w_{li}x_{gli} - w_{lo}x_{gl} + w_{le}x_{gle} + \\ -\frac{\partial M_g}{\partial P}\dot{P} - \frac{\partial M_g}{\partial h_l}\dot{h}_l - \frac{\partial M_g}{\partial y}\dot{y} - \frac{\partial M_g}{\partial x_{gl}}\dot{x}_{gl} \tag{4.58}$$

All the unknown right-hand terms can be considered weak: since most of the CO_2 storage is in the gas phase, the terms x_{gl} is weak; the derivative of h_l is small (since the water storage implies a certain inertia in the enthalpy dynamics), and the term containing the derivative of y is small, since the water level cannot exceed the weir edge by more than some centimetres, which is negligible compared to the height of the gas control volume, which is about 80 cm. Under this assumption, the equations (4.58), relative to all the plates can be integrated as usual with Euler's implicit method to yield $x_{g,k+1}$ and put each in a causal sub-module. The corresponding equations are then solved in sequence from the bottom plate up to the top plate, thus obtaining the values of x_g at step *k+1*. At this point, the remaining blocks of equations (4.46)-(4.48) become causal; the system corresponding to each plate can be discretised and put into another causal sub-module.

The same considerations apply to the reboiler bottom, the only differences being in the calculation of the mass transfer flowrates w_{c1}, w_{c2}, w_{s1}, w_{s2}, and in the liquid outlet flowrate w_{lo}, which is determined by the output flash valve.

	P_1	P_2	P_f	w_v	w_{ai1}	w_{ai2}	x_{gaf}	x_{ga2}	x_{ga1}	h_{l1}	y_1	x_{gl1}	h_{l2}	y_2	x_{gl2}	h_{lf}	y_f	x_{glf}
w_v	X			X														
w_{ai1}	X	X			X													
w_{ai2}		X	X			X												
M_{a1}	X			X	X													
M_{a2}		X			X	X												
M_{ab}			X			X												
M_{gb}			X			X	X											
M_{g2}		X			X	X	X	X										
M_{g1}	X			X	X			X	X									
E_1	X	X		X	X			X	X	X	X	X						
M_{wl1}	X				X			X	X	X	X	X						
M_{gl1}	X				X			X	X	X	X	X						
E_2	X	X	X		X	X	X	X		X	X	X	X	X	X			
M_{wl2}		X				X	X	X			X	X	X	X	X			
M_{gl2}		X				X	X	X			X	X	X	X	X			
E_b		X	X			X	X						X	X	X	X	X	X
M_{wlb}			X				X							X	X	X	X	X
M_{glb}			X				X							X	X	X	X	X

Table 4.1: Incidence matrix of a simplified 2-plate plus bottom column.

These sub-modules can be solved sequentially from the top plate to the bottom plate, thus completing the solution of the whole reboiler system. Each reboiler plate then corresponds to two hydraulic sub-modules (a node and a branch) and to two causal sub-modules.

Table 4.1 shows the incidence matrix describing the solution scheme of a simplified 2-plate plus bottom column, with a top exhaust valve and a fixed gas-vapour mixture flowrate at the reboiler inlet. Subscripts 1, 2, *b* and *v* indicate top plate, mid plate, column bottom and exhaust valve, respectively. The weak variables have not been included in the matrix.

The corresponding solution scheme in the ProcSim environment is shown in Fig. 4.5 (left to right): first the hydraulic network is solved, then the sub-modules relative to x_g are solved in ascending order, then the sub-modules relative to the other variables are solved in descending order. This solution strategy is, to the author's knowledge, completely original.

In the case of the primary separator, since there is no cross-flow of liquid and gas-vapour mixture (unlike in the reboiler components), it is not necessary to decouple eq. (4.45), which can be solved simultaneously with (4.46)-(4.48), after the hydraulic network has been solved.

As a final remark, the problem of modelling a two-component process has been solved by decoupling the fluid composition (x_g) from the pressure-flowrate dynamics, in the same way as the fluid energetic content (h). In the real plant simulation, this approach gave rather satisfactory results, resulting in an upper stability limit for the integration step size of 0.85 s, which was then reduced to 0.6 s to add an adequate safety margin.

A completely different approach would be to generalise the method described in section 3.4.2, dealing with two-component hydraulic networks. In

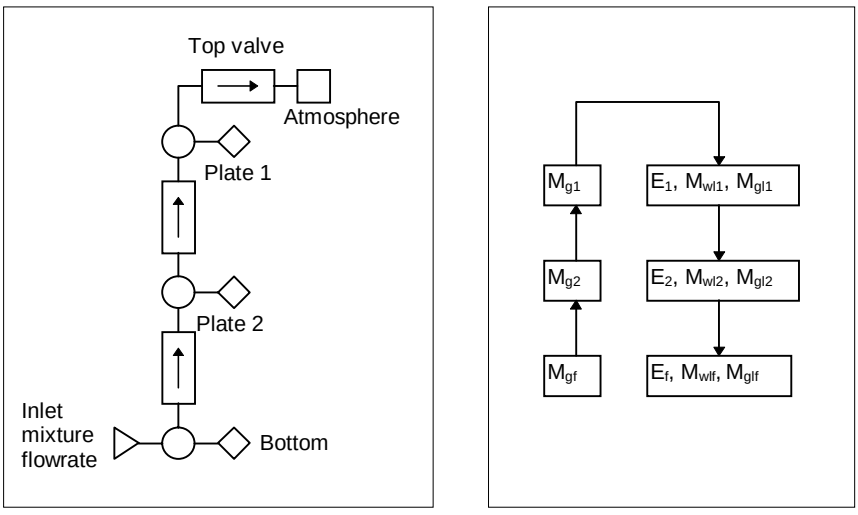

Figure 4.5: Reboiler solution sequence

this generalised approach, two mass conservation equations should be considered for each node, and partial derivatives of the flowrate with respect to the node pressure and the mass fraction of the flow inside each branch should be considered. Following this idea, a generalised hydraulic network solving algorithm could have been devised. This task was not undertaken because it would have implied a major rewriting of a significant portion of the simulation environment, and its effectiveness in enhancing the numerical stability of the integration is unknown.

4.3 Long Pipelines with Wave Propagation

Another issue arising from the Latera process was the correct modelling of the very long reinjection pipelines. Since the total travelling time of the pressure and flow waves is around 10 s, a distributed model must be employed, obtaining a system of PDE's. The pipeline is thermally insulated, guaranteeing a temperature drop of less than 1 °C between the head and the tail. Therefore, the interest for the simulation lies only in the hydrodynamic equations, while the thermal equation is a trivial equation $T=const$.

The flow of a liquid in a pipeline is described by the following mass and momentum conservation PDE's [Str83], [Fer90], in which the kinetic energy term has been neglected, since the fluid speed is much less than the speed of sound:

$$\frac{\rho g A}{c^2}\frac{\partial H}{\partial t}+\frac{\partial w}{\partial x}=0 \tag{4.59}$$

$$\frac{\partial w}{\partial t}+\rho g A\frac{\partial H}{\partial x}+Fw|w|=0 \tag{4.60}$$

$$H=\frac{P}{\rho g}+z\;;\quad F=\frac{c_f\omega}{2\rho A^2} \tag{4.61}$$

where c is the speed of sound along the pipe (including the effect of pipe wall elasticity), ρ is the water density, z is the elevation above a reference level, H is the total water head, ω is the pipe perimeter, A is the (uniform) pipe cross-section and c_f is Moody's friction factor.

Equations (4.59)-(4.60) can be reduced to ODE by the method of the characteristic lines, i.e. taking $\delta x / \delta t = \pm c$, and then integrated along a time step $\delta t = \delta x / c$, yielding the two following equations, which are discretised both in time and in space:

$$\begin{aligned}&\mathrm{A}\rho\,\mathrm{g}\left[H_L(t+\delta t)-H_R(t)\right]-c\left[w_L(t+\delta t)-w_R(t)\right]+\\&-\delta x F w_R(t)|w_R(t)|=0\end{aligned} \tag{4.62}$$

$$\begin{aligned} &\mathrm{A}\rho\, \mathrm{g}\left[H_R(t+\delta t) - H_L(t)\right] + c\left[w_R(t+\delta t) - w_L(t)\right] + \\ &+\delta x F w_L(t)\left|w_L(t)\right| = 0 \end{aligned} \tag{4.63}$$

where the subscript L means Left (i.e. evaluated at the left-hand side of the spatial element of length δx) while the subscript R means Right. Note that the only approximation made in obtaining (4.62) and (4.63) is that, for the considered pipe segment, the friction head losses have been computed by using either the right or the left value of the mass flow-rate, instead of the spatial integral along the segment: this may be shown to yield very small errors as friction is a secondary effect in pressure and flow dynamics for typical pipelines. Therefore, the length δx of the generic pipe segment may be chosen quite large (in our case δx=0.85 km), without significant loss of accuracy. The interesting feature of eq. (4.62)-(4.63) is that they are inherently discrete-time equations, so that they can be included seamlessly in the fixed time step simulation context of ProcSim. Eq. (4.62)-(4.63) will be arranged in order to obtain: two hydraulic sub-modules of branch type, to connect the head and the tail of the pipe to an ordinary hydraulic network, and a causal sub-module, computing the propagation of pressure (head) and flowrate waves along the pipe. Note that the finite speed of sound completely decouples the solution of the two hydraulic networks to whom the pipe head and tail are connected, without any approximation whatsoever. This will be reflected by the sub-module structure. The details of the implementation in the ProcSim environment will be given in Section 5.4.3.

4.4 Hydraulic Networks with Complete Flow Cut-Off

A recurrent situation in the Latera process is the need to model hydraulic networks, constituted by a series of valve and pipe components, (see, e.g., Fig. 4.6), in which the flow can be completely cut off by suitable stop-valves, in order to isolate certain plant units from others.

Most of these branch-type components appearing in those networks are models of head losses which are quadratic with the flowrate. A typical example is the ordinary regulating valve with liquid flow:

$$w = f(\theta) k \sqrt{\rho \Delta P}\,; \tag{4.64}$$

where θ is the valve opening, $f(\theta)$ is the flow characteristic, k is a constant, ρ is the water inlet density and ΔP is the pressure drop across the valve. In general,

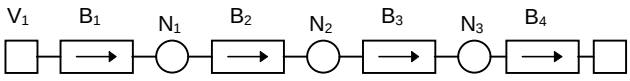

Figure 4.6: "Series" hydraulic network

as will be explained in more detail in Sect. 5.3, all the valve components (liquid and gas, both in normal and choked flow), along with the friction models for pipes, can be given a general formulation which is very similar:

$$w = f(\theta) k \sqrt{z}\ ; \quad z = \frac{\Delta P}{\Delta P_{nom}} \tag{4.65}$$

where ΔP_{nom} is the nominal pressure drop, while k is only weakly dependent on the input and output pressures. Moreover, some valve might be associated to a check valve, i.e. a device which allows the flow in one direction only.

Assume, for instance that B_1 and B_4 are stop valves, B_2 is a pipe carrying liquid water, and B_3 is a regulating valve. Suppose now that B_4 is completely closed, that is θ_4=0. The corresponding operating point should be zero flowrate and zero pressure drop across every branch. If model equations like (4.65) are employed, this causes the numerical integrator to blow up, since the contribution to the network Jacobian (see Sect. 3.4.2) will be either indeterminate or infinite, as can be seen clearly by examining the following equation:

$$\frac{\partial w}{\partial P_{in}} = f(\theta) \left[\frac{\partial k}{\partial P} \sqrt{z} + k \frac{1}{2 \Delta P_{nom} \sqrt{z}} \right]; \tag{4.66}$$

This problem can be solved by introducing a suitable regularisation in (4.65), i.e. performing the following substitution:

$$\sqrt{z} \to \frac{z}{\sqrt{|z| + b}} \cong \begin{cases} \dfrac{z}{\sqrt{b}}, & |z| << b \\ \operatorname{sgn}(z) \sqrt{|z|}, & |z| >> b \end{cases}; \tag{4.67}$$

when the pressure drop is greater than b times the nominal value, (4.65) holds with a good approximation, while for small values of ΔP, a linear relationship holds instead, which by the way makes sense from a physical point of view, since laminar flow takes place instead of turbulent flow in the valve. The contribution to the Jacobian will therefore be finite even for zero flow, giving the correct solution of zero pressure drop across all the other branches:

$$\frac{\partial w}{\partial P_{in}} = f(\theta) \left[\frac{\partial k}{\partial P} \frac{z}{\sqrt{|z| + b}} + k \frac{|z| + 2b}{2 \Delta P_{nom} \sqrt{\left(|z| + b^3 \right)}} \right]; \tag{4.68}$$

Equation (4.67) leads to a symmetrical pressure drop for w<0: this is necessary to ensure numerical robustness to the network solver, since it is possible that, during Newton iterations, the flowrate momentarily assumes (small) negative values.

Consider now the problem of modelling a check valve: its equations are

$$w = \begin{cases} f(\theta)k\sqrt{z}, & w \geq 0 \\ 0, & w < 0 \end{cases} \tag{4.69}$$

Numerical problems here are even more serious, since the derivative is infinite at $z=0^+$, and zero at $z=0^-$. Again, a suitable regularisation must be introduced; for positive z:

$$\sqrt{z} \to \frac{z^2}{\sqrt{|z^3| + b^3}} \cong \begin{cases} \dfrac{z^2}{\sqrt{b^3}}, & 0 \leq |z| << b \\ \sqrt{|z|}, & |z| >> b \end{cases} \tag{4.70}$$

while for $z<0$, $w=0$. The contribution to the Jacobian for $z>0$

$$\frac{\partial w}{\partial P_{in}} = f(\theta)\left[\frac{\partial k}{\partial P}\frac{z^2}{\sqrt{|z^3| + b^3}} + kz\frac{z^3 + 4b^3}{2\Delta P_{nom}\sqrt{\left(z^3 + b^3\right)^3}}\right]; \tag{4.71}$$

is zero at $z=0^+$, thus ensuring that the function is $C^1(\Re)$.

The ideal relationship (4.65), together with the two approximations (4.67) and (4.70) (with b=0.01) are shown in Fig. 4.7 for $-0.1 < z < 1$ (left), and in the neighbourhood of $z=0$ (right). It is clear that the relative error for $\Delta P > 0.1\Delta P_{nom}$ is negligible, while the characteristics behave as needed around $\Delta P=0$.

A reasonable value for the parameter b is 0.01; however, in some situations, it should be increased to facilitate the convergence of Newton's method iterations (the more a function is linear, the faster Newton's method will converge). This is true in particular for the turbine valves PV500XA: their

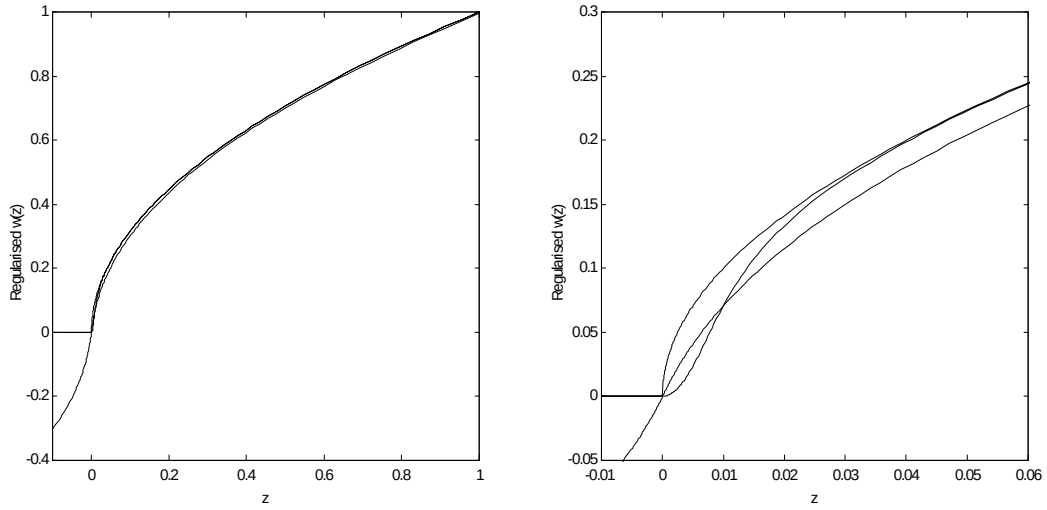

Figure 4.7: Regularised characteristics

nominal ΔP (when fully open) is very low, in order to avoid costly pressure drops at the turbine inlet. In this case the characteristic would be less accurate, but this is not a problem, since the pressure drop is small anyway; when the valves are closed (i.e. when the pressure controllers goes out of saturation to actually control the separator pressures), values of z much greater than unity result, so that the approximation is very good, where is needed.

One very important remark must then be made. Consider again the network in Fig. 4.6. It is rather obvious that, if both B_1 and B_4 are closed, the pressures of the nodes N_1, N_2, N_3 are indetermined; this will correspond to a singular Jacobian matrix, and will lead to a numerical blow-up of the solver. This would not happen if all the three nodes had associated capacitance, since then the $\alpha/\delta t$ contribution to the Jacobian would make it non-singular, thus leading to a constant pressure in the nodes themselves. The conclusion is that, unless all the nodes are associated with components characterised by mass storage, no more than one valve can be closed at the same time. The same situation arises if B_1 is a closed stop valve and B_4 is a check valve: the closure of B_1 implies $w = 0$; in the neighbourhood of this operating point, the regularised characteristic of the check valve is equivalent to that of a closed valve, since its first-order approximation is just $w = 0$. This again would bring to a singularity in the network Jacobian.

Summing up, linear networks like the one of figure 4.6 cannot have more than one closed or check valve at the same time, to avoid numerical problems in the solution. Note that these numerically pathological situations also correspond to physically pathological situations, since it makes no sense, during normal plant operation, to close more than one valve on a segmented pipeline, or to have more than one check valve. Extreme situations, such as maintenance configurations or initial start-up of the line are of course outside the scope of this discussion.

4.5 Special Network Structures

4.5.1 Flow Splitting

Another recurrent configuration in the Latera plant is the one sketched in Fig. 4.8: a tank (e.g. one of the phase separators) is connected to more than one output pipes, e.g. one leading to a pump and another leading to a flashing valve. Since the tank model has only one liquid outlet, the standard solution would be the one of Fig. 4.9.

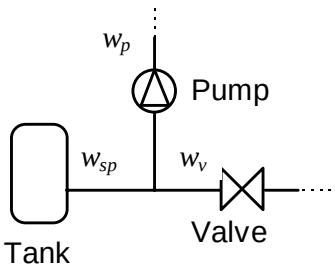

Figure 4.8: Flow splitting

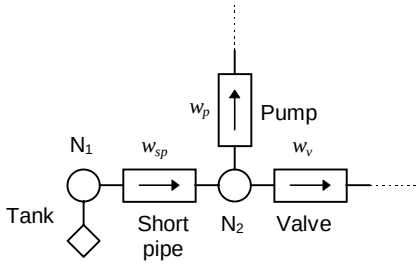

Figure 4.9: Hydraulic network

This solution is not satisfactory, since the pressure drop across the short connecting pipe is irrelevant (and its very small resistance could lead to numerical ill-conditioning of the network Jacobian); moreover, its dimensional parameters (length, diameter etc.) might not be available. Therefore, this solution should be avoided. Moreover, due to the structure of the branch-type module equations, it is not possible to model pipes having $\Delta P = 0$, because that equation does not fit the standard form $w = f(P)$, being its singular case. An alternative approach would be to build a tank model having a parametric number of outputs, but this is somewhat artificial, and is not compliant with the modular approach used within the ProcSim environment, in which every component model should be independent of the components to which it is connected.

The following solution scheme has been devised. The nodes N_1 and N_2 are merged in a single node N, whose pressure will correspond to the tank pressure. The hydraulic network can be solved without any particular problem, calculating the new values of the tank pressure and of the flowrates w_p and w_v. A *causal* sub-module is then introduced, whose purpose is to calculate the outlet flowrate

$$w_{sp} = w_p + w_v, \tag{4.72}$$

which is needed by the causal sub-module of the tank to calculate all its remaining variables (enthalpy, level, etc.). This sub-module must be executed before any other causal sub-modules relative to the components in the network, in order to make the value of w_{sp} at time step $k+1$ available where needed. The solution scheme is sketched in fig. 4.10.

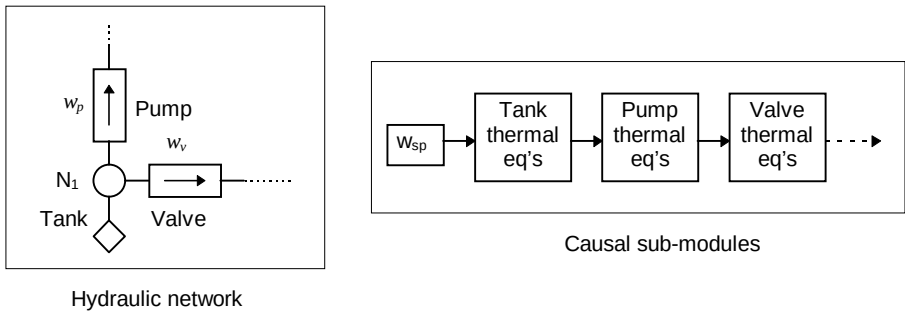

Figure 4.10: Solution scheme with flow splitting

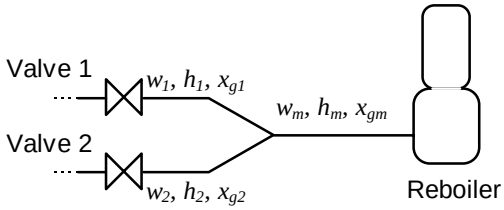

Figure 4.11: Flow mixing

4.5.2 Flow Mixing

The dual situation is also present in many points of the Latera Plant (e.g. at reboiler inlet). Consider the diagram of Fig. 4.11:
again, the reboiler model has one gas-vapour inlet, but it is not convenient to include the short pipe connecting the reboiler to the mixing node, for the same reasons stated above. As before, w_1 and w_2 can be computed without any problem by the hydraulic network. Subsequently, a causal sub-module is needed to calculate the flowrate w_r, along with the mixture enthalpy and CO2 mass fraction after mixing:

$$w_m = w_1 + w_1 \tag{4.73}$$

$$h_m = (w_1 h_1 + w_2 h_2) / w_m \tag{4.74}$$

$$x_{gm} = (w_1 x_{g1} + w_2 x_{g2}) / w_m \tag{4.75}$$

these variables are then used to solve the causal equations of the reboiler, as shown in the solution scheme of Fig. 4.12.

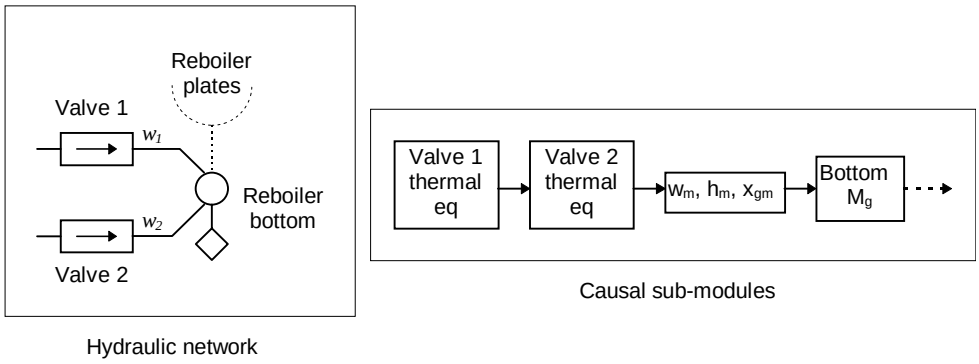

Figure 4.12: Solution scheme for the reboiler inlet

5. MODELLING OF PROCESS COMPONENTS

5.1 Reboiler

The reboiler is the most unusual component for a power generation plant. Basically, from the point of view of mechanical design, it is a plate column, like those used for distillation in the chemical or petro-chemical industry. It is divided into an upper section, with liquid flowrates around 100-200 kg/s, and a lower section, with liquid flowrates around 400-900 kg/s. The eight upper section trays, or plates, are of the so-called *four-pass* type [Per85]: the liquid flows downwards through two or three alternate downcomers, comes into contact with the gas-vapour mixture bubbling from the plate below and then overflows the plate weirs, falling down the next downcomer (Fig. 5.1). This means, by the way, that the liquid flowrate is a function of the liquid build-up in the plate. The six lower trays, instead, are of the so called *dual-flow* type [Per85]: they are very simple perforated plates, where an alternate pulsating flow of rising vapour and falling liquid takes place. They are preferred in situations where the liquid flowrate is huge (Fig. 5.2). The bottom of the column collects the hot water flow from the plates above, providing some storage which is necessary to cope with the flowrate transients. For many reasons, it is out of question here to model explicitly the complex geometry of the flows in the plate, along with complex physical phenomena such as frothing and flooding. These calculations were performed (in steady-state conditions) by

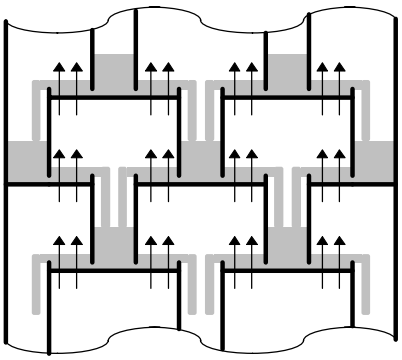

Figure 5.1: Four-pass plate column

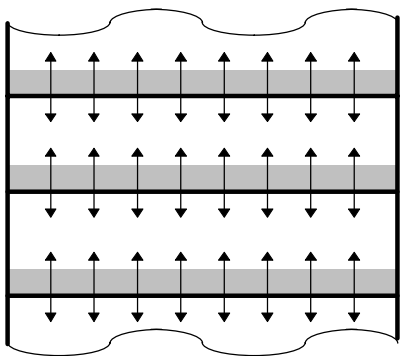

Figure 5.2: Dual-flow plate

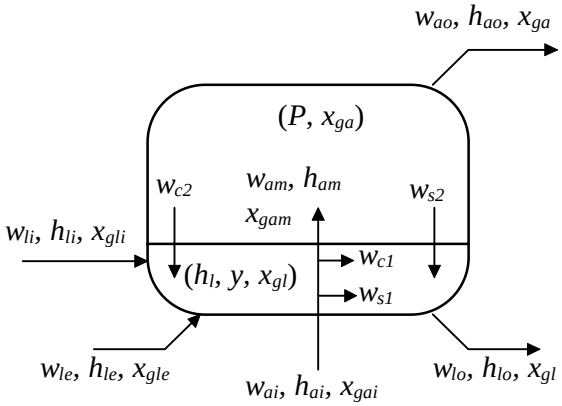

Figure 5.3: Reboiler plate schematic diagram

the designers of the column, using specialised (and proprietary) code, which is not available, and is probably too complex to be extended to dynamic operation. Moreover, the formulae used for component sizing are often devised in order to leave a certain safety margin, rather than to give exact results, which is instead what is needed for accurate simulation. Some simplifying assumptions have then be made, and some of the simplified model parameters have been tuned in order to match the steady-state operating points specified by the column design documentation.

5.1.1 Reboiler Plate

The flow diagram of the plate model, already introduced in Section 4.2.2, is again given in Fig. 5.3.

The following simplifying assumption have been made, in order to obtain a manageable model:

- The liquid and water phases are perfectly separated by a planar surface; their content is perfectly homogeneous (zero-dimensional model). The liquid control volume takes into account both the plate and the downcomer hold-up.
- The liquid output flowrate wlo is a linear function of the level *y*, whose coefficients are tuned according to the two operating points specified in the design document. This is a reasonable approximation for the upper plates; for the lower plates, instead, the flowrate is a function of both the level *y* and of the gas-vapour inlet flowrate w_{ai}. This function is rather complex, subject to high uncertainty, and moreover it introduces a strong mutual coupling between the hydraulic equations and the causal equations. Therefore, a linear level-flowrate relationship has been used also for the lower plates, with a

high value of the coefficient, so that the level is always approximately equal to the nominal level.

- Since the model will not be used for start-up simulation, there will always be a significant flow of gas-vapour mixture through the liquid layer; therefore, it is assumed that the energy and mass transfer between the liquid and the gas phase only takes place there, so that the superficial condensation and solution flowrates w_{c2} and w_{s2} are neglected.
- The two phases are not in thermodynamic equilibrium conditions: the steam fraction is always considered at saturation (see sect. 4.1.2), but the liquid phase can be colder or hotter than the temperature of the saturated steam fraction and its dissolved CO_2 content may be greater or less than the equilibrium value given by Henry's law.
- The mass and energy transfer between the liquid and the gas-vapour mixture is governed by very complex laws (see, e.g., [Col81]), which however are too cumbersome to be used for dynamic simulation. Murphree-like efficiency [Luy90] is then assumed, i.e. the condensation flowrate w_{c1} is a fraction of the theoretical one, which would bring the incoming gas-vapour mixture into an equilibrium condition with the liquid layer. After the release of the condensation flowrate w_{c1} and of the solution flowrate w_{s1}, the gas-vapour mixture enters the gas control volume (subscript *am*).
- Due to the huge dimensions of the reboiler (having a diameter ranging from 3.5 m to 4.6 m), to the relative thinness of the plates (2 mm), and to the very large flowrates involved, the thermal interaction between the fluid and the metal has been neglected. Note that the reboiler is covered by a thermal insulation, so that there is no heat flow from the internal fluid to the atmosphere.

The describing state equations are then the general (4.44)-(4.48), repeated here for convenience

$$\dot{M}_a = w_{ai} - w_{ao} - w_{c1} - w_{s1} - w_{c2} - w_{s2} \tag{5.1}$$

$$\dot{M}_g = w_{ai}x_{gai} - w_{ao}x_g + w_{li}x_{gli} - w_{lo}x_{gl} + w_{le}x_{gle} \tag{5.2}$$

$$\dot{E} = w_{ai}h_{ai} - w_{ao}h_{ao} + w_{li}h_{li} - w_{lo}h_{lo} + w_{le}h_{le} \tag{5.3}$$

$$\dot{M}_{wl} = w_{li}(1-x_{gli}) - w_{lo}(1-x_{gl}) + w_{le}(1-x_{gle}) + w_{c1} + w_{c2} \tag{5.4}$$

$$\dot{M}_{gl} = w_{li}x_{gli} - w_{lo}x_{gl} + w_{le}x_{gle} + w_{s1} + w_{s2} \tag{5.5}$$

the left-hand sides are exactly the same as in (4.49)-(4.53), the gas-vapour inlet flowrate obeys (4.52):

$$\Delta P = k_f w_{ai}^2 + \rho_l \cdot g \cdot y \tag{5.6}$$

and the following assignments are made:

$$h_{lo} = (1 - x_{gl})h_l + x_{gl}h_{gl}(P, h_l) \tag{5.7}$$

$$h_{ao} = h_a(P, x_{ga}) \tag{5.8}$$

$$w_{lo} = k_l \cdot (y - y_o) \tag{5.9}$$

The Murphree-like plate efficiency coefficient η can be defined as:

$$\frac{x_{gam} - x_{gai}}{x_{ga}^* - x_{gai}} = \eta \tag{5.10}$$

where x_{gam} is the CO_2 mass fraction of the mixture actually entering the gas phase and x_{ga}^* is the CO_2 mass fraction corresponding to the equilibrium condition with the liquid phase. Application of mass balances for water and CO_2 through the liquid layer leads to the following equations:

$$x_{gam} = x_{gai} + \eta(x_{ga}^* - x_{gai}) \tag{5.11}$$

$$w_{c1} = \frac{w_{ai}(x_{gam} - x_{gai}) - w_{s1}(1 - x_{gam})}{x_{gam}} \tag{5.12}$$

This choice seems reasonable, since the condensation flow-rate is proportional to the gas mixture flow-rate w_{ai} and to the quantity (x_{ga}* - x_{gai}), which is related to the temperature difference between the incoming gas flow and the liquid layer. If η = 1, an equilibrium model is obtained.
Due to the low solubility and heat of solution (which is actually neglected), the CO_2 flow-rate w_{s1} is a side effect of the process, compared with the main phenomenon of water vapour condensation. As a first approximation, it can be thought of as proportional to the gas mixture flow-rate w_{ai} and to the driving force generated by the difference between the CO_2 partial pressure P_g of the gas mixture entering the gas control volume, and the equilibrium pressure corresponding to the CO_2 mass fraction in the liquid x_{gl}:

$$w_{s1} = k_{s1}w_{ai}\left(P_g(P, x_{gam}) - H(T_l(P, h_l)) \cdot x_{gl}\right) \tag{5.13}$$

where $H(T_l)$ is Henry's constant for CO_2 in water, which is a function of water temperature. When k_{s1} goes to infinity, one obtains the equilibrium condition $P_g = H \cdot x_{gl}$, i.e. Henry's law. Since the solubility of CO_2 in water is rather low, the modelling accuracy of eq. (5.13) is anyway not an issue.

The selection of the hydrodynamic equation and the solution scheme are accomplished as described in section 4.2.2.

5.1.2 Reboiler Bottom

The reboiler bottom model is very similar to the plate model, except for two aspects. First, there are no weirs, so that the liquid outlet flowrate depends

on the outlet valve; second, the entering gas-vapour phase does not bubble through the liquid, but enters directly the gas control volume. Therefore

$$w_{c1} = 0;\ w_{s1} = 0\ . \tag{5.14}$$

Conversely, it is necessary to take into account the superficial phase exchange flows w_{c2} and w_{s2}; during normal operation, the mean residence time of the water and of the gas-vapour pressure is around 10-20 second, so this exchange is rather small. Therefore, a great modelling accuracy is not needed, and the two flows can be simply modelled as proportional to their corresponding driving forces:

$$w_{c2} = k_{c2} \cdot \left[T_a(P, x_{ga}) - T_l(P, h_l) \right] \tag{5.15}$$

$$w_{s2} = k_{s2} \cdot \left[\frac{P_g(P, x_{ga})}{H(T_l(P, h_l))} - x_{gl} \right] \tag{5.16}$$

where T_a is the temperature of the gas-vapour mixture and k_{c2}, k_{s2} are two suitable proportionality constants.

The solution scheme for the reboiler bottom is the same as in the reboiler plate, except that w_{lo} is not computed by the causal sub-module, but is instead a *weak* variable, whose value is computed by the hydraulic network to which the liquid outlet is connected.

5.1.3 Reboiler Assembly

The reboiler sub-modules are assembled in a solution scheme as explained in section 4.2.2 (Fig. 5.4, left to right). Note that the hydraulic network (describing the gas-vapour mixture flow) extends beyond the reboiler inlet up to the primary separators: the resistance of the connecting pipes is too low to permit the splitting of the network without causing instability. The liquid flowrates are either calculated by the causal sub-modules, or considered weak, in the case of the bottom output flowrate and of the two recirculation inlets in the first and eighth plate. This is possible since their mutual interaction with the hydraulic equations is negligible (e.g. a change in the plate pressure causes a change in the recirculation flowrate, but not vice versa), so that they can be decoupled and computed separately by the hydraulic networks describing the recirculation loops and the liquid outlet network. Note that, due to the downcomer structure, the liquid flow leaving one plate enters directly the liquid phase control volume of the plate below, and only then the phase exchange takes place.

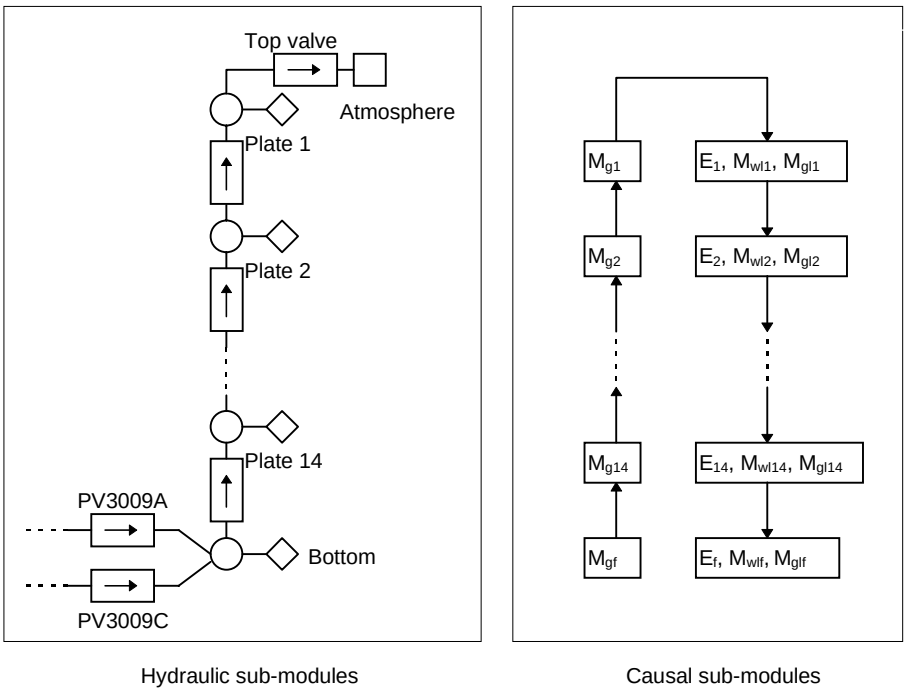

Figure 5.4: Reboiler solution sequence

The efficiency coefficient η has been tuned in order to obtain steady state column boundary conditions (in terms of flowrates and temperatures) equal to those of the design document. The same document suggests that the efficiency of the lower plates will be less than that of the higher ones, due to their simpler structure. This led to a choice of $\eta = 0.57$ for the eight upper plates and $\eta = 0.4$ for the lower six plates. These parameters will be better tuned once some experimental data become available.

In the absence of any further information, the value of k_{s1} has been tuned in order to have a CO_2 exchange flow approximately equal to half of the equilibrium value in the top plate, where the CO_2 partial pressure is higher, and the entering water is almost CO_2-free, coming from the low-pressure phase separator. The values of k_{c2} and k_{s2} for the reboiler bottom have been tuned in order to have exchange flowrates equal to one tenth of the exchange taking place in the reboiler plates.

5.2 Phase Separators

The phase separators are used to separate the two-phase flow which is found after each production well head valve (primary separators) and after each flashing of hot water (secondary generators). They are composed of a Webre-type cyclone separator [Per85], immediately followed by a tank, providing a liquid storage (equivalent to around 20 seconds at the nominal liquid flowrate)

which is necessary to cope with the flowrate transients. The models of primary and secondary separators are quite different. In the former, thermodynamic equilibrium is not assumed, so that it is first necessary to compute the variables relative to the separation of the two-phase inlet fluid, which takes place under equilibrium conditions, and then use them as liquid and gas inlet for a tank model such as the one of Sect. 4.2.2. In the latter, instead, since thermodynamic equilibrium is assumed also in the tank, a simpler model can be used. The assumption which are common to the two models are the following:

- The liquid and water phases are perfectly separated by a planar surface; their content is perfectly homogeneous (zero-dimensional model). The volume of the Webre separator is considered as being part of the gas control volume of the tank; the phase separation process is assumed to take place without any mass storage, so that the equations modelling the process are algebraic ones (see Section 4.1.3)
- The two-phase inlet flowrate depends weakly on the separator pressure; this can be assumed since in every case, a valve under critical or near-critical conditions can be found just upstream the separator. Therefore the input flowrate is a weak variable in the model.
- The thermal exchange with the metal walls is neglected.
- The difference between the gas-vapour mixture pressure and the liquid outlet pressure, due to the water head, is taken into account. This is very important, since water coming out of the separators (in particular the secondary ones) is very close to the saturation state, so that a head of some meter can make quite a difference in the behaviour of the downstream valve.

5.2.1 Primary Separators

The flow diagram of the primary separator is shown in fig. 5.6. The inlet flow, characterised by its flowrate w_{in}, its enthalpy h_{in} and its CO_2 content x_{gin} is first separated into its two phase components at the separator pressure, (which corresponds to the process taking place in the Webre cyclone separator), according to the method and equations given in Section 4.1.3; the partial pressure P_v in the separator is memorised as a state variable, in order to be used at each step as an initial guess for Newton's method iterations. The two flows then enter the corresponding control volumes of a two-phase vessel model, which is identical to the model of the reboiler bottom, from the point of view of the involved equations. Note that the partial pressure of the vapour in the Webre separator (which is an algebraic function of the inlet flow characteristics and of the pressure) is different from that of the tank, which has its own dynamics due to mass storage. The only equation that has to be added

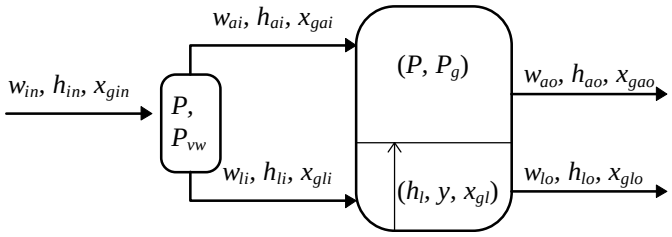

Figure 5.5: Primary separator flow diagram

to the model is the calculation of the pressure at the water outlet, taking into account the additional water head:

$$P_{lo} = P + \rho_l g\left(h_o + y\right) \tag{5.17}$$

where P_{lo} is the pressure at the liquid outlet, r_l is the liquid density, g is the gravitational acceleration, and h_0 is the height of the zero reference for the level above the liquid outlet.

There is one slight difference in the way the equations are solved, though; the mass conservation equation for the gas-vapour mixture (5.1) is again selected for inclusion in a node-type hydraulic sub-module, and solved together with the other network equations; conversely, since there is no cross-flow of liquid and vapour, there is no need to decouple (5.2) from (5.3)-(5.5); hence, one causal sub-module, including the simultaneous solution of (5.2)-(5.6) will be needed, instead of the two needed by the components of the reboiler.

5.2.2 Secondary Separators

The model of a phase separator under thermodynamic equilibrium has already been discussed in Section 4.2.1, together with the procedure to obtain a causal sub-module computing its state and output variable. The schematic flow diagram is shown in Fig. 5.6 for convenience

The only equation that has to be added to the model has to do with the water head:

$$P_{lo} = P + \rho_l g\left(h_o + y\right) \tag{5.18}$$

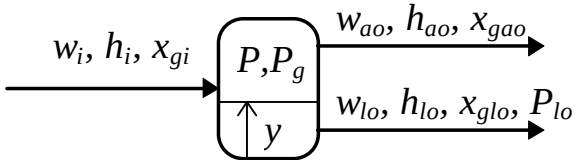

Figure 5.6: Secondary separator flow diagram

where P_{lo} is the pressure at the liquid outlet, r_l is the liquid density, g is the gravitational acceleration, and h_0 is the height of the zero reference for the level above the liquid outlet.

For the reasons already explained in Section 4.2.1, this component does not have a hydraulic sub-module. In general, the separator will be connected to two hydraulic networks, one for the liquid and the other one for the gas-vapour mixture. In these two networks, the separator will be represented by an imposed pressure node, whose imposed value will be P_{lo} and P, respectively.

5.3 Valves

Many different kinds of valves are employed in the whole Latera plant. The models describing them are different, due to functional reasons (regulating valves vs. on-off valves), working fluid (liquid, vapour, gas-vapour mixture, two-phase flow) and operating regime (normal vs. choked, or critical, operation).

The models for the control valves have been based on the American standard ISAS75.01 [ISA75], which is very similar to the European Standard IEC 534. The equations are intended mainly for component *sizing*, but their accuracy is good enough for simulation; in most cases, some rearrangement of the equation is needed to make them easier to use for simulation purposes. The exact flow characteristics (valve *stem position* or *travel* vs. flowrate under standard test conditions) have been included in the models, taking also into account the corrections due to the fittings attached to the valve inlets and outlets, to adapt them to the usually larger diameter of the pipes.

In the case of the flashing valve followed by an orifice, no recognised standard equations exist to describe the two-phase flow through an orifice, [Mur91], so that an approximate model of the valve-orifice complex has been devised.

In the case of on/off valves, which are used as stop valves to isolate a plant unit from another one, a very simplified model has been adopted, which can be used with every kind of working fluid.

For all the kinds of valves, the energy conservation equation is simply:

$$h_{in} = h_{out} \tag{5.19}$$

and the mass fraction of CO2 is conserved between inlet and outlet, so that

$$x_{gin} = x_{gout} \tag{5.20}$$

Equations (5.19)-(5.20) therefore make up the thermal sub-module for all the valve components.

5.3.1 Liquid Water Valve

According to [ISA75], the flow rate of a liquid through a given control valve, assuming turbulent flow (which is always the case with water) is the following:

$$w = NF_p(C_v)C_v(\theta)\sqrt{\rho(P_{in} - P_{out})} \tag{5.21}$$

where w is the mass flowrate, N is a factor depending on the units used in the equation (English or SI units), F_p is the *piping geometry factor*, describing the head loss on the valve fittings, in case the inlet and outlet pipe diameters are different from that of the valve, C_v is the valve flow coefficient, which is a function of the travel θ, ρ is the liquid density at the valve inlet and P_{in}, P_{out} are the pressures at the valve inlet and outlet. Since the C_v coefficient is a function of the valve travel, it is possible to write:

$$Cv(\theta) = f(\theta)\, C_{vmax} \tag{5.22}$$

where $f(\theta)$ is a dimensionless function with range (0–1), describing the valve flow characteristic. The valve travel can be expressed in percent or per unit, according to the user preferences.

The factor F_p, whose effect is noticeable only when the valve is almost completely open, depends on C_v according to the following equation:

$$F_p\left(C_v(\theta)\right) = \frac{1}{\sqrt{1 + AC_v^2(\theta)}} = \frac{1}{\sqrt{1 + \alpha \cdot f^2(\theta)}} \tag{5.23}$$

$$\alpha = A \cdot C_{v\max} \tag{5.24}$$

where A is a suitable constant, depending on the diameters of the valve and of the fittings.

The data obtained from the valve manufacturer are the flow characteristic of the valve without the attached fittings (i.e. $f(\theta)$), plus some calculated operating points, including the valve travel, usually at full opening (100%) and at some intermediate value (50-70%), and the corresponding value of Cv. These data can be used to obtain the values of C_{vmax} and A, thus leading to the valve model employed by the simulator:

$$w = \tilde{f}(\theta) \cdot \tilde{C}_v \sqrt{\rho(P_{in} - P_{out})} \tag{5.25}$$

where

$$\tilde{C}_v = C_{v\max} F_p(C_{v\max}) = \frac{w_{\max}}{\sqrt{\rho(P_{in} - P_{out})}} \tag{5.26}$$

$$\tilde{f}(\theta) = f(\theta)\frac{\sqrt{1+\alpha}}{\sqrt{1+\alpha \cdot f^2(\theta)}} \tag{5.27}$$

Eq. (5.27) shows how the valve flow characteristic is warped by the effect of the pipe fittings. In the following, the tilde signs in (5.25) will be omitted, for the sake of simplicity, thus writing:

$$w = f(\theta) \cdot C_v \sqrt{\rho(P_{in} - P_{out})} \tag{5.28}$$

The last modelling step is to regularise the valve equation as explained in section 4.4: (5.28) is re-written as

$$w = f(\theta) \cdot C_v \sqrt{\rho \Delta P_{nom}} \cdot \sqrt{z} \tag{5.29}$$

where $z = (P_{in} - P_{out}) / \Delta P_{nom}$; then the following substitutions are performed:

$$\sqrt{z} \rightarrow \frac{z}{\sqrt{|z| + b}}; \tag{5.30}$$

for an ordinary control valve, or

$$\sqrt{z} \rightarrow \begin{cases} \dfrac{z^2}{\sqrt{|z^3| + b^3}}, & z \geq 0 \\ 0 & z < 0 \end{cases} \tag{5.31}$$

for a control valve immediately followed by a check-valve.

Note that, in the case of a liquid flow, the inlet density depends weakly on both the fluid enthalpy and pressure; therefore, (5.29), with the substitutions (5.30) or (5.31), can be employed in a branch-type module, using the previously computed enthalpy to calculate ρ, and neglecting the partial derivative of ρ with respect to the inlet pressure when computing the contributions to the network Jacobian.

When the outlet pressure decreases below a certain value, the flowrate stops increasing: in this case the valve is said to be in *critical* or *choked-flow* conditions. This phenomenon is due to the vaporisation of the liquid in the vena contracta, inside the valve, with the flow velocity reaching the speed of sound. The flow equation (5.28) must be replaced by:

$$w = f(\theta) \cdot F_L C_v \sqrt{\rho(P_{in} - P_c)} \tag{5.32}$$

where F_L is the liquid pressure recovery factor, i.e. the ratio of the square root of the pressure drop across the valve to the square root of the difference between the inlet pressure and the pressure in the vena contracta zone, and P_c is the critical pressure, given by

$$P_c = F_F P_v \tag{5.33}$$

$$F_F = 0.96 - 0.28\sqrt{\frac{P_v}{P_{wc}}} \tag{5.34}$$

where P_v is the saturation temperature corresponding to the inlet liquid temperature, and P_{wc} is the water critical pressure (221.1 bars). Note that, when the valve is choked, the flowrate depends only on the inlet pressure, so that the valve is seen downstream like an "ideal flowrate generator" (borrowing from the electrical equivalent terminology); this means that the outlet contributions to the network Jacobian will become zero. Simple calculations show that (5.32) becomes valid instead of (5.26) when

$$P_{out} < P_{2c} \tag{5.35}$$

$$P_{2c} = (1 - F_L^2)P_{in} + F_F F_L^2 P_v \tag{5.36}$$

The contribution to the network Jacobian must be modified accordingly.

5.3.2 Vapour and Gas+Vapour Valves

The flow equations given by [ISA75] for valves using compressible fluids (such as steam or the gas-vapour mixture) are the following:

$$w = N \cdot F_p(C_v) \cdot C_v(\theta) \cdot Y(x)\sqrt{\rho_{in} P_{in} x} \tag{5.37}$$

$$x = \begin{cases} \dfrac{P_{in} - P_{out}}{P_{in}}, & x \le F \cdot x_t \\ F \cdot x_t & x > F \cdot x_t \end{cases} \tag{5.38}$$

$$Y(x) = 1 - \frac{x}{3F \cdot x_t} \tag{5.39}$$

where w is the mass flowrate, N is a factor depending on the units used in the equation (English or SI units), F_p is the *piping geometry factor*, C_v is the valve flow coefficient, which is a function of the travel θ, ρ_{in} is the fluid density at the valve inlet, P_{in} and P_{out} are the absolute pressure at the valve inlet and outlet, x is the ratio of the pressure drop across the valve to the absolute inlet pressure, Y is a factor taking into account the fluid compressibility, F is the specific heat ratio (c_p / c_v) divided by 1.4 (which is the typical value for air at moderate pressures and temperatures), and, finally, x_t is the pressure drop critical ratio, which is a characteristic parameter of the valve.

The same considerations made in Sect 5.3.1 for the liquid flow valve still remain valid; therefore, by using the data provided by the valve manufacturer, it is possible to obtain the following describing equation

$$w = f(\theta) \cdot C_v \cdot Y(x)\sqrt{x P_{in} \rho_{in}} \tag{5.40}$$

where the dimensionless function $f(\theta)$ describes the valve flow characteristic, again taking into account the effect of pipe fittings. Then, regularisation is applied, to avoid problems as the pressure drop goes to zero: (5.40) is re-written as

$$w = f(\theta) \cdot C_v \cdot Y(x) \sqrt{x_{nom} P_{in} \rho_{in}} \cdot \sqrt{z} \tag{5.41}$$

where $z = x / x_{nom}$, and the usual substitutions (5.30) or (5.31) are performed, to obtain the equation either for an ordinary control valve, or for a control valve immediately followed by a check valve.

In case the fluid is pure steam, the inlet density is a function of the pressure and of a thermal variable, i.e. $\rho_{in} = \rho(P_{in}, S_{in})$ or $\rho_{in} = \rho(P_{in}, h_{in})$, according to the steam tables. In order to include the regularised version of (5.40) in a hydraulic sub-module of the branch type, the thermal variable has to be assumed weak (so that its past computed value can be used). This is more or less true, depending on the upstream process: if the upstream component is a valve, then the enthalpy h_{in} is independent of P_{in}, and the weakness assumption holds; conversely, if the upstream component is a pressurised tank, the entropy S_{in} is independent of P_{in}. In the latter case, however, the mass and energy storage will still ensure decoupling, provided the integration stepsize is not too large. Therefore, the thermal variable is assumed weak without any problem.

The same can be said of the gas-vapour mixture, whose density (under the assumption of saturation for the vapour fraction) is a function of the pressure and of the CO_2 mass fraction, i.e. $\rho_{in} = \rho_a(P_{in}, x_{gin})$, according to the equations stated in section 4.1.2. In this case, x_{gin} is assumed weak, which is a reasonable assumption in most cases. Of course, if the pressure varies very rapidly, or in the case of the flow downstream a valve, the hypothesis of saturation for the steam fraction no longer holds; however the error committed on the density calculation is small, and moreover it is mitigated by the density appearing under square root.

Contrary to the case of the liquid flow valve, when computing the contribution to the network Jacobian, i.e.

$$\frac{\partial w}{\partial P_{in}}; \quad \frac{\partial w}{\partial P_{out}} \tag{5.42}$$

it is of paramount importance to take into account the partial derivative of the inlet density with respect to the inlet pressure as well; otherwise, the contribution to the Jacobian would be underestimated approximately by a factor of 2, which would in turn severely compromise the convergence of Newton's iterations, possibly giving rise to limit cycles or even instability, if a single Newton's iteration is performed for each integration step.

5.3.3 Flashing Valve with Orifice

Most of the flashing valves in the Latera plant are followed by an orifice, which is supposed to bear most of the pressure drop, in order to avoid excessive mechanical stress in the valves, which would otherwise be subject to excessive wear. Unfortunately, no widely recognised or standard equations exist to describe the two-phase flow through an orifice. Some equations are available from various sources ([Mur91], [TAI81], [Muk80]), but they are intended primarily for the sizing of relief valves, not for the accurate flow simulation through orifices embedded in a flashing process; therefore, they tend to overestimate the flowrate and are often written in a mathematical form which is too cumbersome to be used in a fast, dynamic simulator; finally, they can be grossly inaccurate in some conditions, since the simplifications that are made in writing their equations (e.g. equal velocity for the liquid and gas phase, and/or thermodynamic equilibrium between the two phases) may not hold at all. In the end, a simplified model of the valve-orifice has been used, which however would be better validated with experimental data, when available. This approximate model may lead, in a certain portion of the operating range, to errors of a factor 2-3 in the gain between valve stem position and flowrate, which however should not be critical, since these valves are used for standard level control.

The component diagram is shown in Fig. 5.7. The idea is to describe the whole complex as a single component, to avoid numerical problems that could arise in computing P_2, if two separate components were included in the hydraulic network.

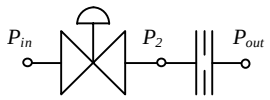

Figure 5.7: Valve + orifice

During normal operation, since the aim of the device is to flash the water, it is assumed that $P_{out} < P_{sat}(T_{in})$, so that the orifice will always be in choked flow conditions. The valve can either be in normal or choked flow conditions, depending on the value of P_2.

The equations describing the flow in the valve, according to [ISA75], are the following (refer to Section 5.3.1)

$$w = \begin{cases} C_v(\theta)\sqrt{\rho_{in}(P_{in} - P_2)}, & P_2 > P_{2c} \\ C_v(\theta)F_L\sqrt{\rho_{in}(P_{in} - F_F P_v)}, & P_2 < P_{2c} \end{cases} \tag{5.43}$$

$$P_{2c} = (1 - F_L^2)P_{in} + F_F F_L^2 P_v \tag{5.44}$$

where P_v is the saturation pressure corresponding to the inlet temperature. When comparing P_{2C} with P_v, it is found that:

$$P_{2c} > P_v \Leftrightarrow P_{in} > F^* P_v \tag{5.45}$$

with

$$F^* = \frac{1 - F_F F_L^2}{1 - F_L^2} > 1 \tag{5.46}$$

This means that, if P_{in} is high enough, as the valve is closed and P_2 gets lower, the choked flow conditions are reached before the valve outlet becomes a two phase liquid. Conversely, first the valve outlet fluid starts being two-phase, and afterward the valve enters the choked flow conditions. Unfortunately, for typical values found in the Latera process (e.g. P_v = 6.1 bars, F_L = 0.9, F_F=0.9134) condition (5.46) implies an additional 2.25 bars over the saturation pressure, which is not the case for all the valves located at the liquid outlets of the secondary separators, where the additional head amounts to some meters, equivalent to some tenth of a bar.

Since no standard formulae are avalilable in the literature, assume now that the orifice flow equation has the same form as the choked valve equation, and that the valve outlet is still in the liquid phase, i.e.:

$$w = K\sqrt{\rho_{in}\left(P_2 - F_F P_v\right)}\,; \tag{5.47}$$

if the system (5.43), (5.47) is solved by eliminating P_2, the following global flow equation is found:

$$w = \begin{cases} \dfrac{C_v K}{\sqrt{C_v^2 + K^2}}\sqrt{\rho_{in}\left(P_{in} - F_F P_v\right)}, & C_v \geq K\dfrac{\sqrt{1 - F_L^2}}{F_L} \quad \text{(a)} \\ C_v F_L \sqrt{\rho_{in}\left(P_{in} - F_F P_v\right)}, & C_v < K\dfrac{\sqrt{1 - F_L^2}}{F_L} \quad \text{(b)} \end{cases} \tag{5.48}$$

When the valve is closed enough (condition *b*), it goes under choked flow conditions, so that the presence of the orifice is irrelevant (at least from the point of view of the flowrate, not from the point of view of mechanical stress), and the equation is accurate, since it corresponds to the ISA standard equation (5.32). The validity of (5.48) in condition *a* is more questionable, especially in those particularly critical conditions when the valve is not yet in choked flow, but its outlet flow (and thus the orifice inlet flow) is a two-phase fluid.

A more accurate equation for the orifice can be written under the following assumptions:

- When the pressure goes below the saturation value, the two phases travel at the same speed through the orifice
- The flow can be divided into two consecutive sections: in the first, as the flow cross-section decreases, the fluid is accelerated isoentropically; when the speed of sound is reached, a shock wave is formed, which brings the fluid pressure directly to the outlet pressure (i.e. zero pressure recovery is assumed)

The application of the momentum conservation equation to the first section leads to the following, general equation:

$$\frac{w}{A} = \eta \frac{1}{v(P)} \sqrt{-2\int_{P_2}^{P} v\left(P^*\right) dP^*} \tag{5.49}$$

where w is the mass flowrate, A is the orifice cross-section, η is an adimensional factor (typically equal to 0.8) taking into account the reduced cross-section of the vena contracta and the friction effects, v is the fluid specific volume, P_2 is the inlet pressure, and P is either the outlet pressure or the pressure in the vena contracta, just immediately before the shock wave.

Assuming v = const (incompressible fluid), the usual flow equation comes out:

$$w = \sqrt{2}\eta \cdot A\sqrt{\rho\left(P_2 - P_{out}\right)}; \tag{5.50}$$

otherwise, assuming that the friction effects have been collected into η, the integral should be calculated along an isoentropic transformation: the liquid specific volume can be assumed constant until $P = P_v$; afterwards, when a two-phase flow takes place, the specific volume will be a function of the pressure according to

$$x = \frac{S_{in} - S_{ls}(P)}{S_{vs}(P) - S_{ls}(P)}; \tag{5.51}$$

$$v(P) = v_{ls}(P) + x(P) \cdot \left(v_{vs}(P) - v_{ls}(P)\right); \tag{5.52}$$

where S is the specific entropy, x is the steam quality, the *ls* subscript refers to saturated liquid, and *vs* refers to saturated vapour. Now, (5.49) should be integrated for increasingly low values of P until either P_{out} is reached (in the case of normal flow condition), or w reaches its maximum value; the latter case corresponds to choked flow conditions, and the corresponding value of P is the critical value P_c of the pressure in the vena contracta, just before the sonic shock wave. Since (5.52) is approximately linear in the interval of interest, the integral (5.49) can be well approximated by the trapezoidal rule, leading to the following approximate equation:

$$w = A\eta \frac{\sqrt{2}}{v\left(P_c\right)} \sqrt{v\left(P_v\right) \cdot \left(P_2 - P_v\right) + \frac{v\left(P_v\right) + v\left(P_c\right)}{2}\left(P_v - P_c\right)} \tag{5.53}$$

By some numerical experiments, it has been found that the critical pressure value P_c can be approximated by (5.33)-(5.34) only when the inlet pressures P_2 is very close to P_v. When the inlet pressure is more than 2-3% greater than P_v, the best approximation for P_c in (5.53) is simply P_v; if $F_F P_v$ is used instead, a much greater flowrate value is found, giving inconsistent results

(i.e. the flowrate initially decreases as the inlet pressure increases). This is not surprising, as the term 1 / $v(P_c)$ rapidly increases when P_c goes below the saturation level. Moreover, it should be considered that (5.33)-(5.34) have been conceived to give good results in (5.32), where the flowrate is a function of the *inlet* density, not of the density at the *vena contracta*, as in (5.53).

Now, while the system (5.43), (5.47) can be solved analytically, giving (5.48), the system (5.43), (5.53) cannot. Since the result of these computations is subject to strong uncertainties anyway, due to the simplifying assumptions involved, the decision was taken not to solve (5.43),(5.53) numerically, but to use (5.48) instead.

The K parameter has then to be tuned, based on the cross-section of the orifice. This is done as follows: first, it is assumed that the orifice inlet pressure is sufficiently close to the saturation value, so that (5.33)-(5.34) hold; then, by equalling the ISA-like formula (5.47) with a simplified version of (5.53), K can be found:

$$K\sqrt{\rho_{in}\left(P_2 - P_c\right)} = 0.8A\eta\frac{\sqrt{2}}{v\left(P_c\right)}\sqrt{\frac{v\left(P_2\right)+v\left(P_c\right)}{2}\left(P_2 - P_c\right)}; \tag{5.54}$$

$$K = \frac{0.8A\sqrt{v\left(P_v\right)+v\left(P_c\right)}}{v\left(P_c\right)\sqrt{\rho_{in}}}\cdot 10^{2.5} \tag{5.55}$$

where the rightmost numerical factor is needed because of the use of the bar instead of the Pascal as pressure unit in the simulator. The value of C_v, instead, is given by the manufacturer, usually in English units; to be used in the simulator (where flowrates are measured in kg/s and pressures in bar) it must be multiplied by the conversion factor $7.597*10^{-3}$. More details on the whole subject can be found in [Cer98].

It is clear from the above discussion that (5.48) is quite uncertain, in particular in the intermediate operating points, when the orifice inlet flow becomes two-phase, without the valve being in choked-flow, and is fully reliable only when condition (b) holds. It is also clear that experimental data are strongly needed, since the various results either found in the literature, or starting from the first principles, are often inconsistent. However, for the time being, (5.48) is employed in the simulator. The contributions to the network Jacobian and residual are computed as usual.

Finally, note that two flashing valves with orifice are inserted in the liquid transport pipes from the wells to the main plant, whose flow can be completely cut off if the stop valves are closed. In this case, critical conditions no longer hold in the valve-orifice complex, and therefore using (5.48) would lead to inconsistency in the solution of the hydraulic network. It is then necessary to introduce a (crude) approximation of the flow equations when $P_{out} > P_c$:

$$w = \begin{cases} \dfrac{C_v K \sqrt{\rho_{in}\left(P_{in} - P_{out}\right)}}{\sqrt{C_v^2 + K^2}}, & C_v \geq K \dfrac{\sqrt{1 - F_L^2}}{F_L} \quad \text{(a)} \\ C_v F_L \sqrt{\rho_{in}\left(P_{in} - P_{out}\right)}, & C_v < K \dfrac{\sqrt{1 - F_L^2}}{F_L} \quad \text{(b)} \end{cases} \tag{5.56}$$

which is then regularised as usual for small values of ($P_{in} - P_{out}$). This last equation is purely conventional, its only purpose being to obtain a consistent behaviour when $\Delta P \to 0$.

5.3.4 On-Off All-Purpose Valve

On-off valves are used in the Latera plant, with the purpose of isolating unit 1 and 2 (production wells) from the main plant. The main feature of these valves is that they are used as stop valves, i.e. they are either fully open (with a very small pressure drop, whose value need not be known with great accuracy), or closed (thus with zero flowrate flowing through them). A strongly simplified flow equation can then be used, since in both cases great modelling accuracy is not needed. This permits to use the same component for liquid, steam, and gas-vapour mixture without the need of any specialisation. The simplified flow equation is

$$w = f(\theta) \cdot k \sqrt{\Delta P} \tag{5.57}$$

where w is the flowrate, θ is the valve stem position (ranging from 0 to 1), ΔP is the pressure drop across the valve, and k is computed from a nominal operating point at full opening (w_{open}, ΔP_{open})

$$k = \frac{w_{open}}{\sqrt{\Delta P_{open}}} \tag{5.58}$$

As usual, (5.58) is rewritten as

$$w = f(\theta) \cdot w_{open} \sqrt{z} \tag{5.59}$$

where $z = \Delta P / \Delta P_{open}$, and then regularised according to either (5.30) or (5.31), depending on the presence of a check valve downstream the on/off valve. The contributions to the network Jacobian and residual are calculated as usual.

Since the valve is meant to operate as a stop valve, the valve stem position θ should not be directly accessible. Instead, the valve is commanded by a Boolean variable d, whose meaning is “open the valve” when true, and “close the valve” when false. The discretised equations for θ, which will be appended to the hydraulic sub-module, are:

$$\theta_{k+1} = \begin{cases} \min\left(1, \theta_k + \dfrac{\delta t}{\tau_c}\right) & d = true \\ \max\left(0, \theta_k - \dfrac{\delta t}{\tau_c}\right) & d = false \end{cases} \tag{5.60}$$

where δt is the integration stepsize, as usual, and τ_c is a user-defined closure time. The flow characteristic $f(\theta)$ is conventionally assumed equal to

$$f(\theta) = \frac{e^{5(\theta-1)} - e^{-5}}{1 - e^{-5}} \tag{5.61}$$

resembling a typical equal percentage valve.

5.4 Pipes for Liquid and Gas Transport

5.4.1 Ordinary Liquid Transport Pipe

These models are needed in two situations: one is the transport of separated liquid from the production units to the main plant, and the other is in the reboiler cycle, for the recirculation pipes. In both cases, the pipe length is significant (around 400 m for the former, and around 80 m for the latter), as is the difference between the head and tail elevation. Since the fluid velocity is rather low (1-2 m/s), a significant energy transport delay is present, which should be modelled; on the other hand, they are not so long as to require a model that takes into account the wave dynamics. Even if the heat capacity of the pipe walls is smaller, compared with typical power plant pipes, since the design pressure is 25 bars, not 100-150 as is often the case in the latter, the effect of the heat exchange with the metal may be noticeable. Needless to say, all the pipes are thermally insulated, so that the thermal flux towards the atmosphere can be neglected.

Consequently, a model of heat exchanger, previously developed in [Cst95], has been re-used, assuming zero external heat flow. The hydraulic sub-module takes into account the fluid inertia, the head loss due to friction, the piezometric effect and the (low) fluid compressibility; the corresponding partial derivative equations of mass and momentum conservation are lumped into two global ordinary differential equations, from which the contributions to the network Jacobian and residual is obtained as usual. The thermal PDE's (conservation of energy for the fluid and for the metal, plus convective heat transfer) have been written in entropic form, to ensure maximum decoupling from the hydraulic equations (see Sect 3.2), and then discretised by lumping them into a finite number of pipe cells, each described by a system of ODE. These have then been discretised with Euler's implicit method, and the

corresponding difference equations have been put in the causal sub-module. More details can be found in [Cst95].

The only modification has to do with the dissolved CO_2, which was not considered in the original model, used for the simulation of a conventional steam generator. Great modelling accuracy is not needed: in the case of the recirculation pipes, the water flowing through them is almost CO_2-free, and in the case of the transport pipes to the main plant, the dynamics of the dissolved CO_2, which is actually a pure time delay, plays no particular role in the overall system behaviour. To avoid a uselessly cumbersome model, the first-order approximation has been employed to model the transport of CO_2: in transfer function form, it can be written as:

$$x_{gout} = \frac{1}{1 + s\tau_t} \tag{5.62}$$

$$\tau_t = \frac{\rho AL}{w} \tag{5.63}$$

where τ_t is the transport delay, r is the liquid density, A the pipe cross-section, L the pipe length, and w the liquid flowrate. Equation (5.62) is then discretised with Euler's implicit method, and the corresponding difference equation is put in the causal sub-module, together with the thermal equations.

5.4.2 Ordinary Gas+Vapour Transport Pipe

A very accurate model of this component would be rather complex, due to the two-component nature of the fluid. In fact, the two phenomena whose modelling is critical for the accuracy of the simulator are the mass storage (since the pipe total volume has the same order of magnitude than the reboiler), and the pressure drop between the production units and the main plant. Thermal effects are negligible, since the pipe is well-insulated and there is no heat generation along the pipe. A sufficiently short section of the pipe will now be considered. The mass conservation equation is

$$\frac{dM}{dt} = w_{in} - w_{out} \tag{5.64}$$

where M is the total mass contained in the section, w_{in} is the inlet flowrate and w_{out} is the outlet flowrate; since the pressure drop due to friction is small when compared with the absolute pressure, the momentum conservation equation can be made trivial by assuming the pressure P along the whole section as uniform and equal to P_{out}, and then lumping the quadratic pressure drop at the section inlet:

$$w_{in} = k\sqrt{\rho\left(P_{in} - P_{out}\right)} \tag{5.65}$$

where the constant k can be calculated once a nominal operating point is known, in terms of nominal pressure drop, flowrate and fluid density (which is the case here, since these steady-state data are known from the design document)

Equations (5.64)-(5.65) are the two hydrodynamic equations, which will correspond to a branch-type sub-module, with an associate upstream capacitance (as explained at the end of Sect. 3.4.2).

Assuming that the fluid composition along the pipe section is constant, it is possible to write

$$M = \rho_a(P, x_g) \cdot A \cdot L \tag{5.66}$$

where A and L are the pipe cross-section and length, respectively, ρ_a is the gas-mixture density (computed as shown in Sect. 4.1.2), and x_g is the mass fraction of CO_2. Equation (5.64) can be written in the standard form (3.39), repeated here for convenience

$$\alpha \frac{dP}{dt} = w_{in} - w_{out} + \Lambda \qquad \text{(mass balance)} \tag{5.67}$$

with

$$\alpha = \frac{\partial M}{\partial P}; \quad \Lambda = -\frac{\partial M}{\partial x_g} \tag{5.68}$$

Equation 5.65 can be regularised as usual:

$$w_{out} = k\sqrt{\rho \Delta P_{nom}} \frac{z}{\sqrt{|z| + b}}; \quad z = \frac{P_{in} - P_{out}}{\Delta P_{nom}} \tag{5.69}$$

The hydraulic sub-module will then be obtained as explained in section 3.4.5., with:

$$\begin{aligned} J_{ii} &= \frac{\partial w_{out}}{\partial P_{in}}_{k} \qquad J_{io} = \frac{\partial w_{out}}{\partial P_{out}}_{k} \qquad r_i = w_{out,k} \\ J_{oi} &= -\frac{\partial w_{out}}{\partial P_{in}}_{k} \qquad J_{oo} = -\frac{\partial w_{out}}{\partial P_{in}}_{k} + \frac{\alpha}{\delta t} \qquad r_o = -w_{out,k} + \frac{\partial M}{\partial x_g}\frac{dx_g}{dt}_{k} \end{aligned} \tag{5.70}$$

Note that, as in the case of the gas valve, when writing the partial derivative of w_{out} with respect to the pressure, the partial derivative of ρ must be taken into account, to avoid errors in the Jacobian leading to bad convergence of Newton's method.

The causal sub-module will contain the equation for x_g and the thermal equation. The first will simply be the CO_2 mass conservation

$$\frac{dM_g}{dt} = w_{in} x_{gin} - w_{out} x_g \tag{5.71}$$

$$M_g = \rho_g(P, x_g) \cdot A \cdot L \tag{5.72}$$

which can be written as

$$\frac{\partial M_g}{\partial x_g}\dot{x}_g = w_{in}x_{gin} - w_{out}x_g - \frac{\partial M_g}{\partial P}\dot{P} \ ; \tag{5.73}$$

the terms w_{in}, x_{gin}, w_{out}, and the term depending on the derivative of P have already been calculated, either by the upstream component, or by the hydraulic sub-component; the remaining equation is discretised according to Euler's implicit method, and the corresponding difference equation put in the causal sub-module.

If the heat exchange with the pipe walls is neglected, which is reasonable since the gas-vapour mixture flows at a sufficiently high speed, the enthalpy dynamics can be approximated by a first-order approximation of the transport delay. In steady state conditions, the equation is exact, since the energy conservation equation states that $h_{in} = h_{out}$; the approximation which has been made is not a problem, since no control loop is strongly affected by the enthalpy dynamics in the transport pipe.

Note that the hydraulic model permits a transient flow reversal, even if the pipe is closed at one end, due to the compressibility effect; the discretised version of (5.73) with negative w_{out}, besides being incorrect (due to the flow reversal) is also numerically unstable; therefore it is convenient to put $w_{out} = 0$ in that equation, whenever the value given by the hydraulic network is negative.

To improve the modelling accuracy of the transport pipes from the production unit to the main plant, each pipe has been represented by three such pipe sections connected in series.

5.4.3 Long Pipelines for Liquid Transport

In section 4.3, the exact modelling of the pressure and flowrate wave dynamics in a long pipeline by means of equations which are discretised both in time and space was discussed. Now, it will be shown how those equations can perfectly fit the hydraulic network structure of the ProcSim environment.

A pipeline of total length L is divided into n segments, whose length is $l = L / N$; the integration stepsize is $\delta t = l / c$, where c is the speed of sound in

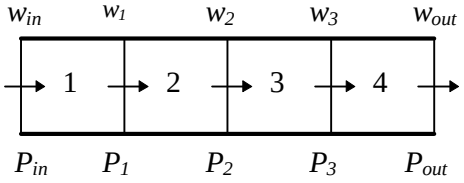

Figure 5.8: Segmented pipeline

the pipe. Therefore, the model will include N+1 flowrates and N+1 pressures, corresponding to the segment boundaries. Assume, for instance, that N = 4 (Fig. 5.8). It will now be shown how the head and tail boundaries will correspond to branch-type sub-modules in the networks to whom the pipe is connected, while the inner boundary values will be calculated by a causal sub-module, whose state variables will be the flowrates $w_1 ... w_{N-1}$ and the pressures $P_1 ... P_{N-1}$.

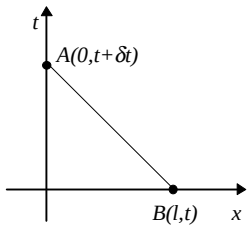

Figure 5.9: Space-time diagram for the leftmost boundary

Consider the leftmost boundary (i.e. the pipe head), and the space-time diagram of Fig. 5.9 (where one of the characteristic lines is represented). Equation (4.62) can be written as:

$$A\rho g(H_A - H_B) - c(w_A - w_B - l \cdot F \cdot w_B|w_B|) = 0 \; ; \tag{5.74}$$

substituting (4.61) for H, writing the equation terms according to the notation given in Fig. 5.8, and solving for $w_{in,k}$, it results

$$w_{in,k+1} = w_{1,k} + (1 / c) \cdot (A\rho g(z_{in} - z_1) + 10^5 (P_{in,k+1} - P_{1,k}) - l \cdot F \cdot w_{1,k}|w_{1,k}|) \tag{5.75}$$

where z_{in}, z_1 are the (fixed) elevations of the boundaries, and the values relative to the right boundary w_1 and P_1 are evaluated at previous time step, so that they can be read from the state vector of the inner boundaries. Note the 10^5 factor, which has been introduced for dimensional consistency reasons, since the pressure values in the ProcSim environment are measured in bar, not in Pascal. Eq. (5.75) is therefore a branch-type equation, whose contributions to the network Jacobian and residual are:

$$J_{ii} = \frac{\partial w_{in,k+1}}{\partial P_{in,k+1}} = 10^5 \frac{A}{c} \tag{5.76}$$

$$r_i = w_{in,k+1}\big|_k = w_{1,k} + \frac{1}{c}\left(A\rho g\left(z_{in} - z_1\right) + 10^5 A\left(P_{in,k} - P_{1,k}\right) - l \cdot F \cdot w_{1,k}\left|w_{1,k}\right|\right) \tag{5.77}$$

Note that the Jacobian can be interpreted as the characteristic impedance of the pipeline, according to the equivalent electrical network paradigm. Note also that P_{in} will be the pressure of the node immediately preceding the pipe.

The same solution strategy can be applied to the rightmost boundary (i.e. the pipe tail), starting from (4.63) and leading to a branch-type component whose contributions to the hydraulic network are:

$$J_{oo} = 10^5 \frac{A}{c} \tag{5.78}$$

$$r_o = w_{N-1,k} - \frac{1}{c}\left(A\rho g\left(z_{out} - z_{N+1}\right) + 10^5 A\left(P_{out,k} - P_{N-1,k}\right) + lFw_{N-1,k}\left|w_{N-1,k}\right|\right) \tag{5.79}$$

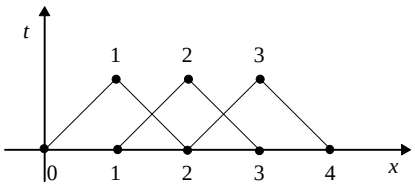

Figure 5.10: Space-time diagram for the whole pipeline

As before, P_{out} will be the pressure of the node immediately following the pipe.

After the two networks, to which the pipe head and tail are connected, have been solved, the new values $P_{in,k+1}$, $w_{in,k+1}$, $P_{out,k+1}$, $w_{out,k+1}$ are available. It is now possible to solve the equations relative to the inner boundaries. Let $P_{*0}...P_{*N}$ be the vector of the boundary pressures, $H_{*0}...H_{*N}$ the vector of the corresponding water heads, and $w_{*0}...w_{*N}$ the corresponding vector of boundary flowrates *at time step k* (which are known), *including the leftmost and the rightmost boundaries*. Consider the space-time diagram of Fig. 5.10, showing the characteristic lines relative to all the section boundaries. Equations (4.62)-(4.63) for the i-th internal boundary can be re-written as

$$A\rho g(H_{i,k+1} - H_{*i+1}) - c(w_{i,k+1} - w_{*i+1} - l\cdot F\cdot w_{*i+1}|w_{*i+1}|) = 0; \quad (5.80)$$

$$A\rho g(H_{i,k+1} - H_{*i-1}) + c(w_{i,k+1} - w_{*i-1} + l\cdot F\cdot w_{*i-1}|w_{*i-1}|) = 0; \quad (5.81)$$

which, after substituting H by (4.61), is a *linear* system of two equations in the unknowns $P_{i,k+1}$, $w_{i,k+1}$, i.e. the new pressure and flowrate values at the inner boundaries of the pipe. System (5.80)-(5.81) can thus be cast into matrix form and easily solved in sequence for each internal boundary i. The corresponding equations will be put in a causal sub-module

Summing up, the overall solution strategy is shown in figure 5.11: first the hydraulic network attached to the pipe head is solved, then the network attached to the pipe tail is solved, and finally the causal sub-module is run. Note that the two networks and the causal sub-module must be synchronous, i.e. for each of them the integration step length must be the same $\delta t = l / c$, otherwise inconsistent results will occur. Finally, note that the solution scheme makes it clear that the wave propagation delay completely decouples the two networks attached to the pipeline, so that they can actually be solved independently, without any approximation.

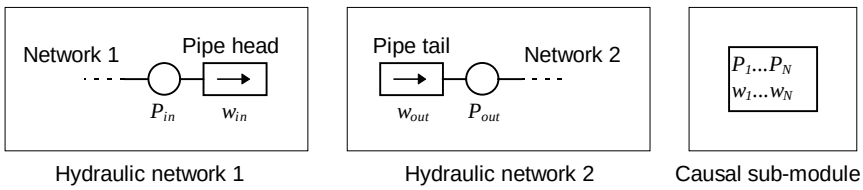

Figure 5.11: Solution sequence for the long pipeline

A special model structure is required for degenerate pipelines (i.e. $N = 1$), which will have modified hydraulic sub-modules for the pipe head and tail, and no causal sub-module. This is too much involved with the inner structure of the ProcSim software, and its description is beyond the scope of this dissertation.

As already said in Sect. 4.3, the thermal dynamics is of no interest in the modelling of this part of the process, since the fluid density remains always approximately the same. It can be assumed either constant, or equal to the density at the inlet, which is a function of the pressure and enthalpy.

5.5 Production and Reinjection Wells

5.5.1 Production Wells

The accurate modelling of the production wells is a very complex matter, since their behaviour is only partially known, being based on experimental results from test wells and on their extrapolation by very complex numerical codes, which simulate the dynamics of the underground production field. The typical pressure-flowrate characteristics of a geothermal well in the Latera production field, after the well start up procedure has been completed and the flow is stabilised, are expected to be like shown in Fig. 5.12, where P is the pressure at the well head and w is the total flowrate. The characteristic curves depend on the CO_2 content of the geothermal fluid (which is expected to get lower through the years as the field is exploited and the CO_2 discharged into the atmosphere), and results from the complex mass, momentum and energy transfer through the whole length of the well bore, which can be more than a thousand meters deep.

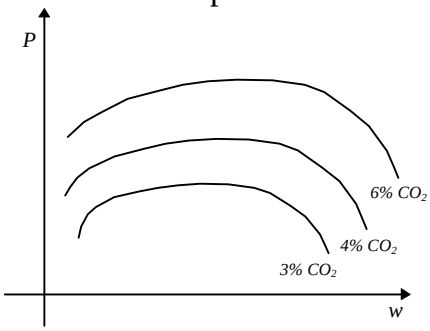

Figure 5.12: Production well characteristics

The direct use of the well simulation code is, of course, out of question, since it is too computationally expensive to be used for dynamic simulation of the plant. Moreover, the very same curves of fig. 5.12 cannot be directly entered into a branch-type component, since the structure of the ProcSim environment requires the flowrate to be a one-valued function of the pressure (see equation 3.41), which is not the case in Fig. 5.12.

On the other hand, a control valve is placed immediately after the well head, and the pressure drop across this valve is usually quite high (several bars), so that the valve is either in critical conditions, or anyway its flowrate depends weakly on the outlet pressure, and is mainly a function of the valve travel. Hence, a simplified model of the well and control valve complex has been used, on the assumption that the production flowrate is a function of the valve travel only. Of course, this model is not valid when the valve outlet pressure gets higher than the well head pressure, but this should never happen, since the pressure control system prevents this situation, by acting on relief valves placed on the gas-vapour outlet of the primary phase separator. The well relief valves have not been included in the model, since they are used only in the initial start-up phase, which is out of the scope of the simulator. The effect of the stop valve, which is placed before the control valve, can be emulated by closing the control valve itself.

The hydraulic equation of the well-valve complex is therefore:

$$w_{out} = f(\theta) w_{\max} \tag{5.82}$$

where w_{max} is the flowrate with the control valve fully open, and $f(\theta)$ is obtained from the flow characteristic of the control valve, as already explained in Section 5.3.1. The well-valve complex is then described as an imposed-flow branch.

The causal equations, describing the geothermal fluid enthalpy and CO_2 content, are two simple fixed assignments:

$$h_{out} = h^* \tag{5.83}$$

$$x_{gout} = x^* \tag{5.84}$$

where h^* lies in the (880–900) kJ/kg range, and x^* lies in the (3%–6%) range, depending on the particular well. Those values can be assumed as constant in the typical time scale of the simulations (1000 seconds).

A more accurate model could be developed, once experimental data become available. Note that all the data available at the time of the simulator implementation were based on samples, some of which were taken 10 years before.

5.5.2 Reinjection Wells

When cold water is pumped into the reinjection wells, they show a quadratic pressure-flow relationship, whose origin is clearly due to friction phenomena. However, when hot water near the saturation state is pumped in, as in the case of the Latera plant reinjection wells, complex phenomena involving two-phase flow occur. The end effect is that the pressure at the well head is

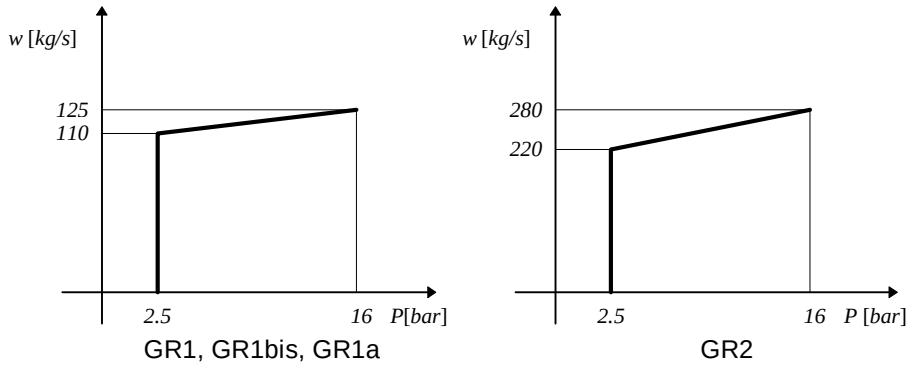

Figure 5.13: Reinjection well flow-pressure relationships

approximately equal to the saturation pressure of the water (between 2 and 3 bars, depending on the operating conditions) for flowrates ranging from zero up to the maximum carrying capacity of the well; if the flowrate increases further, the pressure starts rising very rapidly. The corresponding idealised pressure-flowrate relationships are shown in Fig. 5.13 for the reinjection wells GR1, GR1bis, and GR1a (left) and GR2 (right) (see Fig. 2.1).

For the sake of simplicity, an equivalent “parallel” well model has been used, whose flowrate is the sum of the three wells flowrates at the same pressure. The characteristics which were actually used in the simulator were smoothed versions of the idealised ones, to avoid numerical problems with the hydraulic network solver. A conventional pressure of 2.5 bars was selected for the first part of the curve; theoretically, this value should be updated, according to the actual saturation pressure of the reinjected water. In practice, since the regulating valve just before the wells bears a pressure drop of more than 12 bars, the difference in the computed flowrate would be less than 5%, thus well within the intrinsic uncertainty of the model.

In case some of the reinjection wells is shut down, the characteristic of the equivalent “parallel” well is modified accordingly.

5.6 Other Components

5.6.1 Turbine

In the case of fossil-fired power plants, the steam leaving the turbines is condensed and then pumped back into the boiler, through the economiser, in a closed cycle; this makes it necessary to compute the turbine outlet conditions and the operation of the condenser to simulate the plant effectively. In the case of the Latera plant, instead, the exhaust steam is condensed and then disposed of through a cooling tower system. Moreover, the turbines employed in the Latera plant do not have complex speed-control actuators, since they are

designed to operate always with fully open valves. As a consequence, detailed simulation of the turbine operation is not required, and only a correct boundary condition for the rest of the plant is necessary. It is well known [Maf89] that the turbine inlet flow characteristic is equivalent to a steam valve operating in choked-flow conditions. The two turbines have then been modelled as such, tuning the valve flow coefficient C_v in order to match the operating curves given by the turbine manufacturer. Minor modifications could have been included to take into account the effect of the residual CO_2 contained in the steam; however, this is found to be generally less than 2% in the high pressure turbine, and less than 300 ppm in the low pressure turbine, so that it has actually been neglected for the purpose of computing the pressure-flowrate relationship.

If one is interested in the net mechanical power output of the turbines, a simple formula based on the isoentropic efficiency η_t (which is declared by the manufacturer to be around 76% for these turbines) can be used:

$$W = w_{in} \cdot \eta_t \cdot (h_{in} - h(P_{cond}, S(h_{in}, P_{in})) \tag{5.85}$$

where W is the mechanical power output, w_{in}, h_{in} and P_{in} are the flowrate, specific enthalpy and pressure at the turbine inlet, respectively; $h(P,S)$ and $S(P,h)$ are the steam table functions. The condenser pressure P_{cond} is assumed constant and equal to 0.09 bar, according to the design document.

5.6.2 Centrifugal Pump

The centrifugal pump model was one of the first models to be built in the ProcSim environment [Bar94]. The fundamental equation for a pump processing an incompressible fluid [Dix66] states that there is a quadratic relationship between the two adimensional quantities

$$\frac{\Delta P}{\rho \omega^2 D^2} \qquad \text{(work number)} \tag{5.86}$$

$$\frac{w}{\rho \omega D^3} \qquad \text{(flow number)} \tag{5.87}$$

where ΔP is the pressure difference between the inlet and the outlet, ρ is the fluid density, ω is the number of revolutions per second (r.p.s.), D is the impeller diameter, and w is the mass flowrate. This implies the following equation:

$$\Delta P = -\frac{a}{\rho} w^2 + b\left(\frac{\omega}{\omega_0}\right) w + c\rho\left(\frac{\omega}{\omega_0}\right)^2 \tag{5.88}$$

where ω_0 is a reference r.p.s. number, and a, b, and c are three parameters which depend on the particular pump. The parameters can be tuned if three points of the pressure-flowrate relationship at the reference r.p.s. are known, which is usually the case, since this curve is always given by the manufacturer. Equation (5.88) is then analytically solved for w, and the corresponding equation $w = f(\Delta P, \rho, \omega)$ is put in a branch-type sub-module in the usual way, considering ρ and ω as weak variables. In some cases (but not in the Latera plant), (5.88) is not monotonically decreasing; to allow its inversion, a slightly modified monotone relationship is used instead, which can be inverted in the form $w = f(\Delta P, \rho, \omega)$. More details on the subject can be found in [Bar94].

Last, but not least, flow reversal is allowed, in order to permit the numerical solution to settle to zero flowrate, in case some stop valve in series with the valve is closed.

The exact thermal equation should take into account the mechanical work done on the processed fluid, which in turn requires to know the exact efficiency of the pump, which is a function of the operating point; in practice, when the fluid is a liquid, this contribution is negligible when compared with other heating effects, so that a simplified version of the energy conservation equation

$$h_{in} = h_{out}, \tag{5.89}$$

can be used, h being the specific enthalpy of the fluid. The CO_2 mass conservation equation simply states

$$x_{gin} = x_{gout}. \tag{5.90}$$

These two equations will be put in the pump causal sub-module.

5.6.3 Pressurised Tank

Two pressurised tanks are used in the reinjection system, to damp out the flow and pressure oscillations (Fig. 5.14). The tank contains liquid water up to a certain level, and a fixed quantity of ideal gas, which is supposed to undergo a polytropic transformation of index n. At low frequency, the transformation is isothermal (so that $n = 1$), while at high frequency it can be thought of as adiabatic (and thus $n = 1.4$). A good compromise is to assume $n = 1.3$. The component state will be characterised by a gas pressure P, a liquid level y, and by a pressure at the inlet and outlet P_o, which will be located y_o meters below the zero level reference.

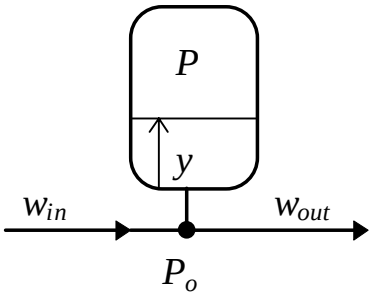

Figure 5.14: Pressurised tank

This component will be used in a part of the process (the reinjection unit) whose thermal

dynamics is of no interest, as already said in Section 5.4.3. Therefore, the liquid density ρ will be assumed as constant, and only the hydrodynamic equation will be written, starting from the mass balance equation

$$\frac{dM_l}{dt} = w_{in} - w_{out} \ . \tag{5.91}$$

This equation should be cast in the standard form (5.67), where the node pressure should be P_o, i.e. the pressure in the point where the branches are actually connected.

Assume now that the tank is cylindrical, so that the gas control volume V is such that

$$V = V(y) = V_0 - A \cdot y \ . \tag{5.92}$$

Due to the assumption of polytropic gas transformation,

$$P \cdot V^n = K \ \Rightarrow \ d(PV^n) = 0 \tag{5.93}$$

$$dP \cdot V^n + nPV^{n-1} \cdot dV \ = 0 \tag{5.94}$$

$$dP \cdot V - nPA \cdot dy \ = 0. \tag{5.95}$$

Now, the water head is such that

$$P_o = P + \rho g(y + y_o) \tag{5.96}$$

$$dP = dP_o - \rho g \cdot dy; \tag{5.97}$$

substituting into (5.90), and solving for dy, one obtains

$$dy = \frac{V}{nAP + \rho g V} dP_o \ , \tag{5.98}$$

so that

$$dM_l = \rho A \cdot dy = \frac{V}{nAP + \rho g V} dP_o \tag{5.99}$$

The mass balance equation (5.86) can thus be written as

$$\alpha \frac{dP}{dt} = w_{in} - w_{out}; \quad \alpha = \frac{\rho V}{nP} \cdot \frac{1}{1 + \dfrac{\rho g V}{10^5 nPA}} \tag{5.100}$$

which perfectly fits the equation form for a node-type hydraulic component.

Once the hydraulic network to which the tank belongs has been solved, the new value of the level y_{k+1} must be computed. The equation relating the outlet pressure to the level, from (5.93), is the following:

$$(P_{g,k+1} - 10^{-5} \rho g (y_{k+1} + y_o)) \cdot (V_0 - A y_{k+1})^n = K \ . \tag{5.101}$$

Equation (5.101) is an implicit equation in y_{k+1} which cannot be solved analytically. It will then be solved by Newton's method, using y_k as the initial

guess. A single iteration is usually enough to achieve good accuracy. The equation corresponding to one iteration of Newton's method applied to (5.101) will be appended to the hydraulic sub-module, which will then also calculate y_{k+1}.

5.6.4 Control Library

The control library contains a number of standard building blocks, which can be used to assemble the control system block diagrams, connecting the sensor inputs with the actuator outputs. The available components include:

- Read access to the process database (representing the sensor)
- Write access to the process database (representing the actuator)
- Normalising block (transforming a measurement into the 0–1 range)
- De-normalising block (transforming a variable in the 0–1 range into the desired range)
- P, I, PI, controllers, with anti-windup features, auto/manual station, and extra inputs for derivative action and feedforward action
- Digital controller (discrete time transfer function)
- Pure algebraic gain
- Relais with hysteresis
- Setpoint generator
- Ramp generator
- Low-pass first-order filter
- Lead-lag filter
- Limited slew-rate block
- Static programmable I/O characteristic

The detailed discussion of the control library is beyond the scope of this dissertation for reasons of space. Anyway, the building blocks are rather standard in the context of CACSD (Computer Aided Control Sistem Design) tools. Future activity might lead to the implementation of a control library, strictly conforming to some recognized standard, but this has yet to be done. Anyway, the library available at present is sufficiently rich for the purpose of control system simulation, yet providing a certain level of abstraction when compared with real CACSD building blocks, which are often much more complete and detailed.

All the continuous-time controllers (such as PI or Pole-Zero filter) were implemented as discrete time dynamic systems according to Euler's implicit method, as usual.

The control system blocks, assembled in control schemes, result in causal sub-modules. The process input variables are read from the process database by the read blocks, then the block diagram (which is a native concept in LabView,

the visual programming language on which ProcSim is based) is executed, and eventually the control variables (generally valve stem positions) are written back to the process database. Note that all the control sub-modules need not be executed synchronously with all the process sub-modules, as explained in Section 3.2, Example 5.

6. THE PROCESS SIMULATOR

6.1 Architecture of the Simulator in the ProcSim Environment

6.1.1 Objectives of the Simulation

As already explained in Chapter 2, the aim of the simulator is to provide a high fidelity representation of the process under consideration, rather than provide simplified models to explain the behaviour of a well-known process, a-posteriori. In particular, the primary aim is to obtain a process model with the degree of accuracy needed for the final checkout of the distributed control system, just before the download of the actual code into the plant controllers. As a consequence, many details had to be included, which are seldom taken into account in power process simulators, such as the exact flow characteristic of each control valve, which is essential to evaluate correctly the controller gains and the possible need for non-linear output compensation for correct operation under large load variations. Other applications are possible, as will be briefly discussed in Section 6.2. The complete lack of previous experience, gained on similar plants, required the use of models based on first principles for most components. In some cases (e.g. flashing valves with orifice, production and reinjection wells), the best models which could be obtained on the grounds of all the available data, are still subject to substantial uncertainty; in those cases, some kind of experimental validation would be extremely helpful, in order to obtain a better process description. Of course, this has not been possible, since the objective of the simulator was to provide answers before the plant was actually built; it could nevertheless be a very interesting subject for further research work. Experimental validation would also (hopefully) confirm that the simplifying assumptions made when modelling the process components were fundamentally correct.

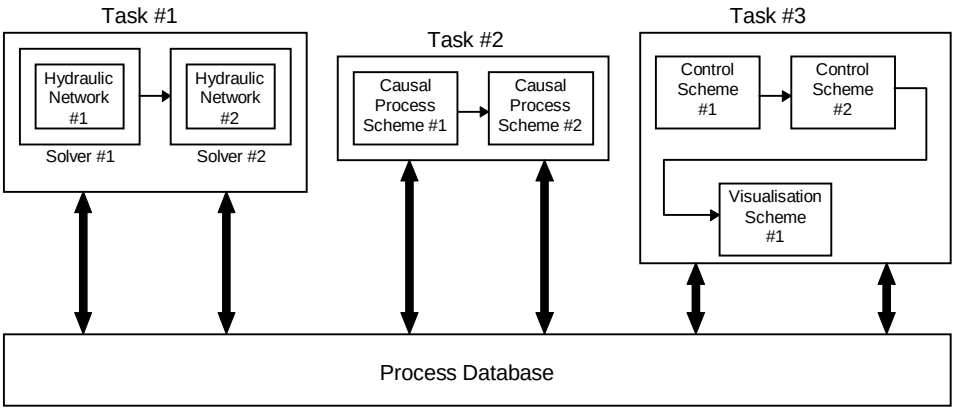

Figure 6.1: The ProcSim Software Architecture

6.1.2 Overview of the ProcSim Software Architecture

The architecture of a process simulator in ProcSim is based on the following hierarchy (Fig. 6.1): the *sub-modules*, corresponding to each process component are assembled in *solution schemes*: in particular the *hydraulic sub-modules* are assembled in *hydraulic networks*, which are embedded in their non-linear equation *solvers*, whose operating principles are described in Section 3.4.2.; the corresponding *causal sub-modules*, which contain the causal equations solved by Euler's implicit method, are assembled in *causal process schemes*, and executed sequentially, usually following the flow direction, as was shown in the examples in Chapters 4 and 5. Finally, the *control systems* are assembled in *control schemes*, by using the standard block-diagram representation which is native in the LabView programming language. These schemes (hydraulic networks with associated solvers, causal process schemes and control schemes) are then collected into different *tasks*, which are executed each with its own integration time step. Note that it is common practice to put all the hydraulic sub-modules relative to a plant section in one task, to put all the corresponding causal sub-modules in another task and, finally, the control schemes and visualisation schemes in yet another task; this is mandatory if multirate integration has to be performed.

The different tasks can be synchronous (an execution priority can be enforced in this case) or asynchronous, if multirate integration is needed, as explained in Sect. 3.2. A task can be active or inactive, in which case all its variables remain frozen at their last computed value.

All the sub-modules communicate with each other only through the *process database*, containing the values taken by all the process variables at the two previous time steps *k* and *k-1*. This last feature is needed when the past value of some derivative is required, due to decoupling, or for particular model

solution strategies, such as the long pipeline models described in Sect 5.4.3. The overall model solution strategy depends on the task execution order, and on the scheme solution order inside each task; note that every process variable is written by a *single* sub-module, and only read by all the others. In some sense, it could be said that every variable "belongs" to some sub-module, and thus it is updated at regular time intervals, depending on the integration step size of the task in which the sub-module is contained. In particular, pressures and flowrates are usually written by hydraulic sub-modules, with some exceptions as the secondary separator models.

The variables which do not belong to any sub-module are called *exogenous variables*; since no sub-module ever writes them, their value is constant, and equal to the initial one. Usually these variables represent boundary conditions (such as atmospheric pressure or the enthalpy and CO_2 content of the fluid leaving the production wells). The whole database can be saved in a so-called process *snapshot*, and loaded to start again the simulation from the same conditions. It is common practice to save snapshots corresponding to steady-state initial conditions, which are then used as a starting point for dynamic simulation. It should be stressed that obtaining the first steady-state snapshot for a new plant is not at all a trivial task, since an initial value must be provided for each variable. Usually, an initial set of (hopefully) compatible values is manually inserted in the initial snapshot. "Slow" control loops are closed on the variables whose initial value is given, and a simulation is run. After an initial transient, the values of the variables settle on the required steady-state, which can be saved for future use. If the plant is assembled incrementally, a good strategy is to obtain a steady state for a portion of the plant (possibly adding some suitable boundary conditions as exogenous variables), and then add some new components, and use the old snapshot as a starting point.

The component parameters are saved in a set of files, one for each component. Different process configurations and control system parameter tunings can thus be saved and retrieved easily.

The different process sub-modules communicate with each other exclusively by reading from and writing to the common process database. The only exception to this rule is given by the control schemes: communication with the database takes place only in the database-read (sensor) and database-write (actuator) blocks. The rest of the scheme is an ordinary block diagram, with data flowing through the wires connecting the various LabView icons, which implement the different control diagram components (e.g. gain, lead-lag filter, normaliser, summing node, PI controller, etc.)

Tasks can also contain sub-modules for data I/O: *trend displays* for real-time visualisation of the trends of variables; *tracers*, to save the trends of selected variables onto a disk file in standard ASCII format, for further

analysis; *graphic plant displays* (such as those commonly found in SCADA systems), to keep critical process variables available at a glance, and to interact with the process, e.g. to open and close the stop valves. Further sub-modules can be included for specialised tasks, such as the calculation of the global process efficiency, or the check of mass and energy balances within certain components or plant sections, or to add enhanced user interfaces. The software architecture is therefore fully open and modular, thus allowing extensions and modifications in a very easy fashion. Moreover, being based on the LabView software tool, the simulation tool can be ported to different computer platform without any effort, since the LabView components are compatible at the binary level on all the CPU's and operating systems where LabView has been ported.

The reader interested in further details on the software implementation of the simulation environment itself should consult the references [Bar94, 96, 98]. Note that the ProcSim simulation environment, apart from the new model libraries, has constantly been enhanced during the years, so that some information in those reference works could be partially obsolete. The fundamental principles, though, have remained unchanged.

6.1.3 The Architecture of the Latera Plant Simulator

The simulator of the Latera plant features seven different tasks. They are listed below, along with the contained schemes. The pictures show how the tasks look like in the LabView graphic programming language; the grey boxes connected by wires enforce the sequential execution of the different schemes. The complete list of the sub-modules is not given, for lack of space; however, it is rather easily inferred by looking at the process flowsheets, shown at the end of Chapter 2. The scheme names, of course recall, the Italian name of their content; the English comment should anyway be clear.

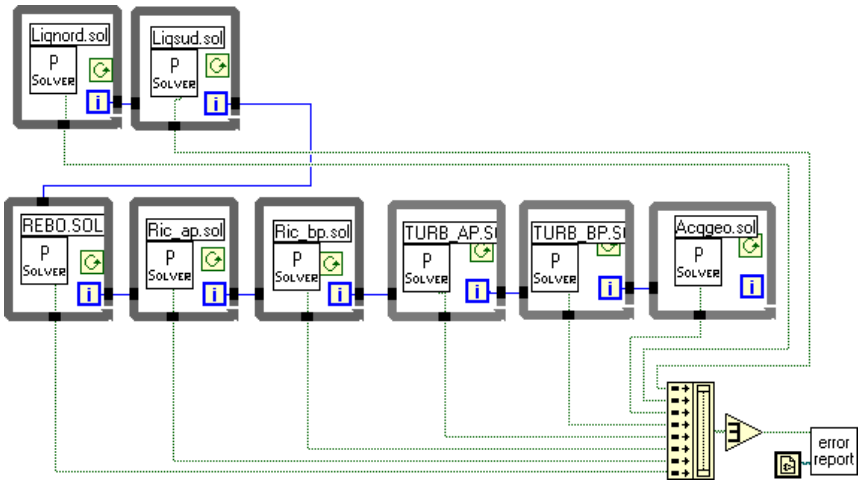

Figure 6.2: IDR_IPV.TSK

TASK 0: **IDR_IPV.TSK** Hydrodynamics of the production units and main plant units. Each hydraulic network is embedded into its solver.

LIQNORD.RET (**LIQNORD.SOL**) Liquid water network for fluid transport from the northern wells to the main plant.
LIQSUD.RET (**LIQSUD.SOL**) Liquid water network for fluid transport from the southern wells to the main plant.
REBO.RET (**REBO.SOL**) Gas-vapour network from the primary separators through to the reboiler top valves. Note that it was not possible to split this network anywhere, so that it counts 28 nodes; this however gave no particular problems during all the simulations.
RIC_AP.RET (**RIC_AP.SOL**) Liquid water network of the high-pressure recirculation circuit.
RIC_BP.RET (**RIC_BP.SOL**) Liquid water network of the low-pressure recirculation circuit.
TURB_AP.RET (**TURB_AP.SOL**) Gas-vapour feed network from the high-pressure separators to the high-pressure turbine.
TURB_BP.RET (**TURB_BP.SOL**) Gas-vapour feed network from the low-pressure separators to the low-pressure turbine.
ACQGEO.RET (**ACQGEO.SOL**) Liquid water network for Unit 4 of the main plant, through to the outlet of LV4002A (Fig. 2.3)

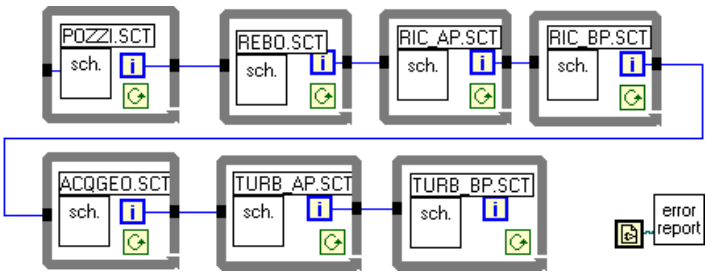

Figure 6.3: TER_IPV.TSK

TASK 1: **TER_IPV.TSK** Causal sub-modules for Units 1 to 5.

POZZI.SCT Production wells, primary separators and transport networks to the main plant.
REBO.SCT Reboiler sub-modules.
RIC_AP.SCT High-pressure recirculation circuit sub-modules.
RIC_BP.SCT Low-pressure recirculation circuit sub-modules.
TURB_AP.SCT High-pressure turbine feed network.
TURB_BP.SCT Low-pressure turbine feed network.
ACQGEO.SCT Unit 4 of the main plant.

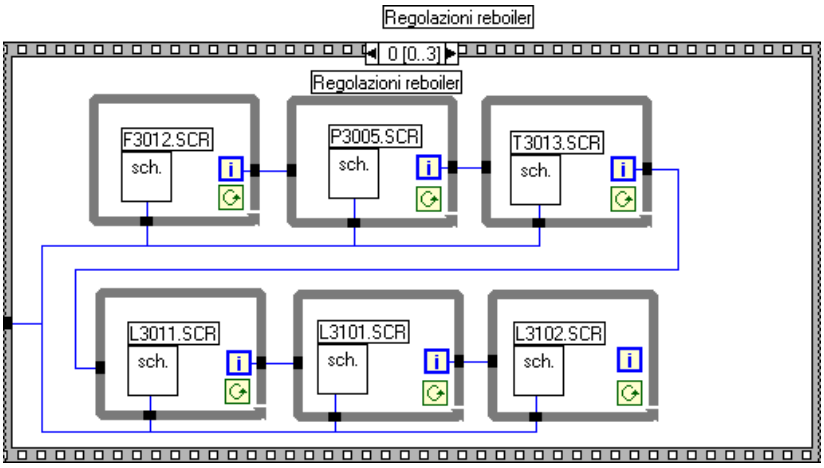

Figure 6.4: REG_IPV.TSK (First frame)

TASK 2: **REG_IPV.TSK** Control systems for Units 1 to 5.

F1044.SCR	**F2044.SCR**	**F3012.SCR**	**L1032.SCR**
L2032.SCR	**L3011.SCR**	**L3101.SCR**	**L3102.SCR**
L4001.SCR	**L4002.SCR**	**P1004.SCR**	**P2004.SCR**
P3001.SCR	**P3002.SCR**	**P3005.SCR**	**P4001.SCR**
P4002.SCR	**P5001.SCR**	**P5002.SCR**	**P5003.SCR**
P5004.SCR	**P6000.SCR**	**T3013.SCR**	**TURBINE.SCR**

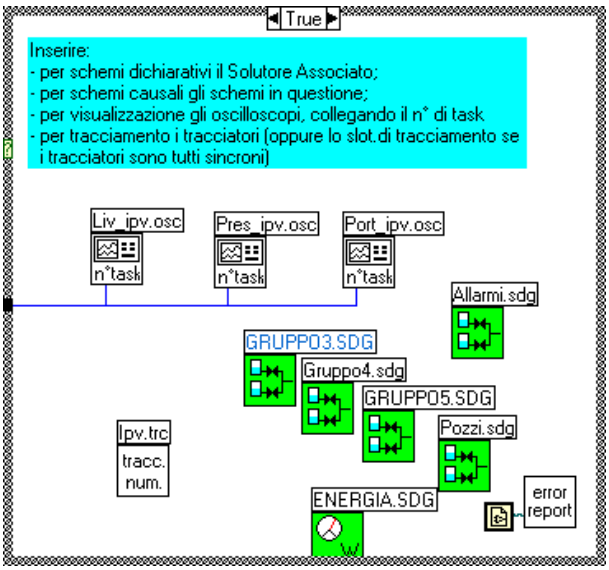

Figure 6.5: VIS_IPV.TSK

TASK 3: **VIS_IPV.TSK** I/O sub-modules for Units 1 to 5.

LIV_IPV.OSC Trend display for the primary separator and main plant levels.
PRES_IPV.OSC Trend display for the primary separator and main plant pressures.
PORT_IPV.OSC Trend display for the primary separator and main plant flowrates.
IPV.TRC Tracer for the variables in Units 1 to 5.
GRUPPO3.SDG Graphic display of Unit 3 (reboiler circuit).
GRUPPO4.SDG Graphic display of Unit 4 (geothermal water circuit).
GRUPPO4.SDG Graphic display of Unit 5 (turbines with feeds).
POZZI.SDG Graphic display of the production well circuit.
ALLARMI.SDG Alarm display.
ENERGIA.SDG Net power output computation.

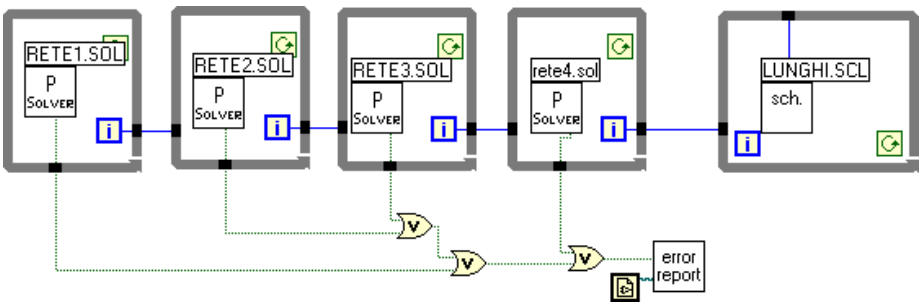

Figure 6.6: IDR_REIN.TSK

TASK 4: **IDR_REIN.TSK** Hydrodynamics of the reinjection unit. Each hydraulic network is embedded into its solver.

RETE1.RET (**RETE1.SOL**) Pipeline head network.
RETE2.RET (**RETE2.SOL**) Top-of-the-hill tank network.
RETE3.RET (**RETE3.SOL**) GR2 well network.
RETE4.RET (**RETE4.SOL**) GR1 well network.
LUNGHI.SCL Causal sub-modules of the long pipelines.

TASK 5: **REG_REIN.TSK** Control system for the reinjection unit.

P6000.SCR

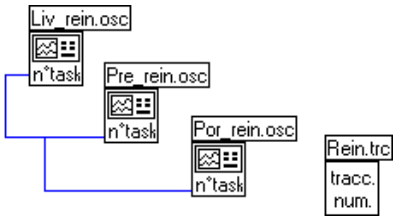

Figure 6.7: VIS_REIN.TSK

TASK 6: **VIS_REIN.TSK** I/O sub-modules for the reinjection unit.

LIV_REIN.OSC Trend display for the reinjection unit levels.
PRE_REIN.OSC Trend display for the reinjection unit pressures.
POR_REIN.OSC Trend display for the reinjection unit flowrates.
REIN.TRC Tracer for the reinjection unit variables.

In the Latera plant, multirate integration (i.e. using shorter step sizes for the hydraulic network integrators and longer step sizes for the remaining ones) did not give satisfactory results, in terms of improved performance and numerical stability. Therefore, Tasks 0 to 3, which correspond to the production units and to the main plant, are executed with a step size of 0.6 seconds, which leaves a reasonable safety margin with respect to the stability limit, which was found around 0.8-0.9 seconds, depending on the operating conditions. Such a short maximum step size is probably due to the coupling between the hydraulic equations and the CO_2 conservation equations, which have been decoupled in the integration algorithm, but this has not been definitely proven. Tasks 4 to 6, instead, run with a step size of 0.85 seconds, which correspond to a length of 850 meters for each pipe section, assuming a speed of sound of 1000 m/s (which is a typical value in hydroelectric plants, where long pressurised pipelines are employed). This section length was chosen because it was (approximately) the greatest common divisor of the lengths of the three pipelines in the network (Fig. 2.4). Note that the reinjection well GR2 was added to the plant at the last moment, as a spare resource in case the three wells GR1, GR1bis, GR1a cannot drain all the exhaust water flow. It was then included into the simulator, but it had not yet been studied thoroughly with respect to the control system design.

This choice of step sizes allows to run simulations in real time on a Pentium class PC, i.e. 1 second in the simulation corresponds to 1 second of CPU time.

The hydraulic network, describing the pumping of exhaust geothermal water from the low-pressure secondary separator through to the reinjection wells, was split just before the first pressurised tank V601. The left sub-network belongs to Task 0, while the right sub-network belongs to Task 4. This

makes it possible to simulate the reinjection unit only, or the main plant without the reinjection unit. In the former case, Tasks 0 to 3 are inactive, and the inlet flow into the tank V601 is an imposed flowrate, which can possibly be varied, by using a suitably configured ramp generator, to test the response of the reinjection control system to flow disturbances, without the need to simulate the whole plant. This makes the simulation about 10 times faster than with the whole simulator running. In the latter case, Tasks 4 to 6 are inactive, so that the pressure at the outlet of the level control valve LV4002A (i.e. the pressure of V601, see Fig. 2.4) is fixed. This allows first to tune the control loops of the main plant without bothering about the reinjection system, then to tune that only at the end of the process. All these operation can be carried out through the user interface, without any programming.

Note that the boundary separating Unit 6 from the rest of the plant does not coincide exactly with the point of network splitting, the former being located immediately before the reinjection pump G401, as shown in Fig. 2.1. However, that is a functional boundary: in case of the failure of the pump (which belongs to the reinjection unit), Unit 5 can still keep working, even though with a reduced flowrate, by discharging the exhaust flow in the V2 well through the control valve LV4002B. The boundary for the splitting of the hydraulic network, instead, is motivated by different reasons, as explained in the paragraph above.

The interested reader can find a more detailed description of the structure of the Latera process simulator in the Report [Cas98e]. Finally, some sample schemes and modules taken from the simulator are shown.

The first example, shown in Fig. 6.8, is the hydraulic network LIQNORD.RET representing the liquid transport network from the primary separator outlet through to the main plant (see also Fig. 2.2).

Note that the structure of the LabView modules in the diagram corresponds one-to-one with the hydraulic network diagrams shown throughout Chapters 3, 4, and 5. The only difference is that the imposed pressure nodes are not represented, since their pressure value is calculated elsewhere. In this case, the pressure at pump inlet is the primary separator pressure, which is calculated by the hydraulic network REBO.RET. Such information is stored inside the sub-modules, which contain a list of the input and output variables. In the same way, the pressures at the outlets of LV4003C and LV4003A are imposed

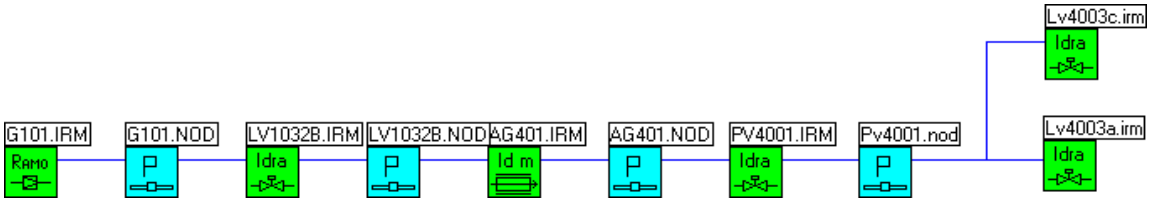

Figure 6.8: Hydraulic network LIQNORD.RET

pressures, the former being the atmospheric pressure (an exogenous variable) and the latter being the pressure inside the separator V401-2, which is calculated by the network REBO.RET. The network REBO.RET would be a very interesting example to show, but it is too big to fit a single page, so that it is not shown here.

A causal process scheme (POZZI.SCT), is shown in Fig. 6.9. The execution order is from left to right, following the flow direction. This scheme contains the causal sub-modules of the components belonging to Units 1 and 2.

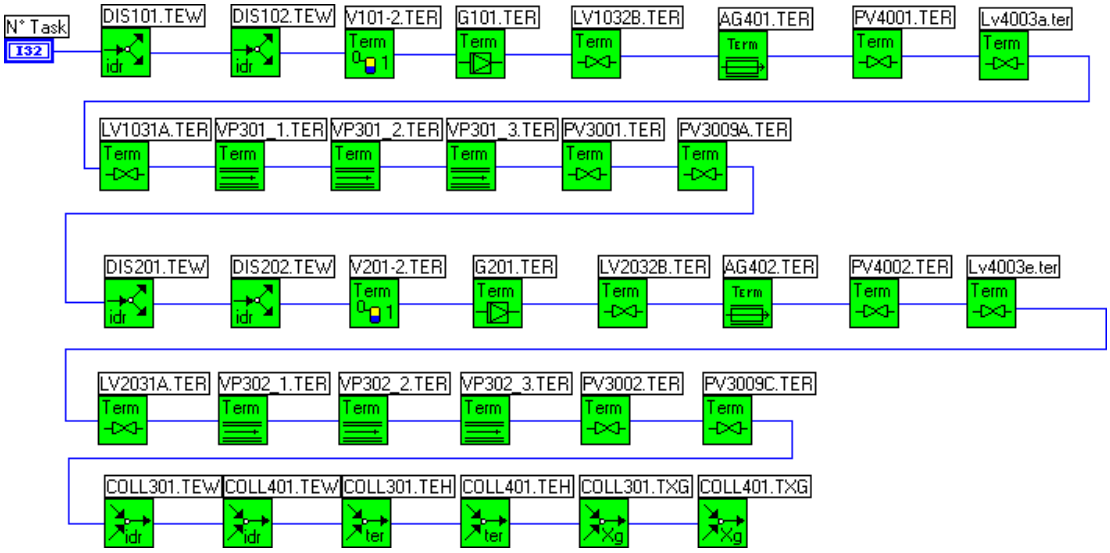

Figure 6.9: Causal process scheme POZZI.SCT

Next, the database interface of a causal sub-module (belonging to the 4th reboiler plate), is shown in Fig. 6.10. Note the input (*lettura*) and output (*scrittura*) variable lists, along with the corresponding units.

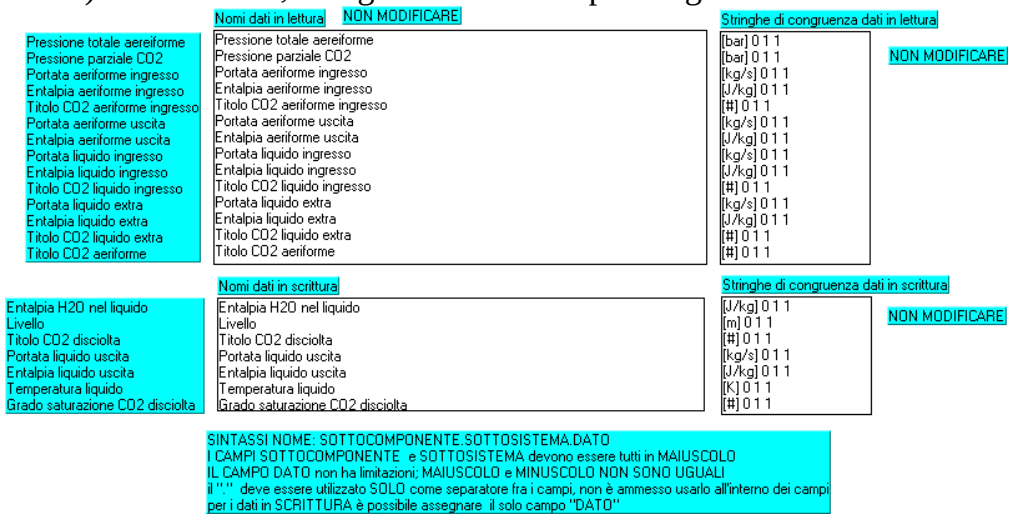

Figure 6.10: Interface with the database of a causal sub-module

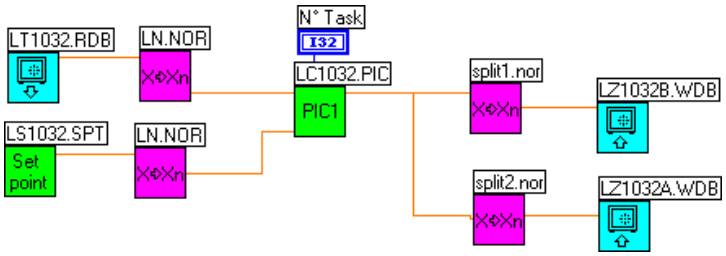

Figure 6.11: Control Scheme L1032

The level control scheme L1032 is shown in Fig. 6.11. The leftmost icon with a safe is the read access to the database, representing the level sensor (or transducer) LT1032, measuring the water level in the tank V101-2 (see Fig. 2.2). The pressure value and the setpoint value are normalised into the range (0–1) and fed to the PI controller. A split-range control strategy is then implemented through the two denormalisers: controller outputs in the range (0-0.5) act on the stem position LZ1032B of the control valve LV1032B; when that is fully open, for PI outputs in the range (0.5-1), also the control valve LV1032A is open, discharging the excess flow into the atmosphere. The write access modules thus write the new values of the variables LZ1032B and LZ1032A, i.e. the stem positions of the relative control valves, in the process database.

The user interfaces of the setpoint and of the PI controller are shown in Fig's 6.12 and 6.13. Note that the setpoint value, manual control value and auto/manual state can be modified by the user either interactively, by acting on the shown interfaces, or by modifying the corresponding variables in a snapshot, for batch simulations.

To make the reader appreciate the complexity and completeness of the Latera plant simulator, the total number of process and control components in

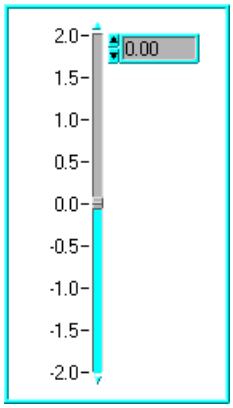

Figure 6.12: Setpoint user interface

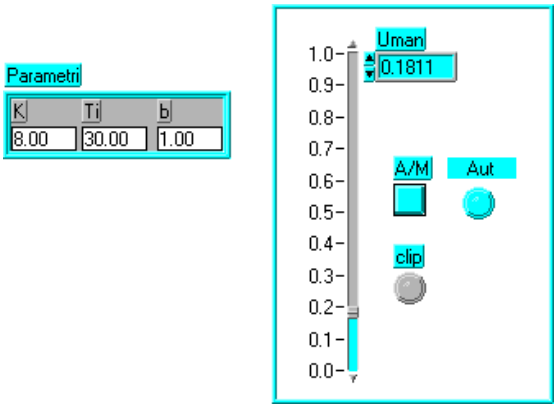

Figure 6.13: PI controller user interface

the simulator is about 300 (each one counting one or more sub-modules), with more than 1000 parameters (including vector parameters, such as the valve flow characteristics or the well characteristic curves); the number of variables in the process database is 734 and, finally, the number of control schemes is 23. The management of such a complex software object is definitely a non-trivial task.

6.1.4 User Interface

The simulator can be used according to three basic operating modes:

1. Fully interactive: a simulation is started from a steady-state database snapshot, and then the user interacts directly with the plant, opening and closing the stop-valves, modifying the control loop setpoints, or directly modifying the values of the exogenous variables through a direct interface with the process database (Fig. 6.13). The results can be observed on-line, by looking at the trend displays, graphic displays, and database interface.
2. One shot simulation: a steady-state snapshot (which is just an ASCII file) is manually modified, e.g. to alter a valve opening in order to obtain a step response. Then a simulation is run, whose duration is predetermined, and some selected variable trends are saved onto disk files by the tracers. Subsequently, the results can be analysed with any suitable tool (e.g. Matlab, a spreadsheet, etc.)
3. Batch simulations: in case one needs to run several similar simulations, it is possible to prepare initial snapshots for each of them, and then to run them in sequence, unattended. In case of errors, the next simulation in the batch is started. Again, the results are saved onto disk files by the tracers.

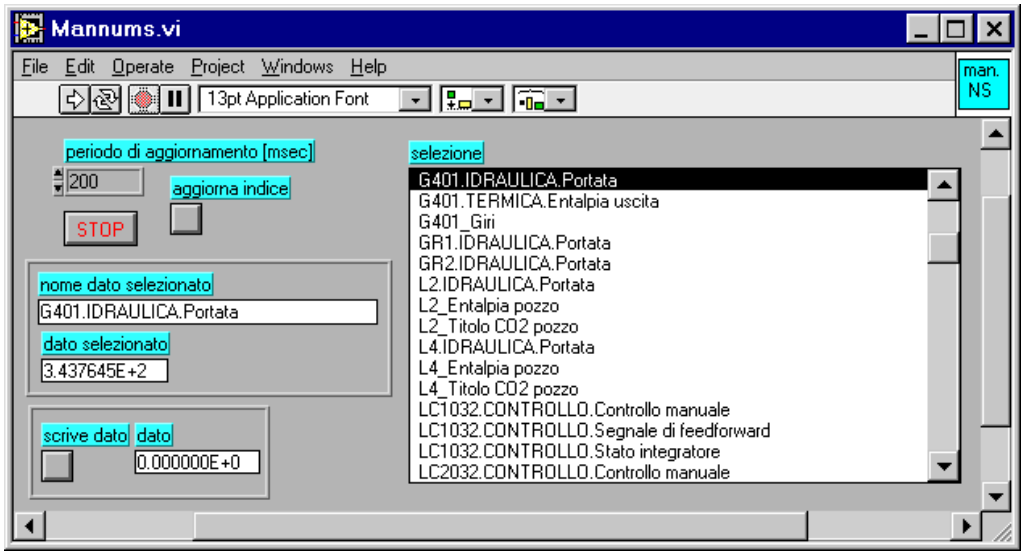

Figure 6.14: Manual interface to the process database

Two visual I/O modules, namely a trend display and the graphic display of the production wells are shown as examples in Fig's. 6.15 and 6.16.

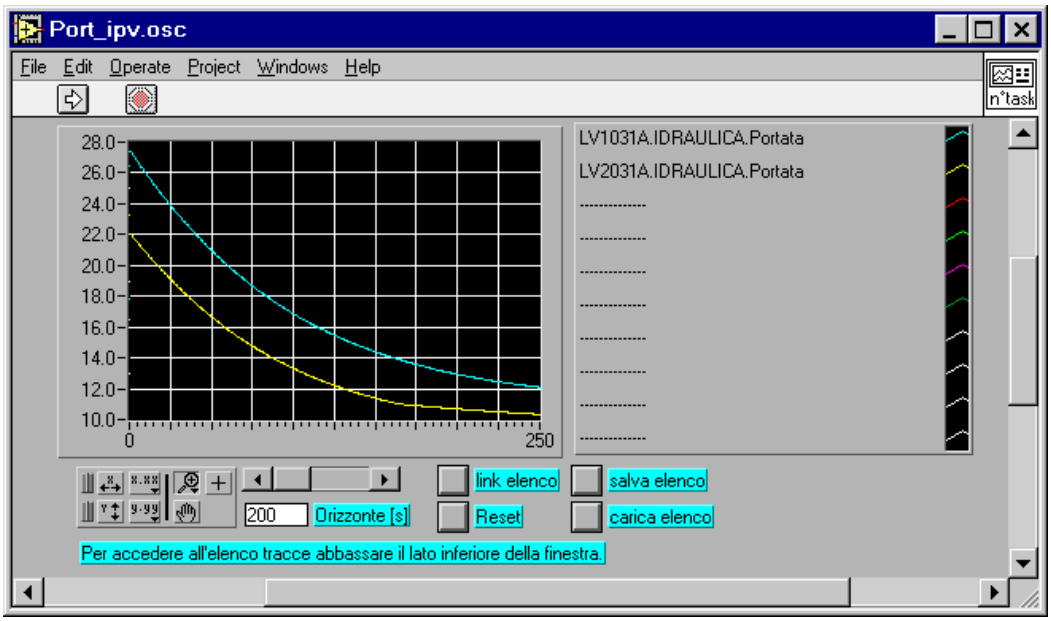

Figure 6.15: Trend display

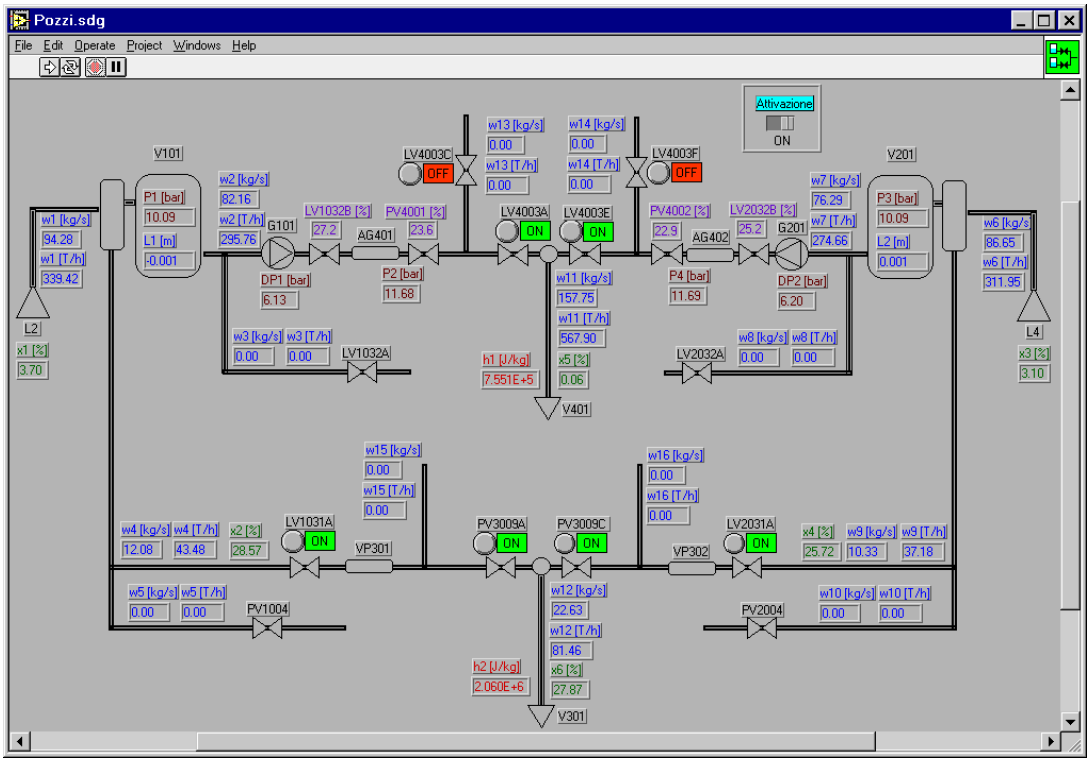

Figure 6.16: Graphic display of Unit 1 and 2

Since the simulation environment is based on a very powerful and flexible GUI, it is very easy to create ad-hoc modules, which can perform any kind of operation based on the values of the process variables, which are available through a database access module (or VI, in LabView terms). As examples of specialised modules which have been built, a module checking mass and energy balances for some sections of the plant, and an alarm display, which signals if some predetermined level and pressure thresholds have been crossed, can be mentioned. Once a suitable template is available, these modules can be easily created and modified by the final user of the simulator, provided he or she is sufficiently proficient in the LabView language, without any need to know the inner implementation details of the simulator.

6.1.5 Operational Limits of the Simulator

The simulator has been designed to cover all the range of allowed operating points, starting from any steady-state. In particular, the reference steady-state is the nominal operating condition, roughly corresponding with the 3A operating point in [ELC89]. In particular, it is possible to isolate some units by closing the corresponding stop-valves, or to analyse the response to pump and turbine trips. Conversely, it is not possible to simulate cold manual start-up operations, such as tank fillings, long pipeline fillings, and initial heating of the reboiler circuit, which would need a considerable additional modelling effort.

During the simulation, it is possible to save snapshots every once in a while automatically, so that the simulation can be recovered in case some error occurs (e.g., if some pressure value goes beyond the saturation level, causing an error in some of the sub-modules), and then re-started, taking the appropriate corrective actions.

6.1.6 Consistency Checks on the Simulator

All the newly built process components were checked thoroughly, in all their possible operating conditions, by running them in ad-hoc, toy plants. This included checks on mass, momentum and energy conservation, both in steady state and in dynamic conditions. Such checks were also performed on some sections of the assembled plant, building specialised modules for that purpose; this allowed to spot some modelling errors, and also an error in the connection of the components, in one particular case.

This approach to model and simulator checking suggested a possible additional feature which could be added to all the component modules, i.e. to always provide the mass and energy storage as output variables. This would permit very easily to check if the balances are preserved on arbitrary sections of

the plant, allowing to locate and remove both modelling errors, and model connection errors easily. This feature has not been implemented yet, but could be an essential part of a future, enhanced version of the simulation environment. Unfortunately, it would require to modify all the library models, in order to provide those additional variables; on the other hand, the added benefit, in terms of reliability of the simulators, could be very high.

6.2 Applications of the Simulator

6.2.1 Single-Loop Tuning and Control System Validation

Assuming a certain control architecture is given, in terms of input and output variables, the simulator can be used to perform the loop tuning, and the validation of the control system behaviour in response to the predicted perturbations (setpoint variations and/or disturbance rejection), in different operating points. This was done by the ENEL personnel themselves, in particular with respect to all the conventional control loops, such as level controls, and pressure controls connected to relief valves. Some examples will be reported in Chapter 7.

6.2.2 Test of Operating Manoeuvre Feasibility

Once the control loops have been tuned, it is possible to test the plant response to the various predicted operating manoeuvres, and to the major fault events. Due to the complexity of the plant, a very large combination of test simulations is possible:

1. Connection of a production unit to the main plant (liquid feed, gas-vapour mixture feed, or both, either on the main plant side or on the production unit side).
2. Disconnection of a production unit from the main plant (liquid feed, gas-vapour mixture feed, or both, either on the main plant side or on the production unit side).
3. Small (±15%) variations in the well production flowrate.
4. Reinjection pump trip, which implies the complete closure of the reinjection valve PV6003 (refer to Fig. 2.4) in 25 seconds, and the reduction to 40% of the full production flowrate on the production units (*reduced flowrate operating mode*).
5. High-pressure turbine trip.
6. Low-pressure turbine trip.

It is not possible to show here the detailed results of all these simulations, for reasons of space. Some conclusions can nevertheless be drawn.

Trials of transients 1. and 2. showed that the automatic control system is able to keep the main plant functional, provided a certain time sequence is followed for the opening and closure of the on-off valves. For instance (refer to Fig. 2.2 for the relative flowsheet), if the liquid transport line has to be cut off on the main plant side, it is necessary first to close the stop-valve LV4003 completely, and only then to start opening the relief valve LV4003C; otherwise undesirable flow reversal phenomena occur.

The transient 3. provided a successful checkout of the control systems for the whole plant, from the production wells through to the reinjection system. As an example, the trends of some key variables are shown for a 15% decrease in the production load setpoints. Note that, since it is very difficult to measure a two-phase flowrate, the production load is quantified by the gas-vapour mixture production flowrate, since the corresponding hot water flowrate is

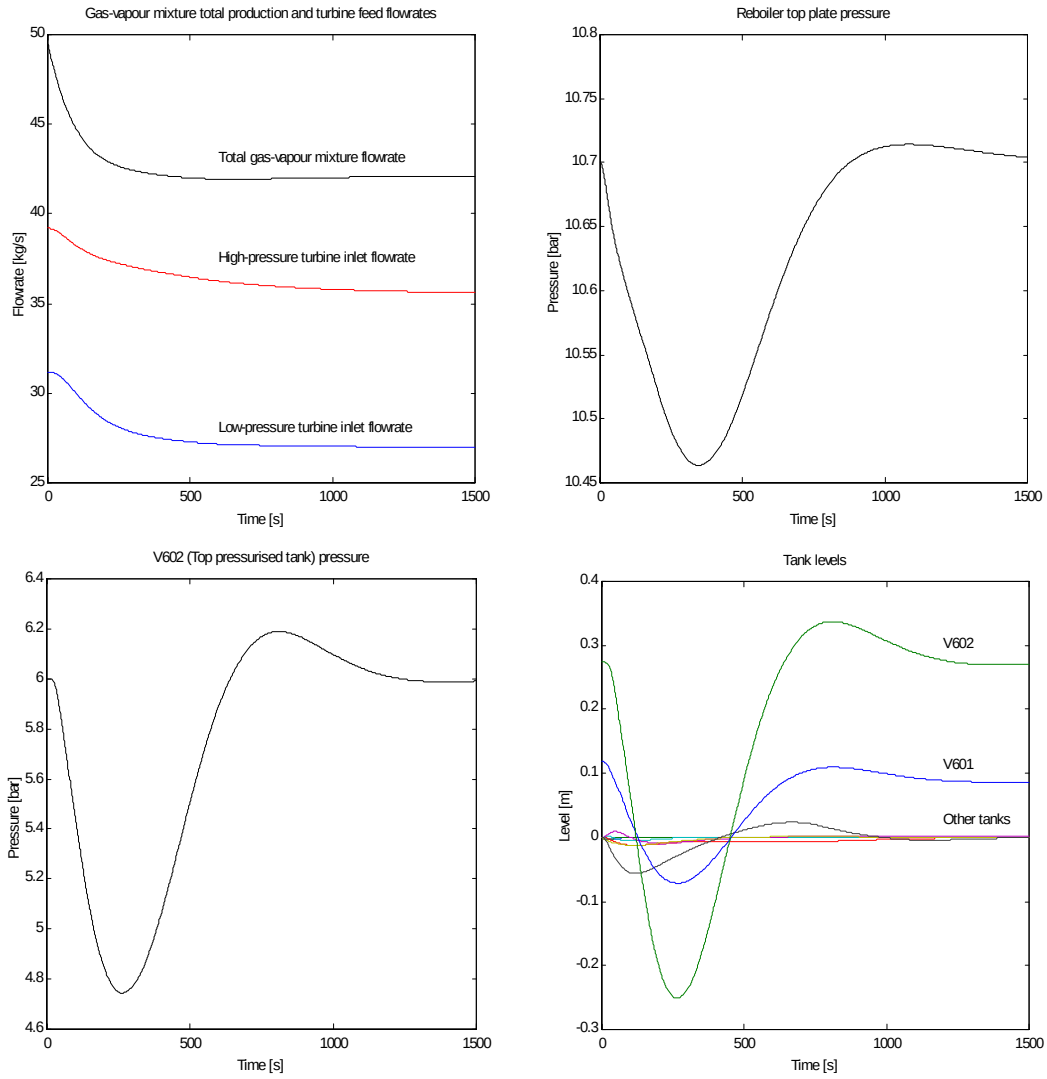

Figure 6.17: Plant response to a -15% load variation

approximately proportional. The simulation results are shown in Fig. 6.17. Note that the rise time of the production flowrate is approximately 200 s, while the turbine inlet flowrate responses are much slower, due to the overall plant inertia. The reboiler pressure transient is not critical (the lower peak is just 2% below the setpoint value of 10.7 bars), and also the top tank pressure transient keeps far away from the lower safety limit of 3 bars. Finally, the tank levels in plant units 1 to 4 show negligible perturbations around the reference value; the variations around the mid-tank reference level in the two pressurised tanks (which are not directly controlled) remain well within the safety limits, since all the tanks are approximately 3 meters high.

The transient 4. is undoubtedly the most critical for the plant; nevertheless, it has been shown that the reinjection system is able to withstand the transient, even with rather narrow safety margin. The same can be said for the rest of the plant: no levels or pressures ever exceeded the safety margins. The trends of some key variables are shown in Fig. 6.18. The bumps on the turbine inlet flowrates are caused by the pressure control systems PC5001 to PC5004 closing the control valves PV5001A to PV5004A, in order to avoid the pressure of the secundary separators going below the setpoint level. Under full-load operation, in fact, these valves are completely open and the corresponding controllers are in saturation state, to avoid any unnecessary pressure drop on the steam going into the turbines. Finally, recall that the maximum allowed pressure for the inlet of PV6003 is 25 bars and the minimum allowed pressure in the tank V602 is 3 bars.

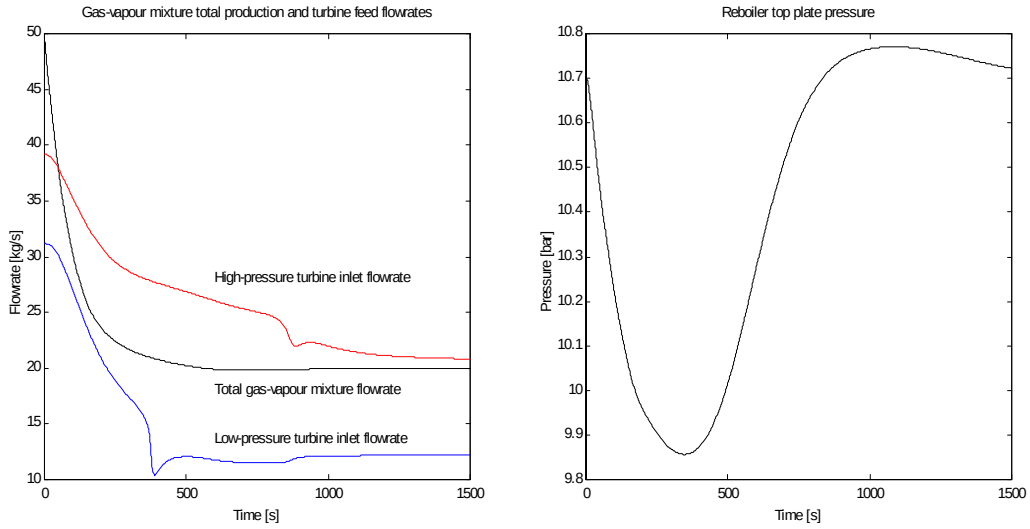

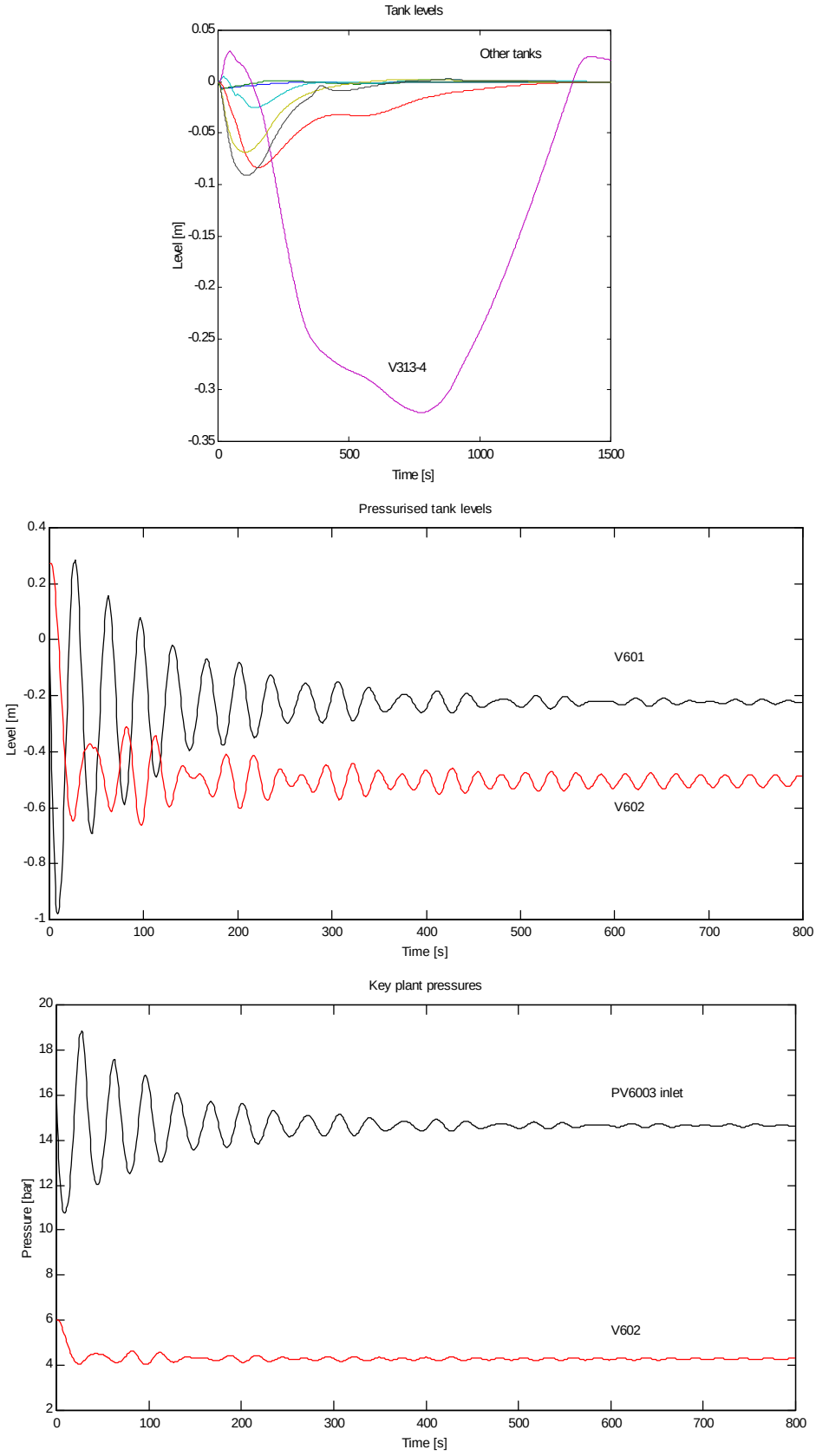

Figure 6.18: Reinjection pump trip and reduction to 40% of full plant load

In the case of the turbine trip (transients 5. and 6.), analysis by simulation showed that the setpoints of the pressure controllers PC5001 to PC5004 have to be suitably adjusted in order to avoid undesirable flow reversal phenomena in the feed circuit.

6.2.3 Aid for the Plant Commissioning Phase

The operations described in the two previous sections can dramatically speed up the plant commissioning phase. First of all, the availability of a preliminary tuning of all the controller parameters permits a substantial saving of time (and money) during the final tuning and checkout of the control system on the field. Moreover, the use of the simulator by the personnel who will be responsible for the plant commissioning, start-up and initial operations, permits them to familiarise with the process in advance, and to spot the right and wrong manoeuvres on the plant in various operating conditions at an early stage. Obviously, this is better done on a computer simulator than on the field, for many reasons including matters of cost, safety, and time; this is even more valid for a completely innovative and complex process, such as the Latera plant.

6.2.4 Plant Personnel Training

All the above considerations apply, in the initial phases of process operation, to highly professional personnel, such as design engineers and control engineers, for whom an engineering simulator can be an invaluable aid. Once the plant has entered the routine operation phase, the simulator can still be useful in the initial training of new personnel, who will then be responsible for routine plant operation, without taking any risk on the real plant. To be used for this purpose, the simulator needs substantial improvement in the user interface, while the process modelling part is more than adequate. Needless to say, the skills needed for such an operation are much more easily found than for the initial modelling and simulator construction phase.

6.3 Simplified Static Model in the gPROMS Environment

6.3.1 Description and Purpose of the Model

During the visit of the Author to the Centre for Process Systems Engineering at the Imperial College of London, a part of the process model was

re-implemented using the gPROMS modelling and simulation environment ([Pan93], [gPR97]). Since the process is very complex, the decision was taken to compare the modelling approach and results, when doing dynamic simulation, taking into account only the reboiler section of the plant. This section accounts for more than 50% of the process equations, but is rather easily implemented in gPROMS due to the repetitive structure of the model and the hierarchical representation facilities provided by the language. Some brief considerations, based on this experience, are given in Section 6.3.3. Subsequently, the same simulation environment has been used to implement a simplified static model of the plant, which allowed some preliminary study on the optimisation issues, which will be presented in the next Chapter. For this purpose, a steady-state model is required, since the optimisation of the transients is of little or no interest in the case of the Latera Plant, which is designed to operate in a steady-state for most of the time.

6.3.2 Simplifying Assumptions

Since a static model is sufficient for the static optimisation analysis, many drastic simplifications can be made in the model. First of all, since there is no interest in the configuration change transients, all the five production wells and phase separators have been represented by a single equivalent well and phase separator. Moreover, no level and pressure control systems are needed, since it is sufficient to include the equations $y(t) = y^*$ and $P(t) = P^*$ for every involved component to get rid of that matter. The pressure drops between the primary separators and the turbine inlets are neglected. Finally, the reinjection system is

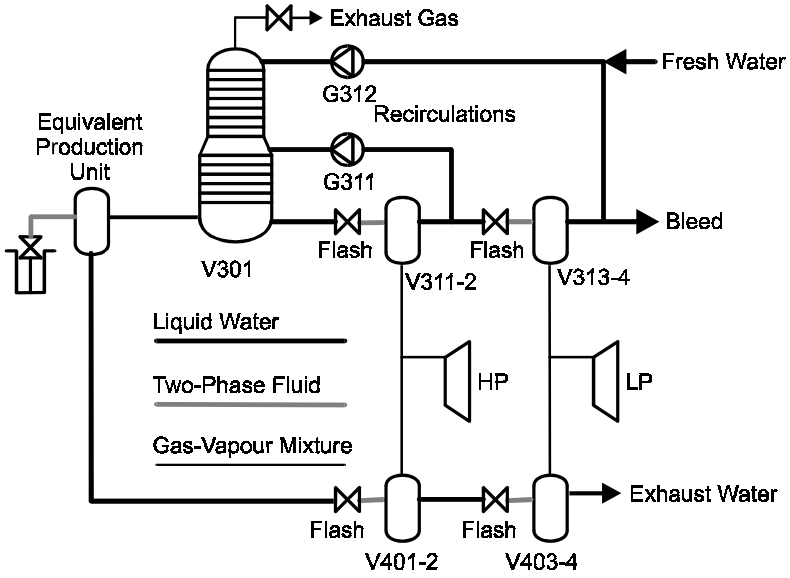

Figure 6.19: Simplified static model

of no interest, since it has no role in determining the plant efficiency, with the only exception of the (steady state) reinjection pump consumption.

The resulting, simplified flowsheet is given in Fig. 6.19. The modelling equations are the same as the ones described in Chapter 5, with the difference that the derivative terms have been eliminated, and that no particular elaboration of the equations is needed, since they can be directly inserted in the gPROMS model. As an example, the (static) plate model is listed below.

```
MODEL Plate
  PARAMETER
     # Dimensional parameters
     A,Vo,yo         AS REAL
     Ks,Kl,Ka,eta    AS REAL
     # physical constants and correlation coefficients
     alpha, R,g,H    AS REAL
     hlcoef          AS ARRAY(4) OF REAL
     hvcoef          AS ARRAY(5) OF REAL
     Tcoef           AS ARRAY(4) OF REAL
     hgcoef          AS ARRAY(4) OF REAL
     rovcoef         AS ARRAY(3) OF REAL
     rolcoef         AS ARRAY(3) OF REAL
     Tlcoef          AS ARRAY(3) OF REAL
  VARIABLE
     P,Pg,Pv,Pgam,Psl            AS Pressure
     xga,xgl,xgai,xgli,xgle      AS MassFraction
     xgao,xglo,xgam,xstar  AS MassFraction
     hl,hai,hli,hle        AS Energy
     hao,hlo,E,ha          AS Energy
     y                     AS Length
     Ma,Mg,Mgl,Mwl         AS Mass
     wai,wli,wle,wao,wlo,wc,ws   AS MassFlowRate
     Va, Vl                AS Volume
     rog,rov,roa,rol             AS Density
     Ta,Tl                 AS Temperature
     PP,PPsl               AS Pressure
     hv, hg, hgl           AS Energy
  STREAM
     GasInlet: wai,hai,xgai AS WHXstream
     GasOutlet: wao,hao,xgao AS WHXstream
     LiquidInlet: wli,hli,xgli AS WHXstream
     LiquidOutlet: wlo,hlo,xglo AS WHXstream
     LiquidExtraInlet: wle,hle,xgle AS WHXstream
  EQUATION
     # Mass & Energy Buildups
     Ma=roa*Va;
     Mg=rol*xgl*Vl+rog*Va;
     E = rol*(hl+xgl*hgl)*Vl + roa*ha*Va - 1e5*P*Vo;
     Mwl = rol*Vl;
     Mgl = rol*xgl*Vl;

     # Mass & Energy balance equations
     0=wai-wao-wc-ws;
     0=wai*xgai-wao*xgao+wli*xgli-wlo*xglo+wle*xgle;
     0=wli*hli+wai*hai-wlo*hlo-wao*hao+wle*hle;
     0=wli*(1-xgli)-wlo*(1-xglo)+wle*(1-xgle)+wc;
     0=wli*xgli-wlo*xglo+wle*xgle+ws;
     # Physical properties
     Pg=alpha*xga*P/(1+(alpha-1)*xga);
     Pv=P-Pg;
     PP=log(Pv);
     Ta=((Tcoef(1)*PP+Tcoef(2))*PP+Tcoef(3))*PP+Tcoef(4);
     rov=(rovcoef(1)*Pv+rovcoef(2))*Pv+rovcoef(3);
     hv=(((hvcoef(1)*PP+hvcoef(2))*PP+hvcoef(3))*PP+
```

```
        hvcoef(4))*PP+hvcoef(5);
     rog=Pg/(R*Ta);
     roa=rog+rov;
     ha=(1-xga)*hv+xga*hg;
     hg=hgcoef(1)+hgcoef(2)*Ta+hgcoef(3)*Ta^2+hgcoef(4)/Ta;
     hgl=hgcoef(1)+hgcoef(2)*Tl+hgcoef(3)*Tl^2+hgcoef(4)/Tl;
     rol= (rolcoef(1)*hl+rolcoef(2))*hl+rolcoef(3);
     Tl=(Tlcoef(1)*hl+Tlcoef(2))*hl+Tlcoef(3);

     # Volumes
     Vl=A*y;
     Va=Vo-Va;

     # Output flows
     wlo=Kl*(y-yo);
     hlo=(1-xgl)*hl+xgl*hgl;
     xglo=xgl;
     hao=ha;
     xgao=xga;

     # Interphase flows
     PPsl=log(Psl);
     Tl=((Tcoef(1)*PPsl+Tcoef(2))*PPsl+Tcoef(3))*PPsl
        +Tcoef(4); # Tl=Tsat(Psl)
     xstar=(P-Psl)/((P-Psl)+alpha*Psl);
     xgam=xgai+eta*(xstar-xgai);
     Pgam=alpha*xgam*P/(1+(alpha-1)*xgam);
     ws=Ks*wai*(Pgam-H*xgl);
     wc=(wai*(xgam-xgai)+ws*(1-xgam))/xgam;
END # Model Plate
```

The thermodynamic properties of saturated water and steam, which are needed in the model, are not directly available in gPROMS, which is not specialised to handle power processes, but is rather oriented to general chemical process simulation. Therefore, they have been approximated by polynomial equations, or by the logarithm of polynomials, whose coefficients have been selected with a least-square algorithm to fit the real saturation curves. Fortunately, by introducing the only approximation that the water density is equal to the density of the saturated water at the same temperature (which is absolutely reasonable at the pressures found in the Latera process, up to 20 bars), the two-entry steam tables (that is, thermodynamic properties outside the saturation conditions, which depend on two state variables) are not needed; otherwise, their implementation through interpolating equations would have been a rather complex issue.

The resulting model was used to compute the overall process efficiency (i.e. net power output per kilogram of extracted geothermal fluid), taking also into account the energy consumption of the recirculation and reinjection pumps, which were given by the manufacturer, and can be very well approximated by quadratic curves. The optimisation tool gOPT, which is integrated in the gPROMS environment [gOP98], was then used to compute the optimal operating points of the plant under different conditions.

6.3.3 ProcSim vs. gPROMS Simulation

Directly comparing a simulation environment such as ProcSim with an equation-oriented tool like gPROMS is quite difficult, since both have their strong and weak points with respect to power process simulation.

Both environments are fully modular, in that models for the single components can be written, irrespective of their connection with other components, and then assembled according to the plant flowsheet. However, the approaches to the system simulation are radically different.

ProcSim is heavily based on decoupling principles, so that the solution of the system of equations describing the whole process is split as much as possible in the sequence of the solution of much smaller problems. This forces to elaborate the process equations, adapting them to the hydraulic or causal solution sub-modules, which is not an easy task for the inexperienced user who wants to create new models. On the other hand, the decoupled solution with fixed step sizes makes it possible, at least in principle, to distribute the computation on many different CPU's, to perform multirate integration (which can be crucial in certain cases, as explained in Section 3.2, Example 5) and to guarantee that hard real-times constraints are satisfied, which is important for training simulators, and mandatory for hardware-in-the-loop testing. In general, it is possible for the user to interact with the simulator as the simulation goes on. Finally, the availability of a model library specialised for power processes and of the steam table modules is very helpful in the construction of new plant models.

The approach followed by gPROMS is completely different: the process equations are directly entered in textual form, irrespective of their being algebraic or differential, explicit or implicit, and the resulting (often very big) system of differential-algebraic equations (DAE) is solved simultaneously. This is possible thanks to the very powerful, fully implicit DAE integrator ([Jar92]), which uses state-of-the-art numerical techniques, such as sparse matrix algorithms and adaptive-order/adaptive-step-size BDF codes. The equation solver is a general purpose solver, so that it does not exploit the particular domain-specific structure and properties of the model equations, as is heavily done in the ProcSim environment; on the other hand, the model developer need not bother at all about how the equations are solved, since this is entirely up to the integrator code. The integration is carried out by adaptive step size algorithms: in some situations (e.g. when the transients are almost settled out) this is much more efficient than the fixed time step approach of ProcSim; on the other hand, if discrete-time models are included (e.g. digital controllers, or pipeline models integrated with the method of the characteristic lines), the integrator has to be stopped and re-initialised at every time step, so that the advantage in terms of efficiency becomes more questionable, in particular in

the presence of hard real-time constraints (such as in hardware-in-the-loop simulations). Moreover, when mixed fast and slow dynamics are present at the same time, no multi-rate integration is possible, since all the equations have to be solved simultaneously. A big advantage is given by the fact that the model is based on the "native" equations, which can be symbolically manipulated, e.g. to solve higher-level problems than simulation, such as static or even dynamic optimisation problems (optimal control problems). On the other hand, the environment has been designed with a "batch simulation" approach in mind, while ProcSim can be used interactively.

Some attempts were made by the Author, at the Imperial College Centre, to adapt the decoupling principles to the gPROMS approach, with the aim of speeding up the numerical solution of the global system by enhancing the block-triangular structure of the Jacobian matrix of the system. However, even if the problem has been given a mathematical formulation, its effectiveness can only be proven by actual numerical simulation of a set of test cases, and this has not been possible for lack of time and resources.

Summing up, a thorough comparison of the two modelling and simulation environments is quite difficult and beyond the scope of this dissertation; moreover, architectural differences (such as different CPU's, different operating systems, etc.) make the task of comparing them directly even more questionable. Nevertheless, some remarks have been made in order to understand at least the similarities and differences, along with the strong and weak points of each one.

7. PLANT CONTROL AND MANAGEMENT

7.1 General Overview

The Latera plant was designed to provide base load power to the electrical grid, due to the intrinsic nature of the geothermal wells, which operate more efficiently if their flow is left unchanged as much as possible. The normal operating mode of the plant is therefore a steady state, and no tracking control of any kind is normally required. Moreover, for various reasons, the designers of the plant opted for a totally decentralised control system (i.e. only single-loop control systems), which is then implemented by advanced PLC-like controllers. Note also that the plant is geographically distributed: the production units are 400 meters away from the main plant, while the main reinjection wells are still farther away (10 km), which is another reason to prefer a decentralised control system. The general control strategy outlined in the original design document [ELC89] has already been explained in Section 2.1: the plant is divided into six functional units, and the control strategy is such that failure or unavailability of any of them should not lead to a shut-down of the others, as long as this is possible and/or convenient.

The 37 control loops found in the original plant design have been reduced to 23, thanks to the simplified representation of the production units, as explained in Sect 2.2.1. With reference to Fig's. 2.2, 2.3, and 2.4, their complete list is the following:

F1044, F2044, F3012, L1032, L2032, L3011, L3101, L3102, L4001, L4002, P1004, P2004, P3001, P3002, P3005, P4001, P4002, P5001, P5002, P5003, P5004, P6000, T3013.

According to their function, they can be divided into four categories:

1. Production rate controllers
2. "Homeostasis" controllers
3. Pressure controllers in the secondary separator and turbine feed circuit.
4. Reboiler cycle controllers

The aim of the controllers belonging to the first category (F1044, F2044) is to control the total production flowrate. If the main plant and the reinjection

wells are fully available, the production rate will be of course 100%, to maximise the power output. However, in some situations (due, e.g. to the unavailability of some reinjection well, or of the whole reinjection unit), it can be necessary to reduce the production rate. The controller structure is rather obvious: since the two-phase flowrate coming out of the production well is very difficult to measure, and the liquid flowrate is strongly coupled with the tank level control, the best indicator of the production rate is the gas-vapour mixture flowrate coming out of the primary separator, which is roughly proportional to the total production rate, at least at a fixed separator pressure, which is guaranteed by the reboiler pressure control. A simple PI, or even I, controller is more than adequate to close the loop on the well head control valve.

The aim of the controllers belonging to the second category, whose name has been borrowed from the field of physiology, is to keep some process variables at their "natural" value, rejecting any disturbance acting on them. Many different controllers belong to this category, which is characterised, among other things, by the fact that the controller structures are rather obvious. First of all, the seven level controllers (L1032, L2032, L3011, L3101, L3102, L4001, L4002), whose aim is to keep the liquid level in the separators tanks and in the reboiler bottom as close as possible to the zero reference value; the control loop acts on the stem position of the outlet valve(s), and simple PI controllers are sufficient to guarantee satisfactory performance, as demonstrated in simulation of the large load variation at the end of Chapter 6. Next, the four pressure controllers P1004, P2004, P3001, P3002, which act on relief valves in case the production units are isolated from the main plant, in order to avoid the pressure in the primary separators growing too high; in this case, even simpler P controllers can be employed. Next, the two controllers P4001 and P4002, whose aim is to keep the pressure in the liquid transport pipelines well above the saturation pressure, in order to avoid a two-phase flow in the final section of the pipes, which could give rise to unpredictable mechanical effects on the pipes themselves; also in this case, simple P or PI controllers are more than adequate to provide satisfactory performance. Last, but not least, the pressure controller P6000, whose aim is to keep the top pressurised tank pressure above the saturation level, to avoid a two-phase flow in the long reinjection pipelines. In this case the purpose of the controller is very clear, but its implementation is more critical, since the only available actuator is the control valve PV6003, but the transfer function of the plant shows a resonance peak (due to the interaction between the tank capacitance and the connecting pipe inertance), and a large phase lag due to the wave propagation delay. The controller has then to be carefully studied. In all the other cases, the controller structure is well-defined from the beginning, and the controller parameters can be easily tuned according to some empirical rules. In

general, a specified rise time in closed loop is sought by simulation, which is roughly equivalent to specify the loop bandwidth; this should be the largest possible, taking into account the limitations given by the sensor's and actuator's own bandwidth. Note that all the valve actuators are of the compressed air kind, and thus very fast, compared to the electrically actuated valves found in other plants.

The purpose of the controllers belonging to the third category, namely P5001, P5002, P5003 and 5004, is to keep the secondary separator pressures within some pre-specified range. The original design document, however, is very concise in this respect, generally suggesting that the pressures should be kept at their reference value. As will be explained in more detail in section 7.2.2, if the issue of energetic efficiency is considered, the control policy has to be completely changed.

The case of the controllers belonging to the fourth category, which includes the three reboiler controllers P3005, F3012, and T3013, is completely different, for many reasons. First, many more measurements (FT3012, FT3013, FT3014, FT3015, FT3102, FT5001, PT3005, TT3013, TT3014) are available than control variables (PV3005A/B, FV3012, TV3013); second, the controller structure (i.e. which should be the controlled variables) is not at all clear a-priori; third, once the controlled variables are selected, there is no "natural" setpoint value for them; in other words, three degrees of freedom (corresponding to the three control variables) are available, which can be used to maximise the plant efficiency. This was not clearly recognised in the design document, as the proposed controller structure lacked a clear view of the purpose of this part of the control system, stated above. The controller structure which was proposed is also questionable, in particular for reduced-load plant operation. This will be the subject of Section 7.4. Unfortunately, this aspects were recognised only towards the end of the research, so that only a preliminary study could be carried out on them. Nevertheless, the whole issue has been given a systematic statement, and future possible directions of research are clearly outlined.

7.2 Conventional Controllers

Most of the data contained in this section are taken from [Cal98], which is based on the use of the simulator by the ENEL engineers. Further details on the subject can be found in that document.

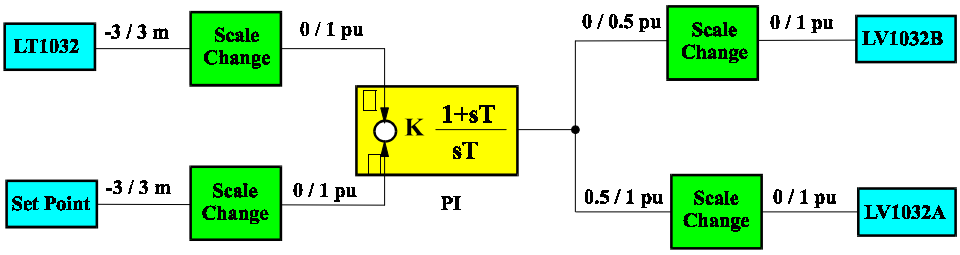

Figure 7.1: L1032 Block Diagram

7.2.1 Level Controls

As an example of level control design, the case of L1032 is briefly discussed. The others have been treated in a similar way.

The block diagram of the controller is shown in Fig. 7.1

The readings from the level transducer and the setpoint are transformed in the range (0-1), and their difference is the input of a PI controller. A split-range structure is employed for the output of the controller: first the LV1032B valve is opened; if this is not enough, the relief valve LV1032A is also open; of course, this happens only when the flow in the liquid transport pipeline is cut off, requiring the production flowrate to be discharged out of the plant circuit.

The plant transfer function is

$$G(s) = K_l \frac{1}{sT_l} \tag{7.1}$$

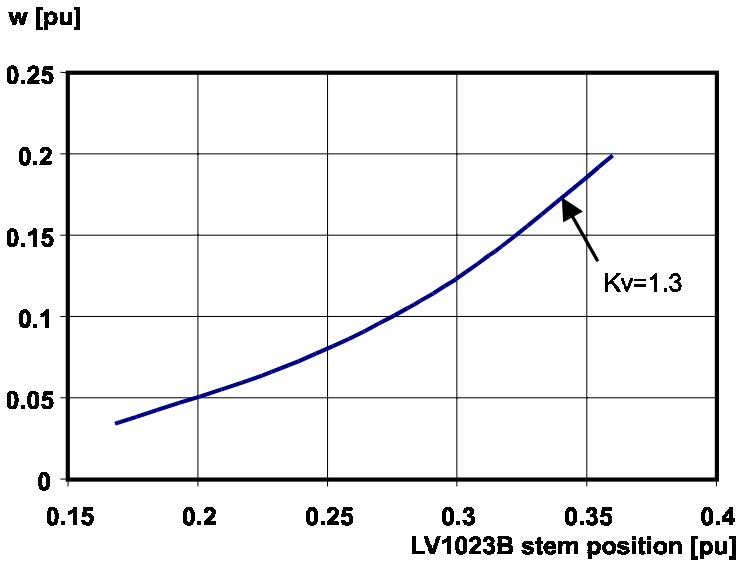

Figure 7.2: Process gain in varying operating conditions

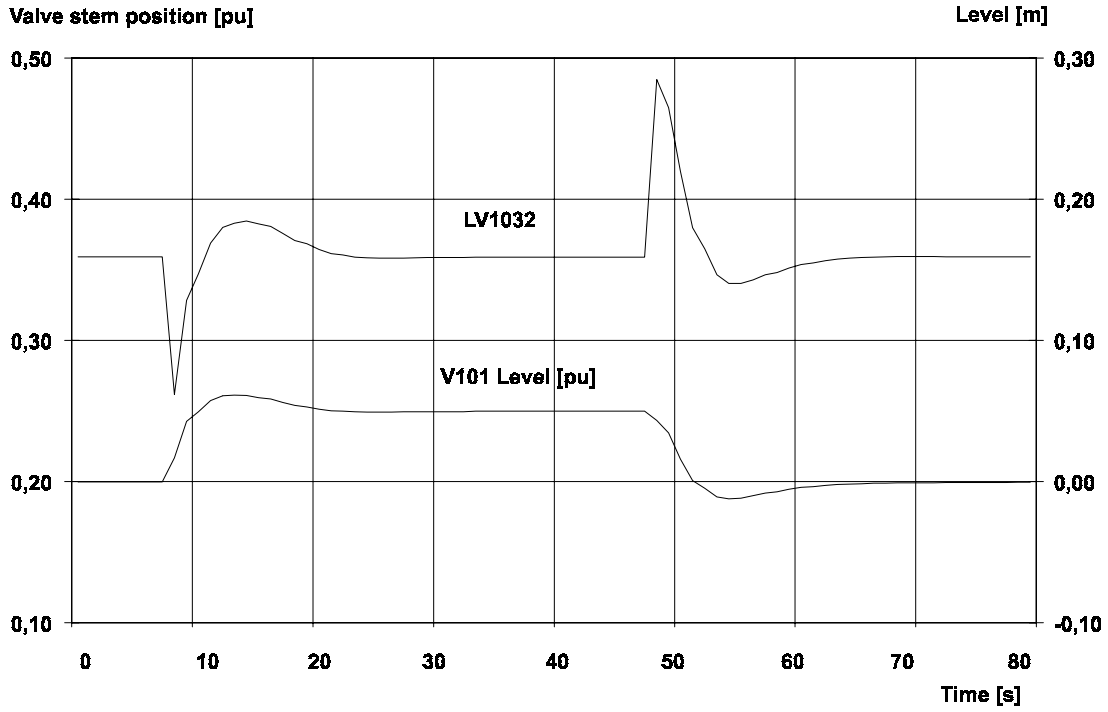

Figure 7.3: L1032 response to step variations in the setpoint

where the characteristic time T_l is given by the ratio of the product of the tank cross-section times the nominal tank height to the nominal flowrate, and the static gain K_l (in p.u.) was found in different operating conditions by varying the production rate, resulting in Fig. 7.2.

The PI controller parameters K = 8 and T = 15 s were selected, leading to a response to step changes of 5 cm in the setpoint (around the nominal operating point 3A) which is shown in Fig. 7.3

The controller has also been tested under large transient conditions, in particular when the stop valve LV4003 is completely closed, so that the split-range structure comes into action. The result is shown in Fig. 7.4, where the valve closing signal is given at time t =10 s; the normalisation values are 250 kg/s for the flowrates and 1 m for the level. Note that the simulator is able to handle zero flowrates correctly, thanks to the modelling expedients described in Section 4.4.

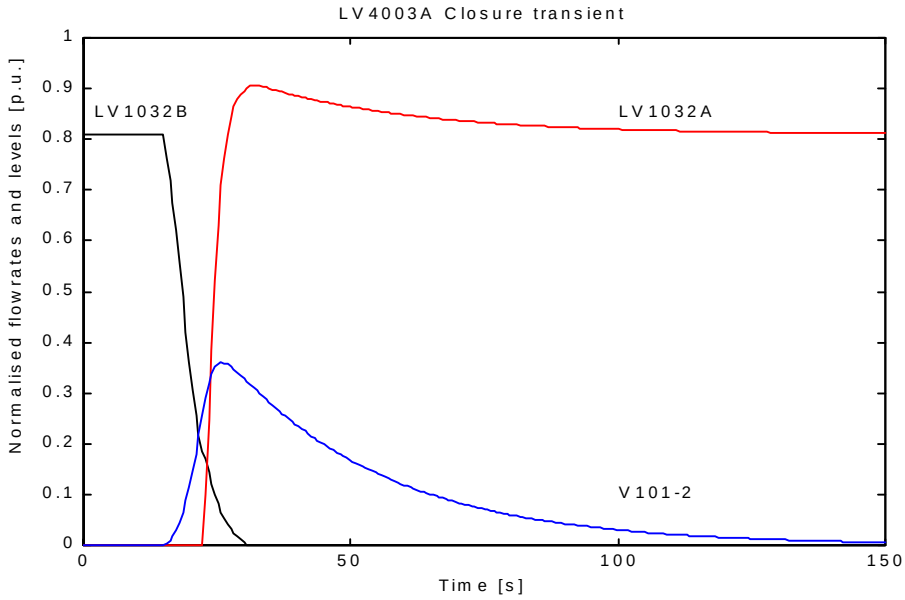

Figure 7.4: LV4003 closure transient

All the other level controllers have been dealt with in the same way. Actually, in the case of the three level controls in the reboiler cycle, namely L3011, L3101, L3102, a better, centralised control structure could be devised, taking into account the fact that the total storage of liquid in the cycle is approximately constant. The valve LV3011 should then control the difference between the liquid storage in the reboiler bottom and in the V311-2, the valve LV3101 the difference between the storage in V311-2 and V313-4, and the valve LV3102 the total amount of liquid stored in the cycle, which undergoes only small variations even if the level in V313-4 varies significantly. All these storage quantities can be expressed as weighted sums of the levels. However, that was not necessary, since the fully decentralised control architecture, shown in Fig. 2.3, is completely adequate, even for the largest transients, such as the one shown in Fig. 6.18.

Nevertheless, it was considered convenient to limit the bleed flowrate through LV3102, possibly using the measurement coming from FT3102. In this way, when the levels in the reboiler bottom and in V311-2 have returned to the reference value, the level in V313-4 will automatically find itself near the reference value. Otherwise, when the level in V313-4 is above the setpoint, the whole circuit will lose a large amount of water; conversely, when the level is below the setpoint, LV3102 will be completely shut, but the fresh water inlet flow (which is limited to a few kg/s) will take a very long time to restore the total liquid storage in the cycle.

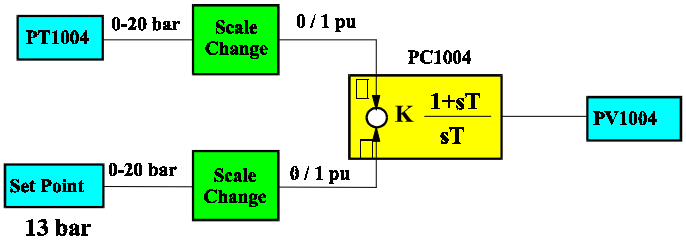

Figure 7.5: P1004 Block diagram

7.2.2 Pressure Controls

As already said, the aim of the pressure controllers P1004, P2004, P3001, P3002 is to open their relative relief valves when the stop valves on the transport pipes are closed. The setpoints must be 1 or 2 bars above the normal operating pressure, to avoid accidental vapour bleeds, and the gain should be tuned empirically, in order to limit the pressure overshoot when the controller comes into action. During normal operation, these controllers remain in a saturation state, with the relative valves completely closed.

As an example, the block diagram of the P1004 controller is Fig. 7.5.

The transient corresponding to the closure of the stop valve LV1031A at time t = 10 and its re-opening at time t = 100 is shown in Fig. 7.6; the normalisation values are 30 kg/s for the flowrates and 15 bars for the pressure. When the stop valve is closed, the primary separator pressure rises until the setpoint value is exceeded; the relief valve then starts opening, and the pressure settles to the setpoint value of 13 bars. When the stop valve is re-opened, the pressure decreases until the relief valve gets completely closed; from this moment on, it will be given by the reboiler pressure, plus the pressure drop across the transport pipe.

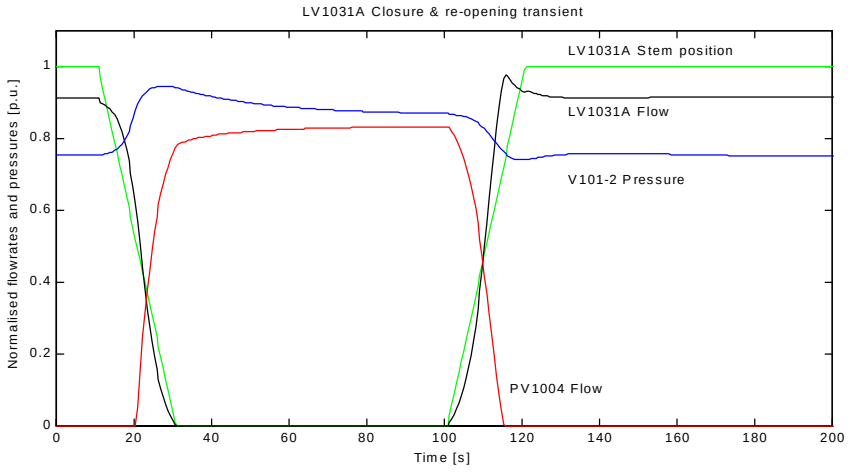

Figure 7.6: LV1031A closure and re-opening transient

The two pressure controllers P4001 and 4002 should ensure that the tail pressure of the two liquid transport pipelines (which by the way have a higher elevation than the production wells) remains well above the saturation level (approximately 9.5 bars). Their gain should be tuned in order to satisfy this constraint with a certain safety margin in every possible operating condition. This can be done by using the simulator, and trying all the planned manoeuvres on the production units.

More details on the subject can be found in [Cal98].

7.2.3 Turbine Feed Pressure Controls

The pressure controllers P5001 to P5004 deserve a special mention. Refer to the flowsheet in Fig. 2.3. The control system structure for P5001 will be described in particular, the others being equal.

The aim of the control system P5001 is to keep the pressure in the secondary separator V311-2 within a specified range. This can be done by partially closing PV5001A, if the pressure gets too low, or partially opening the relief valve 5001B, if the pressure gets too high. It is evident that both actions have a strong impact on the energetic efficiency of the process: in the former case, the steam is subject to a pressure drop just before the valve inlet, an irreversible process which decreases the mechanical energy that can be extracted from the fluid; in the latter case, part of the steam is discharged into the atmosphere, which is clearly undesirable if it is not absolutely necessary. The idea is then to use two PI controllers: PC5001A, whose output is the stem position of PV5001A, which is normally in the state of saturation corresponding to the completely open valve, and the other, acting on the valve PV5001B, which is normally in the state of saturation corresponding to the completely closed valve. The two setpoints correspond to the high and low boundaries of the allowed pressure range. The corresponding control scheme is shown in Fig. 7.7. Generally, the relief valves are opened in case of a turbine

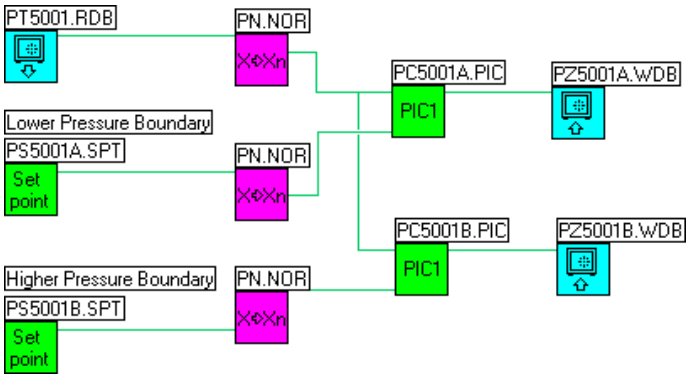

Figure 7.7: P5001 Control Scheme

trip, when the produced steam has to be discharged into the atmosphere; conversely, the in-line valves are closed when the production flowrates (both gas-vapour mixture and hot water) fall below a certain threshold, or even go to zero, in case of unit shutdown. In the last case, the corresponding valve is completely closed by the control system, thus isolating the unit from the rest of the main plant.

Through extended simulations of the whole plant, it has been discovered that the intervention of these control valves invariably decreases the net power output. Therefore, it makes no sense to use these pressure control systems to keep the secondary separators at their reference pressure value; their pressure should instead be given by the pressure-flowrate relationships of the two turbines. This can lead to an increase in the net produced energy of more than 10%.

The pressure boundaries (i.e. controller setpoints) have thus been set according to the following criteria:

- The upper boundaries should be sufficiently higher than the values at full production load , in order to avoid spurious steam bleeds.
- The lower boundary for the high pressure turbine circuit should be higher than the upper boundary of the low-pressure turbine circuit, otherwise no flashing would occur on the valves LV3101 and LV4001A.
- The lower boundary for the low-pressure turbine circuit should be higher than the atmospheric pressure, otherwise the LV4002B valve would not function properly, should it be opened due to a reinjection pump trip.

Summing up, the following pressure ranges have been selected:

- (4.0–7.5) bars for the controllers in the high-pressure turbine circuit
- (1.5–3.5) bars for the controllers in the low-pressure turbine circuit

The bumps in the turbine flowrates that can be seen in fig 6.18 correspond to the PC500XA going out of the saturation state, since the turbine inlet pressures in the reduced flow operating mode would be too low.

7.2.4 Production Rate Controls

As already discussed in the introductory overview, the production rate of each well is controlled by a loop measuring the gas-vapour mixture flowrate coming out of the phase separator (e.g. PT1044), and acting on the stem position of the well head control valve (e.g. FC1044). The loop bandwidth should not be too high, to avoid fast variations in the valve opening. The transients shown in Fig's 6.17 and 6.18 have been obtained by step changes on the setpoints of both controllers (P1044 and P2044), and the response in terms of the sum of the gas-vapour flowrate is shown there.

7.3 Reinjection Control

7.3.1 General Considerations

In some respects, the reinjection unit resembles a hydroelectric plant, due to the presence of very long pipelines with pressurised water, with significant flow and pressure wave propagation phenomena. However (refer to the schematic diagram in Fig. 2.4), the differences far outnumber the similarities. First of all, the total pipeline length (10 km) is much longer than in typical hydro plants, whose penstocks are rarely longer than two kilometres. This implies, on one hand, longer propagation delays; on the other hand, a much stronger effect of the distributed friction, since the pipe is sized just for water transport, not to produce power. The second main difference lays in the first part of the pipeline, which is connected at both sides to pressurised tanks, with no control valve in-between. This means that the oscillations, generated by the interaction between the fluid inertance in the pipe and the capacitance of the tanks (like in a LC equivalent circuit), are damped out only by the distributed friction of the connecting pipe. These oscillations are difficult to control using the valve PV6003, since its controlling action is filtered by the capacitance of the tank V602. Conversely, in a hydro plant penstock, during normal operation, the equivalent resistance of the hydraulic nozzle at the end of the circuit is such that the oscillations have a high damping coefficient. Finally, the presence of a pump to overcome the head caused by the 100-metres-high hill, located between the main plant and the reinjection wells, adds a possible failure mode to the plant, which is particularly critical.

The control system P6003 acts on the valve PV6003, just before the reinjection wells, to keep the pressure of the top-of-the-hill pressurised tank V602 equal to its setpoint value. Two conflicting objectives arise: on one hand, the pressure in V602, being the lowest of all the circuit, has to be kept well above the saturation level (2.5-3 bars), to avoid a two-phase flow in the topmost sections of the pipelines; on the other hand, the pressure should not be too high, in order to remain below the design pressure of the pipeline (25 bars), in particular at the end of the pipe, where the pressure is higher. The setpoint for the pressure inside V602, which is the controlled variable, has been fixed at 6 bars, corresponding to 15.5 bars at the inlet of PV6003. This ensures the widest possible range of oscillations for both values in case of perturbations.

The pressure control system has two different operating modes:

1. Normal operation: a closed-loop, low-bandwidth controller tries to keep the pressure in V602 at the setpoint values, rejecting the disturbances caused by the variations in the pump flowrate.
2. Pump trip: in case of a pump trip, no closed-loop control system will ever be sufficiently fast to guarantee that the pressure in V602 does not fall below

the critical value; consequently, an open-loop closure of PV6003 is triggered, whose optimal duration has been found by simulation to be 25 seconds, in order to provide the largest safety margins on both the critical points of the circuit. The corresponding transient has already been shown in Fig. 6.18.

The focus will now be on the normal operation controller. In the following analysis, the role of the GR2 well is not taken into account, since it was included in the simulator in a later phase of the project.

7.3.2 Linear Analysis

The starting point for the study of the pressure control system is the analysis of the linearised transfer function between the actuator (PV6003 valve stem position) and the sensor (PT6003 sensor, measuring the pressure in the tank V602), around the nominal operating point 3A. To this aim, the partial differential equations (4.59)-(4.61), describing the mass and momentum conservation in the pipes, the pressurised tank equation (5.100), and the liquid valve equation (5.28) have been linearised around the operating point and then Laplace-transformed. The boundary conditions for the plant are assumed to be: exogenous flowrate at the outlet of LV4002A (which is justified both by the presence of the level control loop, and by the high impedance of the valve, seen from the outlet), and fixed pressure at the outlet of PV6003 (which is justified, provided the flowrate is below the maximum well draining capacity). The resulting equations, which contain exponential terms in s, due to the wave propagation delays, have been assembled in a system of equation, which is then solved for $s = j\omega$ to yield the frequency response of the plant. There is no room here to include all the mathematical details; the results in terms of Bode diagrams will instead be given.

Case 1: No distributed friction

The Bode plot of the plant transfer function is shown in Fig. 7.8

The low-frequency behaviour is a low-pass filter, whose pole results from the total tank capacitance and the valve resistance (in terms of equivalent electrical circuit). The first resonance peak is located at around 0.198 rad/s, resulting mainly from the interaction between the capacitance of the tanks and the inertance of the connecting pipe. The successive peaks (at 0.97, 1.88, 2.79 rad/s, etc.) are the higher-order harmonics caused by the wave dynamics between the two tanks, whose damping is very low since, as already said, the valve friction effect is filtered out by the capacitance of V602.

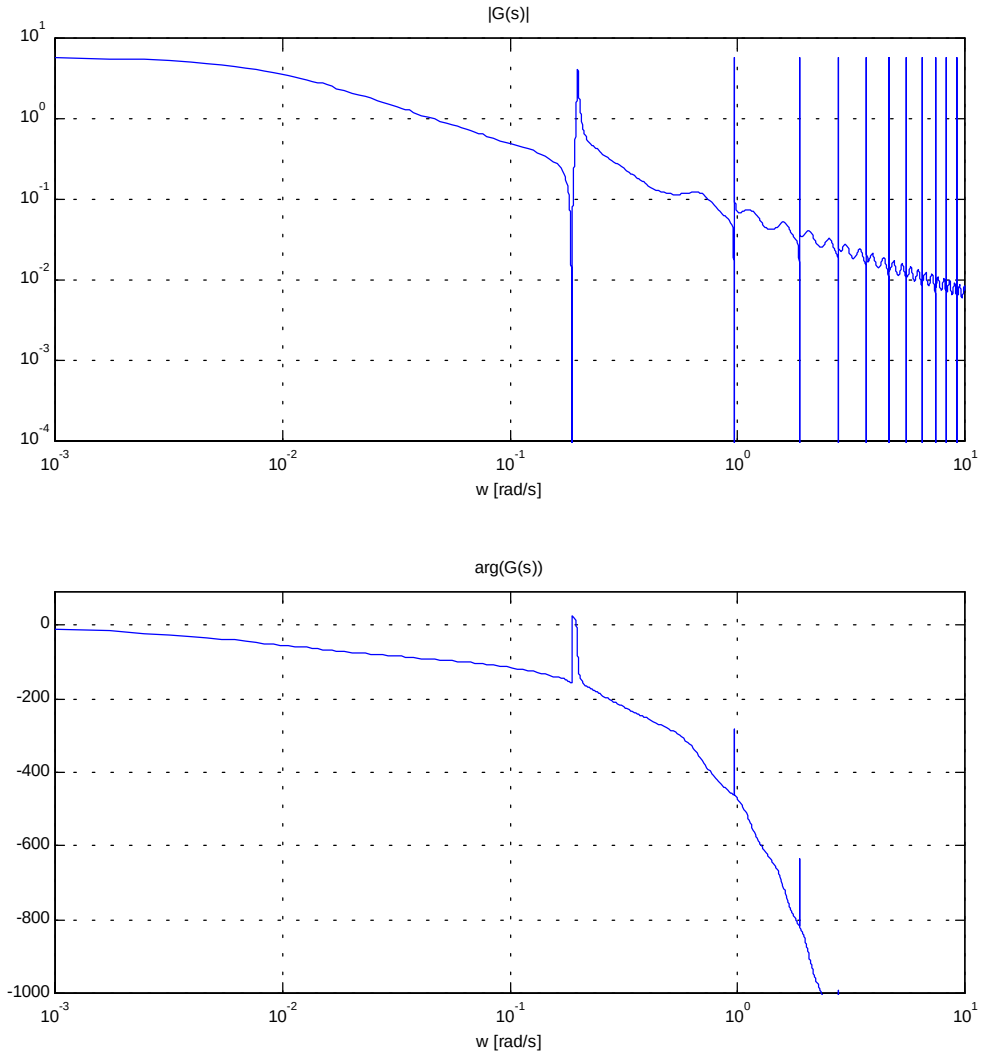

Figure 7.8: Bode plot without friction

Case 2: Distributed friction

If the distributed friction is taken into account, the situation changes completely, as shown in Fig. 7.9. The resonance peaks are smoothed out by the distributed friction, which is of great help in carrying out a conventional PI design.

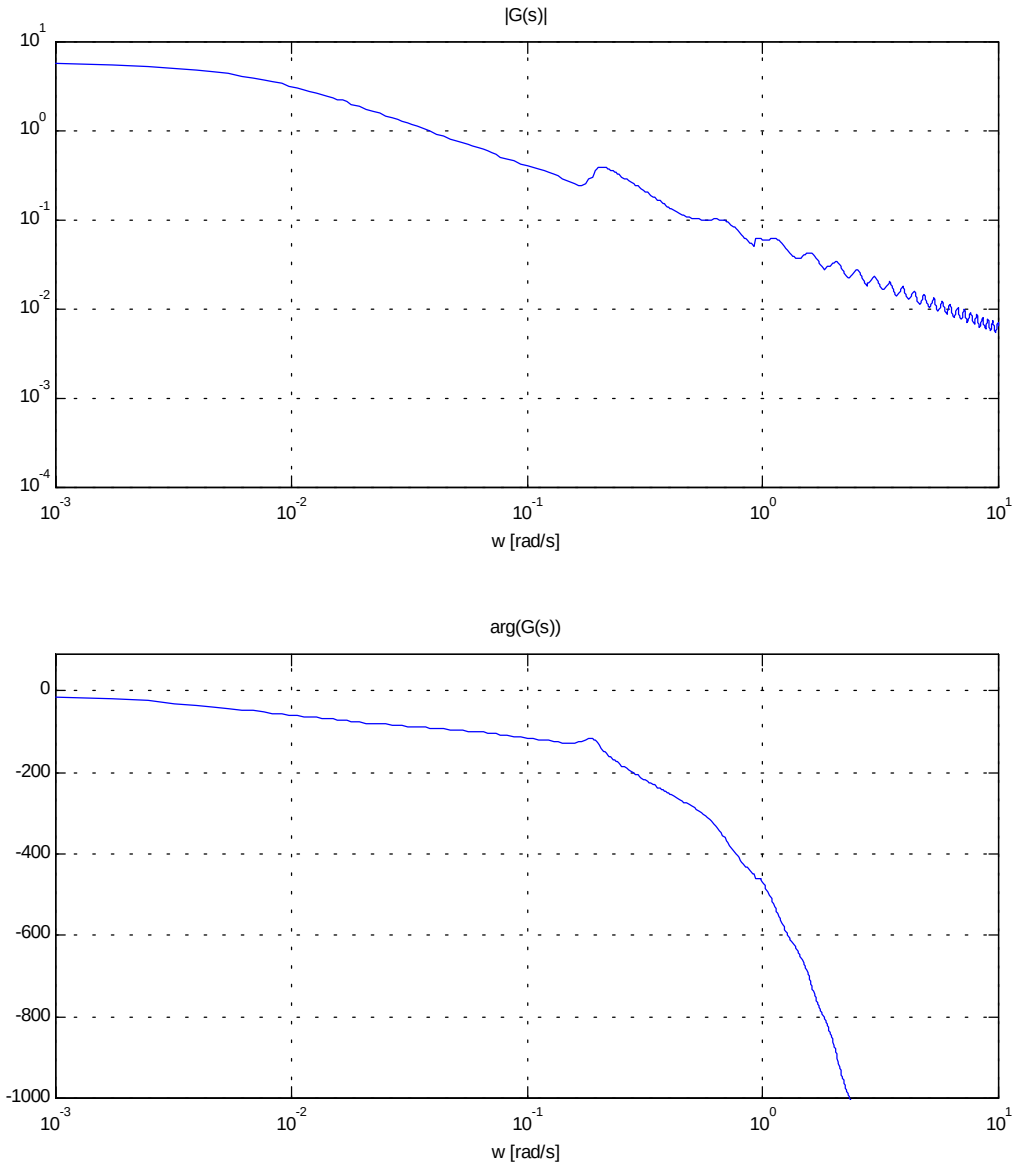

Figure 7.9: Bode plot with friction

7.3.3 Conventional Control

A PI controller can be designed by cancelling the plant pole at T = 100, and by adjusting the gain in order to have a loop bandwidth of 0.05 rad/s. The corresponding phase margin is 75°, and the gain margin is approximately 6 dB. The frequency response of the loop transfer function is shown in Fig. 7.10.

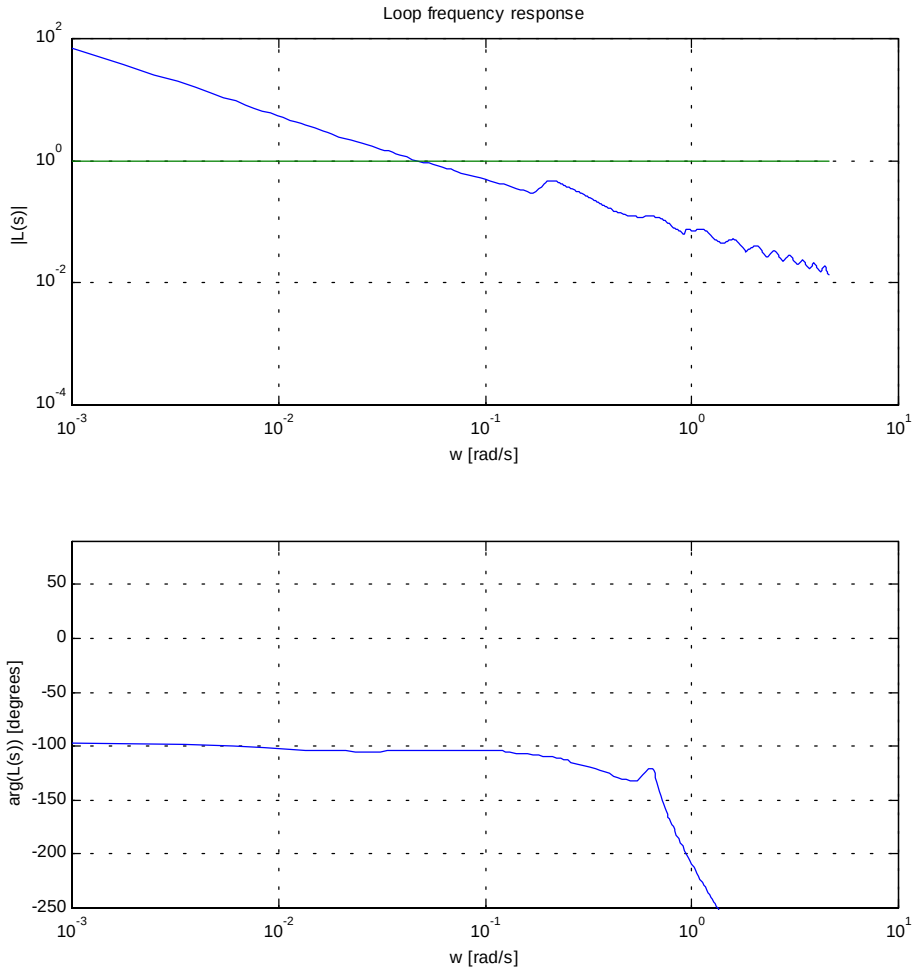

Figure 7.10: Frequency response of loop transfer function

In case the reinjection well approaches the maximum draining capacity, the process gain will decrease, so that the control loop will become slower, but with no risk of unstable behaviour. The response of this control system to a +15% step increase in the pump flowrate is shown in Fig. 7.11. Note that, in this test, the pressure setpoint was set to 5.3 bars.

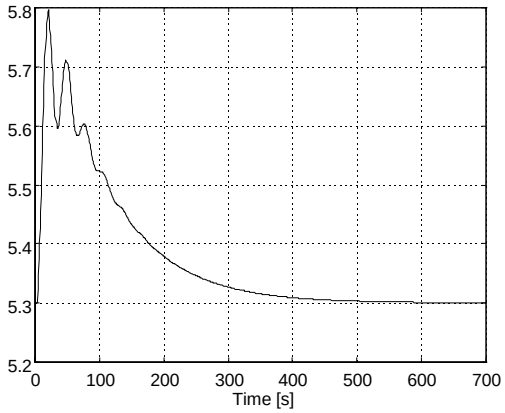

Figure 7.11: Step disturbance response - PI only

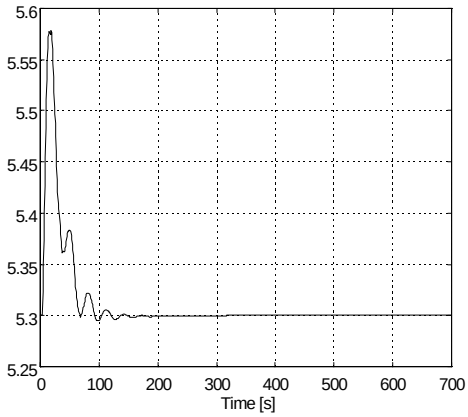

Figure 7.12 Step disturbance response - PI + feedforward

In steady-state conditions, there is fixed relationship between pump flowrate (measured by the sensor FT4001) and the valve stem position. This can be exploited to add a static feed-forward compensation to the control system, enhancing its response to the flowrate disturbances. The response to the same +15% flowrate disturbance in this case is shown in Fig. 7.12. Note that the peak value is slightly decreased, and the transient is much shorter, as expected. Of course, this is true only if the flow-stem position relationship is estimated precisely; otherwise, the settling time of the transient will be longer, but no damage will occur, unless very gross errors are made.

7.3.4 Digital Control

It was shown in [Fer90] that for the processes, where the fundamental dynamics is due to the wave propagation through long pipes, an approach to control based on a peculiar model of the process may lead to considerable improvements. The method consists in finding a pipe segment whose length is the greatest common divisor of the lengths of the pipelines of the plant. In this case, this length is just coincident with the length of the first pipeline (3.4 km), since the second pipeline is 6.8 km long, if the connection to the GR2 well is neglected. Then, the transfer function model is described in the *z*-transform domain, by selecting a sampling time equal to the propagation time through the segment (3.4 s in this case). This amounts to using Eq's. (4.62) and (4.63) for each pipe segment 3.4 km long, combined with the discretised storage tank models (obtained by applying Tustin's formula to (5.100)), the linearized version of the valve equation (5.28), and the same boundary conditions described in section 7.3.2. The resulting overall model is of seventh order, and the transfer function $F(z)$ between the process input (variation in the stem

POLES
$p_{1,2}$ =-0.5553 ± *i*0.5499; $p_{3,4}$ = 0.5434± *i*0.5726 ; $p_{5,6}$ = 0.7849 ± *i*0.6125 ; p_7 = 0.9818
ZEROS
z_1 = 0 ; z_2 = 0 ; $z_{3,4}$ = 0.8110 ± *i*0.5851 ; z_5 = -1

Table 7.1: Poles and zeros of discretised plant

position of PV6003) and output (pressure variation in V602) in the *z*-domain has the poles and zeros of Table 7.1.

The discretised model has been obtained as a worst-case approximation, ignoring friction. Note that the model of the pipes in the *z*-domain is exact, while the tank model has to be discretised by using some suitable approximation method. If Tustin's formula is employed, the property of the continuous-time model of being almost on the stability boundary is preserved. If Euler's explicit method is used, an unstable discrete-time model is obtained, while Euler's implicit formula introduces a fictitious damping (as was already hinted at in Section 3.3.3). In this case, the choice of Tustin's method seems therefore the best one.

Note also that the three non-null zeros are on the unit circle, so that they must appear also in the closed-loop transfer function. Among the poles, the first four are at a relatively high frequency and sufficiently well damped; the last pole is at a low frequency and overdamped, while poles p_5, p_6 are at rather low frequency and slightly damped.

The controller is designed to obtain a closed-loop transfer function, say F_{CL}, which keeps all the zeros and the first four poles of the process transfer function, while replacing the last three poles with 3 coincident positive real poles located at z=0.4 (as a reasonable compromise between speed of response and robustness of the control system). Of course, the desired closed-loop transfer function will have unit gain (this implies that the digital regulator will have a pole at z = 1).

The resulting seventh-order regulator has the following transfer function:

$$R(z) = 0.01\frac{-7.1436z^7 + 18.0568z^6 - 17.8473z^5 + 6.8068z^4 - 2.5211z^3 + 6.6103z^2 - 6.6103z + 2.6459}{z^7 - 1.762z^6 + 0.0612z^5 - 0.2030z^4 + 0.6173z^3 - 0.8619z^2 + 0.1809z - 0.0244} \quad (7.2)$$

The digital controller has been implemented in a control module containing its finite-difference representation, the state vector being the vector of the last seven outputs.

The response of the digital control system to the disturbance specified in Section 7.3.3 is shown in Fig. 7.13. To point out the feedback control capability, no feedforward disturbance compensation has been included in the digital control scheme. Note that the task containing this controller will run with its own step size of 3.4 seconds, while the rest of the simulator keeps

running with the usual step sizes. This is very easily implemented in ProcSim, since multirate integration is possible without any particular problem.

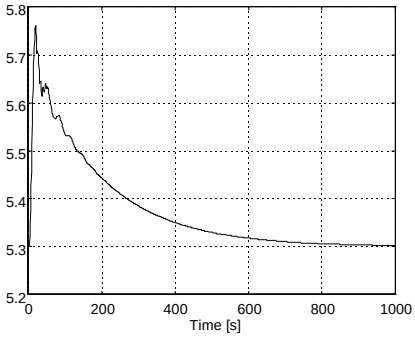

Figure 7.13: Step disturbance response, digital controller

In conclusion, it may be observed that the improvement obtained by a model-based digital control with respect to conventional PI control is not at all dramatic, as it was expected. Thas is because, in the case under examination, the pressure wave dynamics combines with the storage tank capacitance to give the system a low-pass characteristic (see Fig. 7.9), which is not the case in hydroelectric plants, for which this method was invented. In fact, the frequency response of (7.2) closely resembles a PI controller, plus a tuned filter suppressing the first resonance peak. Moreover, friction effects along the transport pipes yield sufficient natural damping to the fundamental oscillation mode. Finally, the controller design has been carried out starting from a frictionless model, which is a worst-case approximation. A better performance of the control system could possibly be obtained by including the friction effect in the discrete-time model of the plant. On the other hand, relying too much on the predicted friction could be dangerous in practice, since friction is a rather uncertain phenomenon, in particular on dynamic conditions.

7.4 Reboiler Control & Plant Efficiency Optimisation

7.4.1 Introduction

As already said in the general overview, the control of the reboiler cycle is perhaps one of the most interesting issues for this plant. Three degrees of freedom (i.e. control variables) are available, namely the stem position of the reboiler top exhaust valves PV3005A/B (which work in a split-range mode, and are thus equivalent to a single actuator), and the stem positions of the two valves at the outlet of the two recirculation pumps, FV3012 and TV3013. Many more measurements are available (i.e. FT3012, FT3013, FT3014, FT3015, FT3102, FT5001, PT3005, TT3013, TT3014). The aim of the controller, as well as its structure and its design, are an open problem, since no “natural” or obvious solution can be easily seen.

The original design document [ELC89] proposes a controller structure, which is the following: the valve PV3005 should be used to control the reboiler pressure (measured by PT3005); the valve TV3013 should be used to keep the

difference between the temperature of the reboiler exhaust and that of the low-temperature recirculation flow at 2 K; finally, the valve FV3012 should be used to provide the largest possible steam flowrate to the high-pressure turbine (measured by FT5001), that is 140 t/hr, or 39 kg/s. The idea behind these last two choices is to limit the vapour waste through the reboiler exhaust, and to fully use the high-pressure turbine, which has a presumably higher efficiency since it processes steam at a higher pressure.

While the use of PV3005 for the reboiler pressure control is the natural solution, as will be seen, the other two choices are highly questionable, for the following reasons:

- The two control loops will be strongly interacting
- The strategy to be followed when switching to the reduced flowrate mode is not even mentioned
- There is no guarantee that this choice is optimal, in any sense.

Early experiments with the simulator showed that decreasing the temperature difference at the reboiler top by increasing the low-temperature recirculation flow could actually decrease the net power output, instead of increasing it, thus contradicting one of the fundamental assumptions. This is a typical situation in process control, where often the aim and structure of the controller is not at all clear at first sight.

The whole problem was then been reconsidered, and it appeared that, it was more an optimisation than a control problem, which had to be solved. The main idea is the following: even though some constraints might exist, the three degrees of freedom provided by the three actuators should be used to *maximise the net power output of the plant.* This is the true aim of the reboiler control system.

The net power output is the outcome of the many complex interactions between the various components. As an example, imagine to increase the low-temperature recirculation flow: the temperature difference between this flow and the reboiler exhaust will decrease, but, at the same time, more low-pressure steam and less high-pressure steam will be produced; this in turn means that the pressure at the low-pressure turbine inlet and in the secondary separator pressure will increase, and thus the low-temperature recirculation liquid will get hotter; as a final outcome, the measured temperature difference will be lower, but the temperature of the exhaust gas-vapour mixture, and thus its wasted steam content, will be higher. In general, the overall efficiency will be the outcome of a complex balance between the pump energy consumption, the waste steam discharged into the atmosphere by the reboiler, and the efficiency of the power generating process based on the four (irreversible) flashing processes and on the turbine efficiency in converting thermal energy into mechanical energy. These aspects can be considered correctly only through the

use of a *complete system model*, and not on partial considerations on the efficiency of a single section of the plant.

Note that the normal operating mode of the plant is a steady state, so that a *static optimisation problem* must be solved. The transients occur only on rare occasions, usually due to faults; needless to say, in these cases the focus is on maintaining the maximum degree of availability of the plant units, rather than optimising the power output.

The optimising control problems can be stated and solved through the following steps (see, e.g., [Sko96, Chapt. 10]):

1. Obtain a static model of the whole plant. A simplified model, described in Section 6.3, has been used in this preliminary study, but a more complete model should be used to obtain better results. Nevertheless, even though simplified, the model captures all the essential interactions between the process components: primary separators, reboiler, secondary separators, turbines, recirculations, fresh water inlet. In this case, *assuming a fixed production flowrate*, the model will have three degrees of freedom.
2. For all the planned operating conditions, perform an optimisation procedure, where the optimised variable is the net power output (which is the turbine power output minus the pump power consumption minus the consumption of the condenser extraction compressor). This procedure will yield the optimal values of *all* the process variables, including the measured ones.
3. Unfortunately, the real plant is different from the model; therefore, the measured variables which are less sensitive to the model uncertainties and to the unmeasured disturbances, more easily controlled, more reliable, and as much independent of each other as possible, should be selected as controlled variables.
4. The input/output pairing, as well as the controller structure (fully centralised, partially decentralised or fully decentralised) should be selected.
5. Finally, the appropriate control laws should be found to actually implement the controller.

Various attempts have been made to give a formal, mathematical statement to all these steps ([Mor89], [Sko96]), but it is very difficult to consider all the aspects simultaneously, and very often, due to the “curse of dimensionality”, the problem becomes intractable if more than 3 or 4 variables are involved. Therefore, a mixture of analytical methods and good judgement on the process-specific features is needed to obtain a satisfactory solution.

On top of that, model-based optimisation procedures require on-line parameter estimation and sensor data reconciliation to provide satisfactory results. These aspects are however beyond the scope of this dissertation.

Unfortunately, time lacked for a thorough analysis of the problem, so that only some preliminary results will be given. They are nevertheless very significant, and can be directly used on the plant giving satisfactory results.

7.4.2 Reboiler Pressure Control

The reboiler pressure is a key variable of the process, since, when all the plant units are connected and functional, it determines the pressure of all the gas-vapour network through to the primary separators, and thus all the quasi-equilibrium conditions in the 14 plates and in the primary separator tanks. The choice of PV3005 as a control variable is quite natural. The open-loop dynamics was quite difficult to predict a-priori, since it depends in a complex way on the mass and energy transfers between the two phases in the plates, and on the boundary condition represented by the gas-vapour mixture feed circuit. The open loop step response of the pressure to a 1% opening of PV3005, starting from the reference state 3A and keeping the other two valve stem positions fixed, is shown in Fig. 7.14

The response is quite slow, despite the very low hydraulic resistance of the plates (about 0.1 bars between the top plate and the bottom plate, including the head due of the water hold-up). This means that the pressure dynamics is fundamentally tied to the condensation dynamics in the plates, which is slow due to the mass and energy storage in the plate hold-ups. Moreover, the counter-current structure is, in some sense, self-stabilising, since any perturbation in one plate is soon restored back near the initial condition by the effect of the adjacent plates. This result holds despite the non-equilibrium

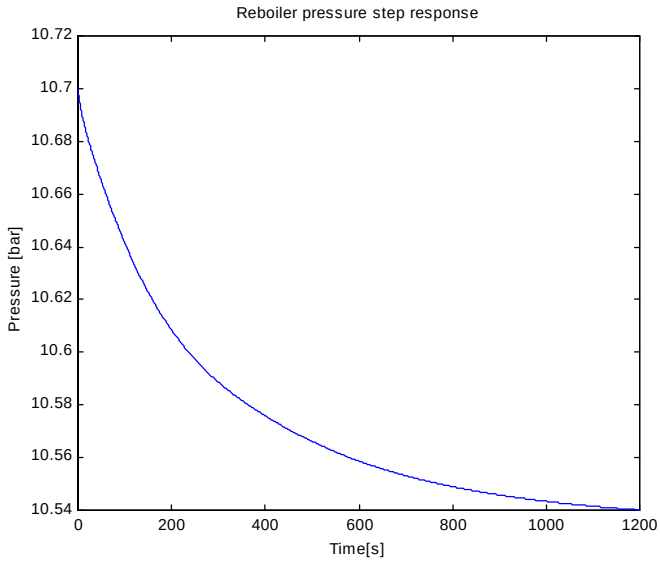

Figure 7.14: Reboiler pressure open-loop step response

hypothesis assumed for the plates, probably due to their relatively high number.

After normalising the pressure values, according to the standard normalisation range employed in the control schemes (0-20 bar), the transfer function has been estimated with a least-square procedure to be approximately equal to

$$G(s) = \mu \frac{1 + s\tau}{(1 + sT_1)(1 + sT_2)} \tag{7.3}$$

where μ = -0.81, τ = 94 s, T_1 = 174 s and T_2 = 361 s. The Bode plot is approximately equal to that of a first-order transfer function having the same gain and a time constant around T = 200 s. It can be seen that a 1% opening on the other valves has a much lesser influence on the reboiler pressure, so that this loop is well-decoupled from the other two. A PI controller was then used, with the zero having a time constant of 200 seconds, and a gain such that the closed loop time constant is reduced to 50 s. This tuning, by the way, provided satisfactory performance in all the transients which were tried on the simulator for the various experiments.

7.4.3 Plant Optimising Control

Once the pressure control problem has been solved, the simplified static model, presented in Section 6.3, is considered for the following analysis. The schematic diagram is shown again in Fig. 7.15 for convenience.

The main assumption is that the production flowrate is given, independently of the pressure value. This is unrealistic if the reboiler pressure

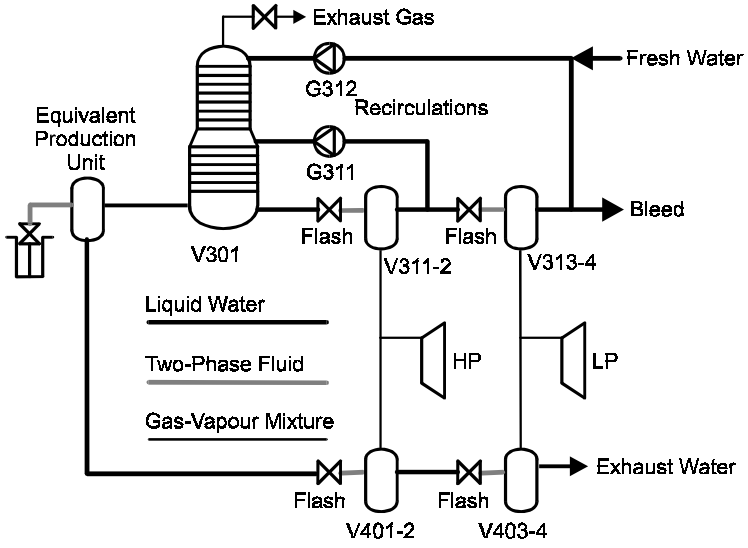

Figure 7.15: Simplified static model

(and thus the primary separator pressure) goes beyond 15 bars, since the well will not be able to sustain the full load flowrate with that head pressure, even if the well head control valve is fully open. Moreover, no lower constraints are taken into account for the recirculation flowrates and for the phase separator pressures, which again might be unrealistic for very low production flowrates.

Under these hypotheses, the static model of the process is a function of four parameters, namely: the reboiler pressure P_r [bar], the production flowrate w_p [kg/s], the CO_2 content in the geothermal fluid x_g [%] and the plate efficiency η (nominal, *n*, or reduced by 30%, *r*). The geothermal fluid enthalpy is considered constant at 900 kJ/kg, and the fresh water inlet flowrate is considered constant at 5 kg/s, with a temperature of 25 °C. The influence of this last parameter could be worth studying, but time lacked to do that.

The output variables which will be considered are the two recirculation flowrates, w_{311} [kg/s] and w_{312} [kg/s], the total gas-vapour mixture flowrate at the reboiler inlet w_{reb} [kg/s], the pressures and flowrates at the turbine inlets, P_{HP} [bar], P_{LP} [bar], w_{HP} [kg/s], w_{LP} [kg/s], the temperature difference between the reboiler exhaust mixture and the low-temperature recirculation ΔT[K], and finally the net power output W[MW], which is the optimised variable. Since the production flowrate is considered as given, the optimised quantity is actually the energy obtained per unit mass of geothermal fluid, i.e. the specific efficiency of the process. Another possible optimisation objective, which is not considered here, could be to maximise the power output, irrespective of the specific efficiency.

Some cases, reported in Table 7.2, will now be discussed. The optimal values have been obtained using the gOPT tool on the gPROMS simplified model of the plant sketched in Fig. 7.15.

Case #1 is the reference case 3A. If the operating point is optimised, keeping the pressure fixed at 10.7 bars, Case #2 is obtained: the optimal recirculation flowrates change by -25% and +8%, respectively, but the corresponding net power output is increased by a mere 0.6%. This means that 3A is already near-optimal. If P_r is included in the set of the optimisation variables, as in Case #3, with the constraint $P_r < 16$ bars, the optimal solution

#	P_r	w_p	x_g	η	w_{311}	w_{312}	w_{reb}	P_{HP}	P_{LP}	w_{HP}	w_{LP}	ΔT	W
1	10.7	430	3.4	*n*	599	138	49.5	6.22	2.63	39.2	31.8	2.03	29.54
2	10.7	430	3.4	*n*	480	149	49.1	6.14	2.64	38.7	31.9	3.32	29.71
3	16.0	430	3.4	*n*	209	63.4	36.7	6.68	2.53	42.1	30.6	6.07	30.83
4	10.7	200	3.4	*n*	187	23.0	22.9	4.16	1.21	26.2	14.6	9.40	15.12
5	10.7	430	3.4	*r*	393	175	49.1	5.99	2.67	37.8	32.2	7.39	29.42
6	10.7	430	3.4	*r*	480	149	49.1	6.09	2.62	38.4	31.8	10.9	29.38
7	10.7	200	3.4	*r*	187	23.0	22.9	4.11	1.20	25.9	14.5	35.9	14.87
8	10.7	430	6.0	*n*	281	289	65.9	5.75	2.79	36.2	33.8	2.0	28.88

Table 7.2: Some results on the simplified model

hits the pressure constraint, with a power output increase of 4%. This is reasonable, since higher pressures correspond to higher temperatures and, in general, higher efficiency. However, the production wells cannot yield a production flowrate of 430 kg/s at such a high pressure. This means that, to include P_r among the optimisation variables, the hypothesis of a fixed production flowrate must be abandoned, and a detailed model of the production well must be included. This was not possible for many reasons; therefore, in the following discussion, the reboiler pressure will always be kept fixed at the nominal value 10.7 bars.

Case #4 is the reduced flowrate case, with optimised operating point. Note the value of ΔT = 9.4. Also note that the fresh water flowrate amounts to 1/5 of the low-temperature recirculation flow.

Case #5 is the 3A case with a 30% reduction in plate efficiency, and optimised operating point. A 1% reduction in power output is obtained, compared to Case #2. If the nominal optimised recirculation flows are used (Case #6), even though the recirculation flowrates are substantially different (+22% and -14%), the loss in power output with respect to the optimal value is less than 0.2%.

Case #7 is the reduced flowrate case, with a 30% reduction in plate efficiency and optimised operating point. A loss of 1.7% in the power output is the result of the plate efficiency reduction.

Finally, Case #8 examines the 3A case, but with 6% CO_2 fraction in the geothermal fluid, with optimised operating point. A substantial change in the recirculation flowrates takes place. If however, the optimal flowrates of Case #2 are used (those obtained with 3.4% CO_2), the loss in power output is less than 1%.

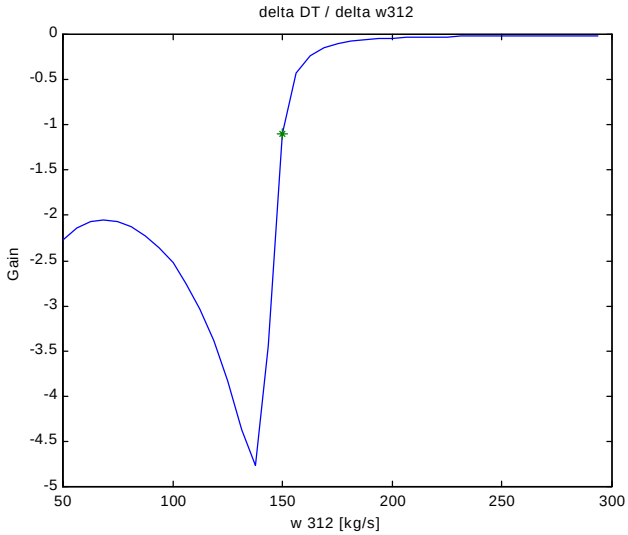

Figure 7.16: ΔT / w_{312} Gain

Some concluding remarks can be done. First, in the various cases, the value of ΔT changes considerably, demonstrating that controlling it to a fixed value of 2 K is not a good choice. Moreover, controlling this ΔT through the low-temperature flowrate is not an easy task: as an example, the graph of the gain between the variation in the recirculation flowrate and the variation in ΔT is given in Fig. 7.16. The gain varies widely (and the poles and zeros as well), in particular around the optimal operating point (marked by a star), which makes it difficult to tune a fast and robust controller.

After all these considerations, a very simple, yet effective, solution can be devised for the optimising control of the reboiler. First of all, since the flows w_{311} and w_{312} are measured by the sensors FT3012, FT3013, local control loops can be used to control those flowrates by acting on the stem position of FV3012 and TV3013. Since the plant transfer function is determined essentially by the sensor and actuator dynamics, these loops can have a wide bandwidth, and thus be very accurate. Moreover, their mutual coupling is negligible. The flowrate setpoints will then be the new control variables. Now, consider that, if the secondary separator pressures (and thus the recirculation temperatures) were fixed, the recirculation flows should be proportional to the reboiler inlet flowrate, which is measured by FT3014 and 3015. This is not true, since the separator pressures vary with the turbine flowrates, but a roughly proportional relationship should hold. For the nominal values of the parameters x_g and η, the curves relating the inlet flowrates with the recirculation flowrates in the optimal operating points are shown in Fig. 7.17.

It has been demonstrated, through various simulations not shown here, that applying the control law given by Fig. 7.17, in case of variations of x_g up to

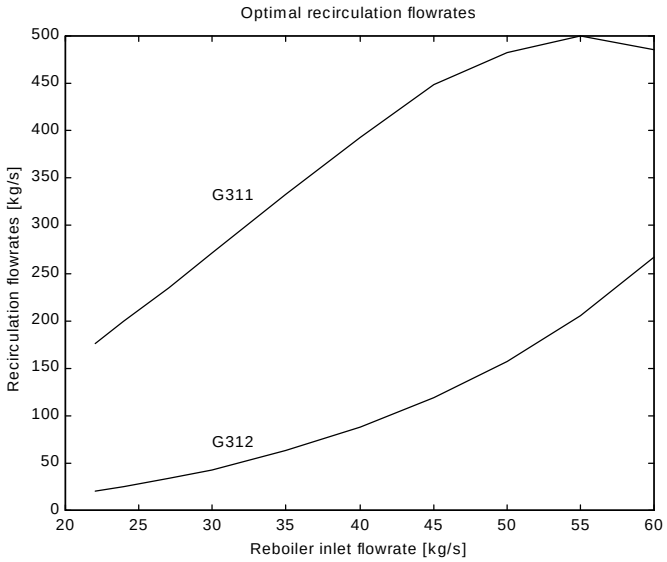

Figure 7.17: Optimal recirculation flowrates

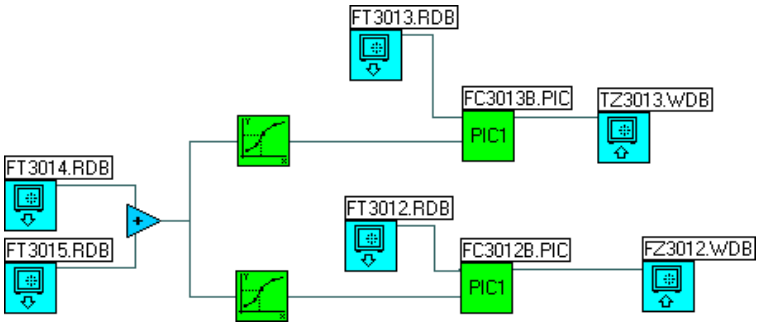

Figure 7.18: Control scheme for the reboiler cycle

6% and of η up to ±30%, a sub-optimal operating point is obtained, whose power output is 1.5% less than the optimal one in the worst case. This result can be considered satisfactory, since modelling and measurement errors will always be present, causing some degree of sub-optimality. The corresponding control scheme is shown in Fig. 7.18.

This control scheme (apart from the flowrate loops, which are fast and robust) has the great advantage of being a feed-forward scheme: this implies that the fast transients caused by the changes in the production rate are immediately followed by the reboiler state, without any slow transients and any danger of instability, since there is no feedback loop closed on the reboiler variables.

Finally, to show that the precision in the recirculation flowrates is not

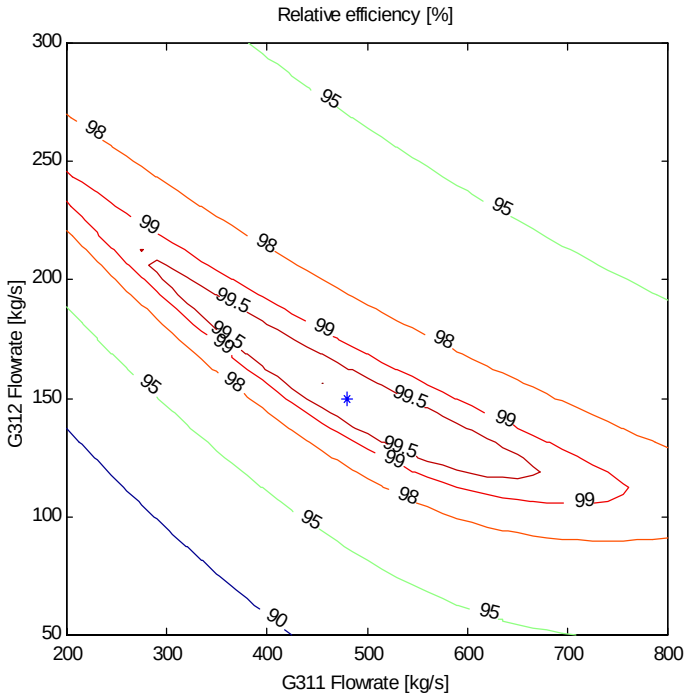

Figure 7.19: Relative efficiency as a function of the recirculation flowrates

critical, the contour plot of the relative efficiency (i.e. the ratio of actual power output to optimal power output) in the case 3A, as a function of the two recirculation flowrates, is shown in Fig. 7.19. Note that there is a certain trade-off between the two flowrates, and that the 98% relative efficiency zone is quite large. The plot is of course valid for a given production flowrate, with the optimal point (marked by a cross) located according to Fig. 7.17.

This is of course only a preliminary study on the subject; the following enhancements are possible:

- Include a better model for the production wells, and also optimise the reboiler pressure;
- Find more robust solutions, making the best possible use of all the available measurements;
- Include in the optimisation procedure the constraints enforced by the pressure control system on the secondary separator pressures, and the constraints on the minimum recirculation flowrates;
- Study the effect of the fresh water input flowrate on the process efficiency.

7.5 Towards a DSS for Plant Management

At the moment, the supervisory level of the Latera plant control system is simply a remote operator console, with a graphic display showing all the relevant measurements coming from the plant. Therefore, the operator is completely unassisted when taking operating decisions, such as connecting or disconnecting some production wells from the main plant, changing the reboiler setpoint pressure, changing the well production rates, and so on.

The system study of the plant, carried out in this research work, was mainly focused on modelling and control issues, with some preliminary study on optimisation issues; it could be carried further on, with the final aim to provide the operator a Decision Support System (DSS), assisting him/her in the plant management task.

The first necessary step is to validate the model, and possibly to implement on-line data reconciliation and parameter estimation procedures, in order to constantly have an updated model available. This model could then be employed to provide, besides the optimisation of the actual operating point, the estimate of parameters which are not directly measured, such as the CO_2 content in the geothermal wells, and a series of possible alternative scenarios, which could arise if some actions are taken by the operator, complete with all the data needed by the operator to evaluate them. As an example, contour plots of efficiency like the one in Fig. 7.19, estimates on the plant efficiency and net power output, evaluation of the consequences of possible faults, could be given for a series of possible actions (e.g. connecting or disconnecting a production

well from the main plant, or changing the production rate, etc.). The operator would then face a series of detailed descriptions of the possible outcome of his/her decisions, allowing him/her to select the best one, according to his/her judgement, which, however, would be based on a richer information than available from a simple graphic plant display. This very promising research direction is completely open.

8. CONCLUSIONS AND FUTURE DIRECTIONS

8.1. Main Results

In this research work, the complete and detailed simulation study of the dynamics of an innovative geothermal power plant was carried out. A full non-linear engineering simulator of the process was built, which implied a major effort to model all the process components which are not standard in the field of power generation processes, such as the reboiler, and, more in general, all the components processing a two-phase two-component fluid. Apart from the simulator itself, some results were obtained, which could have a more general interest, such as the study on the numerical stability of the solution of hydraulic networks, or the systematic approach to valve modelling, to allow the complete flow cut-off in hydraulic networks.

The simulator, which has been built as a fundamental part of the research work, has already had a significant impact on its end users, i.e. the engineers at ENEL which are in charge for the control system specification and checkout, along with all the personnel involved in the final design, commissioning, start-up, and initial operation of the plant.

The simulator has allowed to evaluate the dynamic behaviour of the plant in many different situations and operating conditions; on one hand, this permitted the study and preliminary tuning of the control system; on the other hand, its results confirmed that the plant can operate safely both in normal operating condition and in case of major faults. This result is of great value, since no previous experience was available on similar plants.

Finally, the study of the control system for the reboiler cycle made it clear that optimisation issues should be considered in the control system design, a fact which was absolutely not clear at the beginning of the research. Some very interesting, although preliminary, results were given.

8.2. Future Directions

The possible future research, based on this work, could take many different directions. First of all, once the plant is actually operating, extensive

model validation should be performed, to check the soundness of the modelling approach and simplifications, which were employed throughout all the research work.

A rather easy task could then be to enhance the engineering simulator, which is one of the outcomes of this research, to obtain a simulator for personnel training. Basically, this would require to implement a better user interface, without need of any further modelling effort.

A much more challenging project would be instead to evaluate, and possibly implement, a DSS for plant management, such as the one sketched in Section 7.5. This would require both substantial theoretical work and software implementation work, but the final outcome could be of great interest, and possibly be re-used in other similar contexts.

REFERENCES

ProcSim

[Bar94] A. Bartolini, "Ambiente multitasking per la modellizzazione e la simulazione dinamica interattiva di processi termoidraulici (A Multi-Tasking Environment for Interactive Modelling and Simulation of Thermo-Hydraulic Processes)", *Graduation Thesis (in Italian),* Politecnico di Milano, 1994.

[Bar95] A. Bartolini, A. Leva, C. Maffezzoni, "Power Plant Simulator Embedded in a Visual Programming Environment", *Proc. 2nd IFAC Symp. on Power Plants and Power Systems,* Cancùn, 1995, pp. 119-124.

[Bar96] A. Bartolini, A. Leva, C. Maffezzoni, "A Visual Environment for Building Process Simulators", *Proceedings ITEC '96,* Le Hague, 1996, pp. 381-389.

[Bar98] A. Bartolini, A. Leva, C. Maffezzoni, "A Process Simulation Environment Based on Visual programming and Dynamic Decoupling", *Simulation,* 1998 (to appear)

[Bel96] G. Bellani, G. Buzzini, "Validazione e sviluppo di una libreria di modelli termoidraulici in ambiente ProcSim (Validation and Development of a Thermo-Hydraulic Model Library in the ProcSim Environment)", *Graduation Thesis (in Italian),* Politecnico di Milano, 1996.

[Cst95] M. Castoro, S. Oldrati, "Simulatore di una caldaia a recupero basato su criteri di disaccoppiamento (Simulator of a Drum Boiler Based on Decoupling Criteria)", *Graduation Thesis (in Italian),* Politecnico di Milano, 1995.

[Col96] F. Colombo, L. Corti, "Simulazione di un impianto a vapore per desalinizzazione soggetto a molteplici condizioni operative (Simulation of a Steam Plant for Desalinisation under Multiple Operating Conditions)", *Graduation Thesis (in Italian),* Politecnico di Milano, 1996.

[Lev99] A. Leva, C. Maffezzoni, G. Benelli, "Validation of Power Plant Models through Complete Dynamic Tests", *IFAC Journal Control Engineering Practice,* 1999 (to appear).

[Lab97] LabView® 4.0 User's Manual, National Instruments Inc., 1997

Latera Plant

[Cal98] P. Calabrese, “Sistemi di regolazione per l’impianto di Latera: simulazione, analisi dinamica e progetto dei loop di regolazione (Control Systems for the Latera Plant: Simulation, dynamic analysis and control loop design)”, *ENEL/PEA internal report (in Italian)*, September 1998.

[Cas98a] F. Casella, A. Leva, C. Maffezzoni, “Dynamic Simulation of a Condensation Plate Column by Dynamic Decoupling”, *Proc. of the 3rd EUROSIM International Congress*, Helsinki, April 1998.

[Cas98b] F. Casella, C. Maffezzoni, “Reinjection Control in a Geothermal Power Plant”, *Proc. 1998 IEEE Conf. on Control Applications*, Trieste, Italy, Sept. 1998, pp. 314-318.

[Cas98e] F. Casella, “Simulazione, analisi dinamica e progetto dei loop di regolazione dell’impianto geotermoelettrico di Latera. Relazione Conclusiva (Simulation, Dynamic Analysis and Control Loop Design for the Latera Geothermal Plant. Final Report)”, *Technical Report for ENEL S.p.A. (in Italian)*, Politecnico di Milano, 1998.

[Car99] E. Carpanzano, C Maffezzoni, “Simplification in Object-Oriented Modelling of Large Scale Continuous Systems”, *to appear in Mathematics and Computers in Simulation, Trans. of the IMACS*, 1999.

[ELC89] ELC S.p.A., “Centrale Geotermica di Latera, Produzione di vapore per la centrale, Progetto di Massima (Latera Geothermal Power Plant, Steam Production for the Power Station, General Design Document)”, *ENEL Report T.621.01.23.581 (in Italian),* 1989.

Modelling and Simulation

[ASM93] ASME Committe on properties of steam, *Steam tables: Thermodynamic and Transport Properties of Steam,* preparated by C. A. Meyer et. al., 6th ed. ASME New York, 1993.

[Atk89] K. E. Atkinson, *An Introduction to Numerical Analysis*, 2nd ed, Wiley, 1989, Chapt. 6.

[Brt94] P. I. Barton, C. C. Pantelides, "Modelling of Combined Discrete-Continuous Processes", *AIChE J.*, 40, 1994, pp. 966-979.

[Bre96] K. E. Brenan, S.L. Campbell, L. R. Petzold, *The Numerical Solution of Initial-Value Problems in Differential-Algebraic Equations,* SIAM series, Classics in Applied Mathematics, 1996.

[Bus85] T. Busi, P. Colombo, A. De Marco, "An efficient modelling technique for power plant training simulators: the FAST method", *Proc. of the 11th IMACS World Congress,* Oslo, 1985.

[Cas98c] F. Casella, C. Maffezzoni: "Exploiting Weak Interactions in Object-Oriented Modelling", *EUROSIM Simulation News,* March 1998, pp. 8-10.

[Cas98d] F. Casella, A. Leva, C. Maffezzoni: "Dynamic Simulation of a Condensation Plate Column by Dynamic Decoupling", *Proc. of the 3rd EUROSIM International Congress,* Helsinki, April 1998, pp. 368-374.

[Cel91] F.E. Cellier, *Continuous system modeling,* Springer-Verlag, 1991.

[Cer98] A. Cera, "Calcolo della portata in un orifizio tarato in condizioni di efflusso critico (Flow computation in an orifice under choked-flow conditions)" (in Italian), *Technical Report, Politecnico di Milano,* 1998.

[Chi59] K. L. Chien, E. I. Ergin, C. Ling, A. Lee, "Dynamic Analysis of a Boiler", *Transaction of the ASME,* 80, 1958

[Col81] J. G. Collier, *Convective Boiling and Condensation,* 2nd ed., Mc-Graw Hill, 1981.

[Dix66] F. L. Dixon, *Fluid Mechanics, Thermodynamics of Turbomachinery,* Pergamon Press, 1966.

[Dom90] P. A. Domenico, F. W. Schwartz, *Physical & Chemical Hydrogeology,* Wiley, 1990, pp. 422-426

[DYM94] H. Elmqvist, *Dymola - Dynamic Modeling Language. User's Manual.* Dynasim AB, 1994.

[Fer90] G. Ferretti, C. Maffezzoni, V. Rossi, "A Novel Approach to Speed Control of Hydro Power Stations", *IFAC Automatica,* Vol. 26 n.3, 1990, pp. 557-565.

[Ger76] W. Gerrard, *Solubility of Gases & Liquids: a Graphic Approach. Data, Causes, Prediction,* Plenum Press, NY, 1976, pp.90-93.

[Gea91] C. W. Gear, *Numerical Initial Value Problems in Ordinary Differential Equations,* Prentice-Hall 1991.

[gPR97] gPROMS Introductory User's Guide, Process System Enterprise Ltd, 1997.

[gOP98] gPROMS Advanced User's Guide, Process System Enterprise Ltd, 1998.

[Hai96] E.Hairer, G.Wanner, *Solving Ordinary Differential Equations II - Stiff and Differential-Algebraic Problems*, 2nd ed., Springer, 1996

[Hol88] J. P. Holman, *Thermodynamics,* McGraw-Hill, 1988.

[How87] J. R. Howell, R. O. Buckius, *Fundamentals of Engineering Thermodynamics*, McGraw Hill, 1987.

[ISA75] Instrument Society of America: *Flow Equations for Sizing Control Valves, Standard ANSI/ISA-S75.01,* 1986.

[Jar92] R. B. Jarvis, C. C. Pantelides, "DASOLV: A Differential-Algebraic Equation Solver", *Technical Report*, Centre for Process Systems Engineering, Imperial College, London, 1992.

[KWU83] G. K. Lausterer, J. Franke , E. Eitelberg, "Modular Modelling Applied to a Benson Boiler", *Proc. of the 1st IFAC Workshop on Modelling and Control of Electric Power Plants,* Como, Italy, 1983.

[Lam91] J.D. Lambert, *Numerical methods for Ordinary Differential Equations*, Wiley 1991.

[Luy90] W. L. Luyben, *Process Modeling, Simulation and Control*, 2nd ed., McGraw Hill, 1990.

[LEG83] C. Maffezzoni, G. Magnani, L. Marcocci, "Computer Aided Modelling of Large Power Plants", *Proc. of the 1st IFAC Workshop no Modelling and Control of Electric Power Plants,* Como, Italy, 1983.

[Maf89] C. Maffezzoni, *Dinamica dei generatori di vapore (Dynamics of Steam Generators) (in Italian),* Masson, Milano, 1989.

[Maf92] C. Maffezzoni, "Issues in Modelling and Simulation of Power Plants", *Proc. of the IFAC Symposium on Control of Power Plants and Power Systems,* Munich, Germany, March 1992, pp. 19-27.

[Maf98] C. Maffezzoni, R. Girelli, "MOSES: Modular Modelling in an Object Oriented Database", *to appear in Mathematical Modelling of Systems,* 1998.

[Mat93a] S. E. Mattsson, M. Andersson, K. J. Åström, "Object-Oriented Modelling and Simulation" *in CAD for Control Systems* (D. A. Linkens, Ed.), Chapt. 2, pp. 31-69, Marcel Dekker, Inc., New York, 1993.

[Mat93b] S. E. Mattsson, M. Andersson, “OMOLA: an Object Oriented Modelling Language”, *in Recent Advances in Conputer Aided Control Systems. Studies in Automation and Control, M. Jamshidi , C. J. Heget, Eds.,* Vol. 9, Elsevier Science Publisher, 1993, pp. 291-310.

[Muk80] A. Mukerji, “How to size relief valves”, *Chemical Engineering*, Jun 1980

[Mur91] P. Muroni, *Valvole di regolazione per processi industriali (Control valves for industrial processes) (in Italian)*, PEG, Milano, 1991.

[Ord94] A. W. Ordys, A. W. Pike, M. A. Johnson, R. M. Katebi, M. J. Grimble, *Modelling and Simulation of Power Generation Plants,* Springer-Verlag, 1994.

[Pan93] C. C. Pantelides, P. I. Barton, “Equation Oriented Dynamic Simulation: Current Status and Future Perspectives”, *Computers and Chem. Eng.,* 17S, 1993, S263-S285.

[Per85] R. H. Perry, D. Green (Ed’s.), *Perry’s Chemical Engineers’ Handbook,* McGraw-Hill, 1984.

[SIC72] M. Perrin, G. Marsot, C. Boudy, *Modèle de simulation mathématique de tranches thermiques et nucleaires - Code SICLE (Model for Mathematic Simulation of Thermal and Nuclear Sections, SICLE code) (in French),* EDF Direction des Etudes et Recherches Internal Report HI 888/02, July 1972.

[SIC79] M. J. P. Maxant, M. H. Perrin, “Mathematical modelling of thermal and nuclear power plants - System code SICLE”, *Proc. of the 2nd Multiphase Flow and Heat Transfer Symposium,* Miami, USA, 1979.

[Str83] V. Streeter, B. Wyley, *Fluid Transients,* FEB, Ann Arbor, MI, USA, 1983.

[TAI81] T. A. I., *Calcolo delle valvole di sicurezza per liquidi vaporizzanti (Sizing of relief valves for vaporising liquid) (in Italian)*, Internal Report, June 1981.

[War88] K. Wark, *Thermodynamics,* McGraw-Hill, 1988.

Control

[Fos73] A. S. Foss "Critique of Chemical Process Control Theory", *IEEE Trans on Automatic Control*, Vol AC-18, 1973, pp 646-52.

[Fra90] P. M. Frank, “Fault diagnosis in dynamic systems using analytical and knowledge-based redondance- A survey”, *IFAC Automatica*, Vol 26, n. 3, 1990, pp. 459-474.

[Fra96] P. M. Frank, “Analytical and Qualitative Model-based Fault Diagnosis - Asurvey and Some New Results”, *European J. of Control*, Vol.2, 1996, pp. 6-28.

[Mor89] M. Morari, Zafiriou, *Robust Process Control*, Prentice-Hall, 1989.

[Sko96] S. Skogestad, R.P. Postlethwaithe, *Multivariable Feedback Control: Analysis and Design*, Wiley 1996.